REPORT DOCUMENTATION PAGE

AFRL-SR-BL-TR-02-

0139

1. AGENCY USE ONLY *(Leave blank)*	2. REPORT DATE	3. RE
	SEPTEMBER 2001	FINAL (29 SEP 00 TO 29 SEP 01)

4. TITLE AND SUBTITLE
A SECOND LAW BASED INEGRATED THERMOECONOMIC MODELING AND OPTIMIZATION STRATEGY FOR AIRCRAFT/AEROSPAVE ENERGY SYSTEM SYNTHESIS AND DESIGN

5. FUNDING NUMBERS
F49620-00-1-0142

6. AUTHOR(S)
M. R. VON SPAKOVSKY

7. PERFORMING ORGANIZATION NAME(S) AND ADDRESS(ES)
VIRGIIA POLYTECHNIC INSTITURE AND STATE UNIVERSITY
DEPART OF MECHANICAL ENGINEERING
BLACKSBURG, VA 24061

8. PERFORMING ORGANIZATION REPORT NUMBER

9. SPONSORING/MONITORING AGENCY NAME(S) AND ADDRESS(ES)
AFOSR/NA
801 RANDOLPH STREET, ROOM 732
ARLINGTON, VA 22203-1977

10. SPONSORING/MONITORING AGENCY REPORT NUMBER

11. SUPPLEMENTARY NOTES

12a. DISTRIBUTION AVAILABILITY STATEMENT

12b. DISTRIBUTION CODE

13. ABSTRACT *(Maximum 200 words)*

As part of this project over the past two years, a general methodology (ILGO) for the decomposed synthesis/design optimization of highly coupled, highly dynamic energy system has been developed applied to an aircraft propulsion sub-system (PS) coupled to an environmental control sub-system (ECS) and is being applied to a combination of coupled aircraft sub-system, namely, a PS, and ECS, a TMS (thermal management sub-system) and a SS (structural sub-system). It is our intention at the completion of this project to have solved this problem in its entirety, resulting in a Ph.D. dissertation already completed and submitted as our annual report in year one of this project and an M.S. thesis. The latter of these will serve as our final report for the final phase of this project to be complete next year. In the meantime, however, for the purpose of this project, some preliminary results are presented showing the influence of the various coupling function (an integral part of ILGO) on the unit-level and system-level, unit-based synthesis/design optimization of the PS, ECS, and TMS (i.e. fuel loop sub-system (FLS) and vapor refrigeration /PAO loops sub-system (VC/PAOS). Furthermore, for the time being, no decision variables are used for the SS, which is solved as an integral part of the PS.

14. SUBJECT TERMS

20020419 176

15. NUMBER OF PAGES
130

16. PRICE CODE

17. SECURITY CLASSIFICATION OF REPORT	18. SECURITY CLASSIFICATION OF THIS PAGE	19. SECURITY CLASSIFICATION OF ABSTRACT	20. LIMITATION OF ABSTRACT
unclassified	unclassified	unclassified	

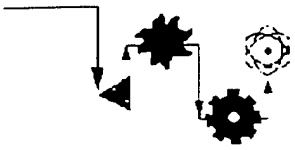

ENERGY
MANAGEMENT
INSTITUTE

Virginia Tech

A SECOND LAW BASED INTEGRATED THERMOECONOMIC MODELING AND OPTIMIZATION STRATEGY FOR AIRCRAFT / AEROSPACE ENERGY SYSTEM SYNTHESIS AND DESIGN

(Grant No. F49620-00-1-0142 – Annual Report)

D.F. Rancruel, J. R. Muñoz and M. R. von Spakovsky
Energy Management Institute
Department of Mechanical Engineering
Virginia Polytechnic Institute and State University
Blacksburg, VA 24061

September, 2001

TABLE OF CONTENTS

ABSTRACT

As part of this project over the past two years, a general methodology (ILGO) for the decomposed synthesis / design optimization of highly coupled, highly dynamic energy systems has been developed and applied to an aircraft propulsion sub-system (PS) coupled to an environmental control sub-system (ECS) and is currently being applied to a combination of coupled aircraft sub-systems, namely, a PS, an ECS, a TMS (thermal management sub-system) and a SS (structural sub-system). It is our intention at the completion of this project to have solved this problem in its entirety, resulting in a Ph.D. dissertation already completed and submitted as our annual report in year one of this project and an M.S. thesis. The latter of these will serve as our final report for the final phase of this project to be complete next year. In the meantime, however, for the purpose of this report, some preliminary results are presented showing the influence of the various coupling function (an integral part of ILGO) on the unit-level and system-level, unit-based synthesis / design optimization of the PS, ECS, and TMS (i.e. fuel loop sub-system (FLS) and vapor refrigeration / PAO loops sub-system (VC/PAOS)). Furthermore, for the time being, no decision variables are used for the SS, which is solved as an integral part of the PS. A breakdown of what this report contains is as follows:

- *Chapter 2* describes the decomposition strategies of LGO and ILGO for the synthesis / design optimization of highly dynamic, highly complex energy systems.
- *Chapter 3* defines the system synthesis / design optimization problem for the coupled PS, ECS, TMS (VC/PAOS and FLS) and SS.
- *Chapter 4* shows how ILGO is applied to the synthesis / design optimization problem outlined in Chapter 3.
- *Chapter 5* goes into greater detail on the TMS optimization sub-problem and its associated model for the synthesis / design optimization.
- *Chapter 6* details the SS optimization sub-problem and its associated model for the synthesis / design optimization of the airfoil.
- *Chapter 7* presents a discussion of preliminary results for the PS, ECS and TMS synthesis / design optimization sub-problems in the context of the overall system-level aircraft synthesis / design optimization problem.
- *Chapter 8* ends this report with some conclusions.

ACKNOWLEDGMENTS

The authors wish to thank Dr. Peter King of Virginia Tech Mechanical Engineering Department for his support, suggestions, and important information which were used to develop the Aerodynamic and Propulsion system models. Special thanks are due to our industrial engine manufacturer for allowing us to use their engine simulator. The comments and suggestions made by Lockheed Martin TAS and in particular to Mr. James A. Louviere are also greatly appreciated.

CHAPTER 1

1. INTRODUCTION

The overall problem of *integrated* aircraft synthesis / design *optimization*[1] with variable loads and/or environmental conditions is a very complex and difficult problem to solve. In its entirety, it represents a mixed integer, non-linear programming (MINLP) problem for which no *general* solution has been found. This is further complicated by the need to examine the largest number and most complete set of alternative syntheses and designs at each level of the problem in the shortest amount of time possible. *Decomposition* is seen as a tool for overcoming the mathematical, cultural, and software difficulties that can occur if this synthesis / design problem is formulated as a single problem for the system as a whole. *Decomposition* not only permits the solution of the overall synthesis / design problem by dividing it into smaller sub-problems but facilitates the difficult task of sub-system integration. The problem of integration is not only that the synthesis / design of the different sub-systems usually present in complex systems is accomplished by teams generally in different areas of expertise each using tools possibly incompatible with those used in other areas but also that these teams encompass a wide variety of engineering disciplines. In addition, the synthesis / design of the different sub-systems may, in many cases, be done at different stages and times, crossing company lines. Furthermore, it is not uncommon to have design teams that are not located entirely at one facility, which added to cultural differences, complicate the task at hand even further. The methods presented here are seen to match and enhance existing design practices and are in tune with the current need for concurrent, collaborative environments that make use of multiprocessing as well as parallel and internet capabilities.

As part of this project over the past two years, a general methodology for the decomposed synthesis / design optimization of highly coupled, highly dynamic energy systems has been developed and applied (Muñoz, 2000; Muñoz and von Spakovsky, 2001a,b) to an aircraft propulsion sub-system (PS) coupled to an environmental control sub-system (ECS) and is currently being applied to a combination of coupled aircraft sub-systems, namely, a PS, an ECS, a TMS (thermal management sub-system) and a SS (structural sub-system). Some preliminary results for the latter application are presented in this report. The approach is based on the physical division of the system into units (sub-systems, components or disciplines) subject to functions describing the energy, cost and other couplings between them. Two versions of the approach are proposed. The first approach is called the Local-Global Optimization (LGO) Approach. LGO requires unit optimizations to be carried out with respect to purely local decision variables for various combinations of the functions that connect the units. The results are used to create an Optimum Response Surface (ORS) for the entire problem. The ORS is then searched by a system-level optimizer to find the values of the coupling functions that lead to an

[1] *Optimization* is used here in a "mathematical" as opposed to "trade study" sense.

optimum system-level solution. The second approach proposed is an iterative[2] version of LGO (ILGO). In this case, the ORS is closely approximated using a linear Taylor series expansion. The partial derivatives resulting from such an approximation are seen to correspond to the shadow prices typically used in the thermoeconomic literature. ILGO effectively and significantly reduces the number of unit optimizations required. The properties used to describe the coupling functions play a critical role in the convergence of ILGO to a global system-level optimum. A discussion of this and its implication for the choice of First or Second Law of thermodynamics based quantities for the optimization of systems is given in subsequent chapters.

The generality of the decomposition methods presented here are such that they are applicable to both stationary or aircraft/aerospace systems. It is assumed throughout this work that any system modeling may require a high level of detail (and is, therefore, expensive to simulate and optimize) and may involve large numbers of continuous and discrete variables. The synthesis/design problem is set up in a general way so that products and feedbacks (i.e. couplings) between units[3] may be represented by energy (or exergy) or by any other relevant quantity that may, for example, facilitate the interface with non-energy systems. This contrasts with the El-Sayed and Evans (1970) formalism and other thermoeconomic formulations (e.g., Frangopoulos, 1983; Tsatsaronis, 1985; von Spakovsky, 1986; Valero et al., 1986; Benelmir, 1990; etc.), which were developed under the assumption that the properties of the energy system being considered are best expressed in terms of exergy. These formulations used exergy due to the belief that cost accounting is more rationally achieved with the use of exergy. For analysis purposes, this is indeed the case! However, even the most enthusiastic proponents of Second Law analysis know that exergy is not an essential requirement for optimization although in certain cases there may be an associated advantage to its use[4]. In this paper, the final choice of quantity (or quantities) used to represent products and feedbacks (i.e. couplings) is based on ensuring that the shadow prices associated with these quantities exhibit certain desirable properties (e.g., aid in *decomposition* and sub-system integration). Whether the choice is exergy or energy or something else depends on this and certain practical considerations such as the details of the simulations tools available, the level of expertise present, the number of different disciplines required, etc.

Fundamental issues, which have been and are being examined, include the following:

---

[2] It should be pointed out here that the use of the word *iterative* to distinguish between ILGO and LGO is somewhat misleading from the standpoint that both approaches are iterative in nature. What fundamentally separates these two is that the former intelligently introduces *shadow price* information (see subsequent chapters) into the optimization procedure in order to significantly reduce the computational burden (whether on- or off-line), which LGO requires.

[3] Units in this context refer to either sub-systems or components.

[4] For example, it may be used as the basis of a search engine for finding the global optimum; or in certain cases, it may enhance *decomposition* itself.

1. the effects of decomposition on convergence to a global optimum or a set of near-global optima for the system as a whole; the system itself may consist of a number of sub-systems, a single sub-system, or a single component;
2. the mathematical basis or justification for decomposition and its relationship to the global optima found without decomposition;
3. the effects on decomposition and the search for global optima that a mixed discrete and continuous decision variable space will have; this relates to the complete MINLP problem and will be examined here but only partially implemented;
4. the effects of material and geometric changes at the component or sub-component level on the thermodynamic and heat and mass transfer phenomena occurring within individual components or sub-components (e.g., heat exchangers, turbo-machinery, ram air nozzles, zones within specific components, etc.);
5. the couplings between the physical phenomena at the component and sub-component levels and the thermodynamic, heat and mass transfer and even aerodynamic phenomena (e.g., ram-air inlet) found elsewhere in the system;
6. the couplings between the dynamics of the overall system and the dynamic or transient responses of individual sub-systems and components and the effects these have on component geometry and material selections as well as component and sub-system integration;
7. the effect, which changes in the physical phenomena at the component or sub-system level under off-design conditions, have on overall system synthesis and design;
8. the coupling between the non-energy-based sub-system (or discipline) phenomena (aerodynamic and structural) and an aircraft's energy-based sub-system / component phenomena;
9. the relevance of using the Second Law of thermodynamics as a measure of the relative importance of the physical phenomena taking place in the system and as a guide to component and system level changes which alter these phenomena in ways consistent with the global optima for the synthesis and design sought;
10. the significance of using Second Law as opposed to First Law of thermodynamics based quantities on decomposition and convergence to global synthesis and design optima;
11. the fundamental difference if any between the optima exhibited by a purely thermodynamic Second Law-based approach for synthesis and design and one based on a combination of costs and the Second Law;
12. the limits on decomposition imposed by thermodynamic as well as cost-based considerations;

Fundamental issues 1 to 3 above deal with the mathematical foundations of decomposition and the nature of the design spaces created by modeling and optimizing the system as well as its sub-systems and components. Establishing and understanding the basis for decomposition and the characteristics of the design spaces involved is

essential for being able to deal effectively with this highly complex problem of interrelated physical phenomena.

A clearer understanding of these physical phenomena and their interrelationships is also essential. The next four issues (4 to 7) deal with these, i.e. the fundamental aspects of how and why these occur at the component and sub-component levels as well as at the sub-system and system levels and how they are affected by other phenomena occurring locally, upstream / downstream, or in some place not directly linked to the phenomenon or phenomena in question. Obviously, the dynamic and off-design aspects of these phenomena are also of importance and will be examined in order to deduce their impact on the overall problem. Studying these phenomena and their interrelationships will require the use of results from CFD as well as experimental models (particularly as they relate to heat exchangers and their interactions within an overall system) coupled to the type of lumped-parameter models used at the sub-system and system levels for optimization.

The next issue, issue 8, will be studied in order to gain a better understanding of the fundamental basis for decomposition as applied to non-energy based aircraft sub-systems. It will also lead to an understanding of the coupling, which exists, between the physical phenomena occurring in these sub-systems and those occurring in an aircraft's energy-based sub-systems.

The remaining four issues (9 to 12) are essential for establishing and understanding the fundamental basis for using the Second Law of thermodynamics in modeling the physical phenomena present and the impact this has on being able to effectively synthesize and design components / sub-components and sub-systems. Optima based on costs as well the Second Law will also be examined in order to establish if a fundamental difference exists between these optima and those based purely on the Second Law. This question will, of course, only have relevance when operational considerations predominate throughout (i.e. capital is comparatively negligible). Obviously, when capital no longer is negligible, a difference will and must exist.

The research plan outlined here represents a unique opportunity to study the fundamental nature of the couplings which exist between the basic physical phenomena occurring within a given component / sub-component and those occurring elsewhere in the sub-system / sub-systems with which the component / sub-component interacts. Understanding the fundamental scientific basis for these couplings is, in fact, as important as understanding the individual phenomena, which occur locally. The work, which has been and is being carried out in this project, provides a platform for doing so.

As mentioned earlier, practically demonstrating the effectiveness of the decomposition approach that we have developed requires applying it to a set of coupled, complex aircraft sub-systems. This has been done for a coupled aircraft PS and ECS (Muñoz, 2000; Muñoz and von Spakovsky, 2001a,b) and is currently being worked on for a coupled PS, ECS, TMS, and SS. Thus, the synthesis / design task at hand is to perform the integrated optimization of four sub-systems, which are part of an advanced military

aircraft. The problem is to carry out the conceptual design of a low-bypass turbofan engine with afterburning (PS), the full synthesis / design optimization of an air-cycle environmental control sub-system (ECS) and a thermal management sub-system (TMS), and the design optimization of a structural sub-system (SS). The TMS is itself comprised of two sub-systems: a vapor compression refrigeration / PAO loops sub-system (VC/PAOS) and a fuel loop sub-system (FLS).

It is our intention at the completion of this project to have solved this problem in its entirety, resulting in a Ph.D. dissertation already completed and submitted as our annual report in year one of this project and an M.S. thesis. The latter of these will serve as our final report for the final phase of this project to be complete next year[5]. In the meantime, however, for the purpose of this report, we will present some preliminary results showing the influence of the various coupling function on the unit-level and system-level, unit-based synthesis / design optimization of the PS, ECS, and TMS (i.e. FLS and VC/PAOS). Furthermore, for the time being, no decision variables are used for the SS, which is solved as an integral part of the PS by applying the procedure described by Mattingly (1999) and previously applied in Muñoz (2000) and Muñoz and von Spakovsky (2001a,b). A breakdown of what this report contains is as follows:

- *Chapter 2* describes the decomposition strategies of LGO and ILGO for the synthesis / design optimization of highly dynamic, highly complex energy systems.
- *Chapter 3* defines the system synthesis / design optimization problem for the coupled PS, ECS, TMS (VC/PAOS and FLS) and SS.
- *Chapter 4* shows how ILGO is applied to the synthesis / design optimization problem outlined in Chapter 3.
- *Chapter 5* goes into greater detail on the TMS optimization sub-problem and its associated model for the synthesis / design optimization.
- *Chapter 6* details the SS optimization sub-problem and its associated model for the synthesis / design optimization of the airfoil.
- *Chapter 7* presents a discussion of preliminary results for the PS, ECS and TMS synthesis / design optimization sub-problems in the context of the overall system-level aircraft synthesis / design optimization problem.
- *Chapter 8* ends this report with some conclusions.

[5] We have received a 6 month no-cost extension (i.e. an extension of the funds originally allocated to this project through May of next year).

CHAPTER 2

2. DECOMPOSITION STRATEGIES FOR THE SYNTHESIS / DESIGN OPTIMIZATION OF HIGHLY DYNAMIC, HIGHLY COMPLEX ENERGY SYSTEMS

Highly complex, dynamic systems in general and energy systems in particular have special attributes and pose great challenges to the practical application of any of the decomposition methods for large-scale optimization found in the literature. To begin with, consider the non-hierarchical energy system of Figure 2.1, which is composed of m units. The functions u_{ij}, which connect the m units, are called coupling, compatibility, interdisciplinary, linking, or connecting functions or parameters. The coupling functions can also be considered intermediate forward and backward feedback functions (Muñoz, 2000; Muñoz and von Spakovsky, 2000a,b,c; 2001a,b). Each unit, i, has a contribution f_i to the overall or system-level objective or cost function f. In typical energy systems, for example, each unit's contribution to the overall objective function has the form

$$f_i = k_i R_i + Z_i \tag{2.1}$$

where the functions R_i $(i = 1,...,m)$ represent the external resources (e.g., fuel) used to perform the required tasks. These tasks are assumed known. The functions Z_i are related to the physical dimensions and material and technology choice for the unit and can, therefore, be given in terms of mass, area, volume, and/or capital cost. The Z_i will, thus, be called the *capital* functions. The constant k_i is an appropriate conversion factor.

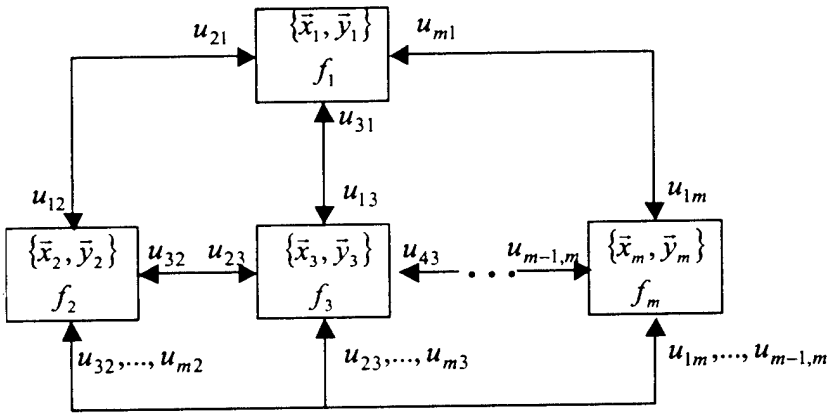

Figure 2.1. A coupled non-hierarchical energy system.

One of the features of dynamic energy systems, for example, is that the amount of external resources can be varied at different instants in time. Likewise, under certain circumstances, the capital functions can take different values over time. One such circumstance is when the capital function represents costs that may be influenced by operating conditions (e.g., maintenance costs). Another feature of energy systems is that the coupling functions u_{ij} may be interpreted as intermediate

products of unit i but in turn become intermediate resources for unit j. In some cases, the coupling functions can be considered as attributes of j that are passed back to i, i.e. they effectively act as intermediate feedback functions.

Time variations in the local or unit-level (as opposed to system-level) objective functions are accomplished by the definition of independent synthesis / design and operational variable vectors $\vec{x}_i$ and $\vec{y}_i$, respectively, for each unit. The synthesis / design variables, $\vec{x}_i$, typically correspond to geometric parameters (physical dimensions of energy and non-energy components[1]), design flow rates, design pressure ratios, and in a wider sense some integer (e.g., material or technology choice) or binary (e.g., existence or nonexistence of a unit in the system configuration) parameters. By definition, synthesis / design variables remain constant in time. Operational variables, $\vec{y}_i$, are parameters which can be controlled over time so that off-design operation is at an optimum. Operational variables can be continuous variables (e.g., flow rates, angles of attack), binary variables (e.g., units on or off), or integer variables (e.g., valve settings).

Given the dynamic nature of the problem, it is often convenient to work with objective functions in rate form. The functional relationships for the local or unit-level objective functions at an instant t are then given by

$$\begin{aligned} \dot{R}_1 &= \dot{r}_1\left(\vec{x}_1, \vec{y}_{1_t}, u_{12}, \ldots, u_{1m}, u_{21}, \ldots, u_{m1}\right) \\ &\vdots \\ \dot{R}_m &= \dot{r}_m\left(\vec{x}_m, \vec{y}_{m_t}, u_{m1}, \ldots, u_{m\,m-1}, u_{1,}, \ldots, u_{m-1\,m}\right) \end{aligned} \tag{2.2}$$

$$\begin{aligned} \dot{Z}_1 &= \dot{Z}_1\left(\vec{x}_1, \vec{y}_{1_t}, u_{12}, \ldots, u_{1m}, u_{21}, \ldots, u_{m1}\right) \\ &\vdots \\ \dot{Z}_m &= \dot{Z}_m\left(\vec{x}_m, \vec{y}_{m_t}, u_{m1}, \ldots, u_{m\,m-1}, u_{1,}, \ldots, u_{m-1\,m}\right) \end{aligned} \tag{2.3}$$

and

$$\begin{aligned} \dot{f}_1 &= \dot{f}_1\left(\vec{x}_1, \vec{y}_{1_t}, u_{12}, \ldots, u_{1m}, u_{21}, \ldots, u_{m1}\right) \\ &\vdots \\ \dot{f}_m &= \dot{f}_m\left(\vec{x}_m, \vec{y}_{m_t}, u_{m1}, \ldots, u_{m\,m-1}, u_{1,}, \ldots, u_{m-1\,m}\right) \end{aligned} \tag{2.4}$$

At an instant t, the coupling functions are in general given by

$$u_{ij_t} = u_{ij}(\vec{x}_i, \vec{x}_j, \vec{y}_{i_t}, \vec{y}_{j_t}) \tag{2.5}$$

With this in mind and after choosing the independent variables, the system-level synthesis / design problem is formulated as

---

[1] For example, these might include turbine/compressor blade geometries, tube fin geometries, tube lengths and diameters, ram air inlet/exit geometries, aspect ratios, wing areas and thickness ratios, wing chord sweeps, etc.

$$\text{Minimize } f = \int_{time}\left(\sum_{i=1}^{m}\dot{f}_{i_t}\right)dt \tag{2.6}$$

w.r.t. $\vec{X}^T = \{\vec{x}_1, \vec{x}_2, \cdots, \vec{x}_m\}$, $\vec{Y}^T = \{\vec{Y}_t\}^T = \{\vec{y}_{1_t}, \vec{y}_{2_t}, \cdots, \vec{y}_{m_t}\}$

subject to

$$\vec{H} = \{\vec{H}_t\} = \begin{Bmatrix} \vec{h}_{1_t} \\ \vdots \\ \vec{h}_{m_t} \end{Bmatrix} = \vec{0}$$

$$\vec{\Gamma} = \{\vec{G}_t\} = \begin{Bmatrix} \vec{g}_{1_t} \\ \vdots \\ \vec{g}_{m_t} \end{Bmatrix} \le \vec{0} \tag{2.6.2}$$

where

$$\dot{f}_i = k_i \dot{R}_i + \dot{Z}_i \tag{2.6.3}$$

The vectors of equality and inequality constraints at various instants of time, $\vec{H}_t$ and $\vec{G}_t$, respectively, represent, for example, the thermodynamic, aerodynamic, physical, and cost models (i.e. the analysis system of equations) and the restrictions imposed on the synthesis / design. One such restriction is the desired product for each of the units. Thus, the n_{th} element of any vector of equality constraints $\vec{h}_i$ at any instant t is given by

$$h_{i,n_t} = \dot{P}_{i_t} - \dot{P}^o_{i_t} \tag{2.6.4}$$

where $\dot{P}_{i_t}$ is the actual product rate and $\dot{P}^o_{i_t}$ the product rate required for unit i.

In most cases it is advisable to discretize the time integral by taking time segments (independent of each other or not[2]) over the entire load and/or range of environmental conditions. The number of these segments depends on the nature of the load and the level of detail desired. A discretized version of equation (2.6) can be written as

$$\text{Minimize } f = \sum_{t=1}^{\tau}\left(\sum_{i=1}^{m}\dot{f}_i\right)\Delta t_t \tag{2.7}$$

w.r.t. $\vec{X}^T = \{\vec{x}_1, \vec{x}_2, \cdots, \vec{x}_m\}$ $\vec{Y}^T = \{\vec{Y}_t\}^T = \{\vec{y}_{1_t}, \vec{y}_{2_t}, \cdots, \vec{y}_{m_t}\}$ $\quad t = 1,\ldots,\delta,\ldots,\tau$

subject to

$$\vec{H} = \{\vec{H}_t\} = \begin{Bmatrix} \vec{h}_{1_t} \\ \vdots \\ \vec{h}_{m_t} \end{Bmatrix} = \vec{0} \qquad t = 1,\ldots,\delta,\ldots,\tau \tag{2.7.1}$$

---

[2] A problem with dependent time segments is one where transient effects are important.

$$\vec{\Gamma} = \left\{\vec{G}_t\right\} = \begin{Bmatrix} \vec{g}_{1t} \\ \vdots \\ \vec{g}_{mt} \end{Bmatrix} \leq \vec{0} \qquad t = 1,\ldots,\delta,\ldots,\tau \tag{2.7.2}$$

Here the subscript t refers to the τ different segments into which the load/environmental conditions have been divided. Note that in equation (2.7), the time segments can have different durations.

Now, assume that the sizes of the synthesis / design and operational variable vectors are d and o, respectively. The total number of independent variables (or degrees of freedom) is, therefore, $d+o\tau$. For complex, highly dynamic energy / non-energy systems, which may require high levels of detail or have large numbers of units, the total combined number of variables, discrete and continuous may grow very large. In addition, the fact that the response of energy / non-energy system components and sub-systems is typically highly nonlinear and the nature of the synthesis / design space is non-contiguous (due to the presence of discrete variables) make the problem very expensive computationally and in some cases, even impossible to be solved with existing optimization algorithms. In fact, the resulting mixed-integer, non-linear programming (MINLP) problem has a known solution only under very special, restricted conditions (Floudas, 1995; Bruno et al., 1998).

The alternatives normally considered are to reduce the number of independent variables either by varying only a few synthesis / design variables at a time (trade-off analysis), considering a severely limited number of synthesis / design variables while accounting for only one of the operating conditions (one-point design), and/or linearizing the problem in order to transform it into a mixed integer linear programming (MILP) or linear programming (LP) problem. These alternatives may be avoided through the use of decomposition so that the solution to the original problem does not compromise the quality of the final synthesis / design.

However, as mentioned above, the purpose of decomposition is not just to decrease the size of the synthesis / design problem. An equally important reason is to facilitate the difficult task of sub-system and, in some cases, discipline integration. In many existing industrial design processes, the synthesis/design of system units are carried out by different groups and oftentimes different departments within a company or even different companies. The different design philosophies, tools and procedures are in many cases not compatible with each other, making the solution of the entire problem as a single block simply impractical. These difficulties are only worsened by the fact that the synthesis / design of the different units is done at different times.

Therefore, in many practical settings, decomposition is an absolute necessity. In the research being conducted in our funded AFOSR project, two types of decomposition are considered. The first is *time decomposition* and the second *physical* (i.e. unit) *decomposition*. Physical or unit decomposition uses the mathematical concepts for LGO and ILGO defined in Muñoz (2000) and Muñoz and von Spakovsky (2000a,b,c; 2001a,b).

2.1 Time Decomposition

Time decomposition exploits the fundamental differences that exist between the synthesis/design and operational variables to create a set of hierarchical problems each with a lower dimensionality than the overall system-level problem. Different types of time decomposition can be defined. The most common time decomposition schemes (e.g., Frangopoulos (1989), Olsommer, von Spakovsky, and Favrat (1999a,b)) are depicted in Figure 2.2. In both cases the synthesis / design variables are selected by a high-level optimizer. Once the synthesis / design variables ($\vec{X}$) are fixed, they are used by a low-level optimizer to find the optimum operational decision variables ($\vec{Y}$). This second step can be done taking all of the time segments into which the load/environmental conditions have been divided and using them in a single problem as illustrated in Figure 2.2a. If the number of operational decision variables (e.g., the size of the vector $\vec{Y}$) and/or the number of time segments is large, it may be advisable to define a set of τ optimization problems, one for each of the time segments (each with respect to the instantaneous operational variables ($\vec{Y}_t$) as indicated in Figure 2.2b). Once the low-level problems are solved, the optimum values of the objective functions corresponding to the given synthesis / design variables, (indicated in Figure 2.2 as f_x^*) are sent back to the high-level optimizer for analysis and the whole process repeated again and again until the optimum synthesis/design is found.

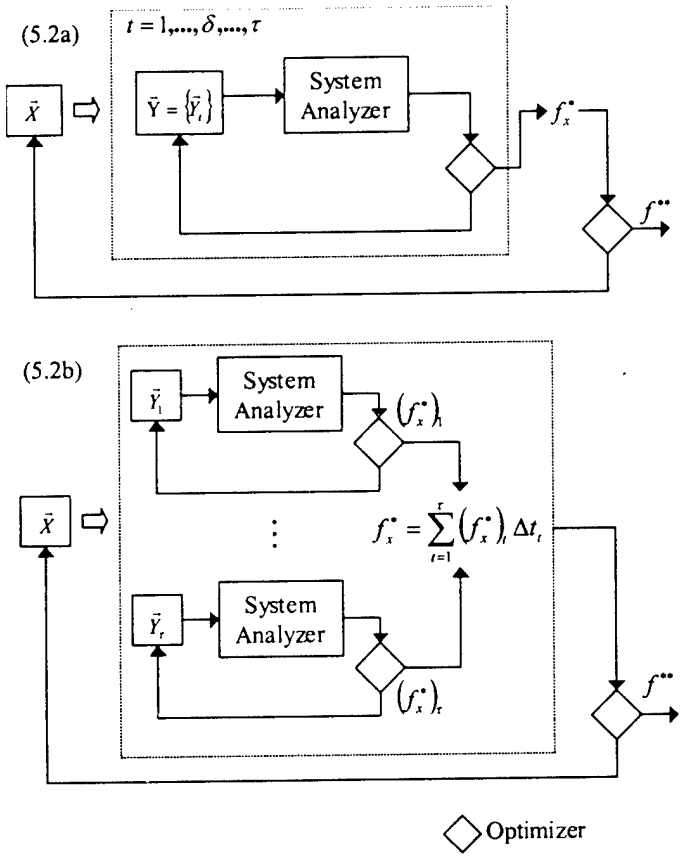

Figure 2.2. Variable-based time decomposition schemes.

Time decomposition effectively reduces the size of the overall problem from $d+o\tau$ variables by solving two problems of size d and $o\tau$, respectively, in the case of Figure 2.2a. In the case of Figure 2.2b, the original problem is replaced by one problem of size d and τ problems of size o/τ.

The main disadvantages of the time decomposition approaches outlined above are

- the very large expense of the nested optimizations that result from applying either approach (i.e. all the time segments as a single problem or each time segment as an individual problem).
- the size of the sub-problems may still be too large even with time decomposition.
- other forms of decomposition, e.g., physical decomposition, are difficult to implement at the synthesis / design level.
- it is likely that a large number of combinations of the synthesis / design variables $\vec{X}$ when used in the low-level problem(s) (to find the optimum $\vec{Y}_t$) will not lead to feasible solutions.

Other than the third disadvantage above, all of these drawbacks are alleviated somewhat by the fact that both approaches are easily parallelized in various ways. Thus, for example, multiple processors may simultaneously handle different combinations of the synthesis / design variables along with the optimizations with respect to the operational variables. Another possibility is to have multiple processors execute the optimizations at different time segments as shown in Figure 2.2b.

To get around the disadvantages listed above and in particular the third one, the type of time decomposition that is proposed and used here is depicted in Figure 2.3. The approach, which is not based on a nested scheme, consists of selecting one time segment, say segment δ, which has the most demanding[3] load requirements and/or environmental conditions[4], as the synthesis / design point[5]. The system is then synthesized / designed for this point by solving the restricted problem:

$$\text{Minimize } f_\delta = \left[\left(\sum_{i=1}^{m} \dot{f}_i\right)\cdot \Delta t\right]_\delta \tag{2.8}$$

$$\text{w.r.t. } \vec{X}^T = \{\vec{x}_1, \vec{x}_2, \cdots, \vec{x}_m\} \quad \vec{Y}^T = \{\vec{Y}_\delta\}^T = \{\vec{y}_{1\delta}, \vec{y}_{2\delta}, \cdots, \vec{y}_{m\delta}\}$$

[3] The most demanding segment could be the one that uses the greatest amount of external resources and/or poses the greatest challenges in terms of meeting the system analyzer equations including the external demand for the system's products.

[4] Actually, more than one segment could be chosen especially if a priori it were not clear which segment is the most demanding or if two or more segments are relatively close in significance. Of course, each additional segment complicates the process and too many defeats the purpose of this type of time decomposition all together.

[5] A single reference condition is normally called the synthesis / design point. In this context, such a designation is somewhat misleading since one is trying to obtain the synthesis / design that minimizes the cost over the entire load / environmental profile.

Subject to

$$\vec{H}_\delta = \begin{Bmatrix} \vec{h}_{1\delta} \\ \vdots \\ \vec{h}_{m\delta} \end{Bmatrix} = 0 \ , \ \text{and} \quad \vec{G}_\delta = \begin{Bmatrix} \vec{g}_{1\delta} \\ \vdots \\ \vec{g}_{m\delta} \end{Bmatrix} \le \vec{0} \tag{2.8.1}$$

where Δt is the length of time considered for time segment δ and m the number of units in the system. The subscript δ refers to the segment chosen for the "synthesis / design" of the system.

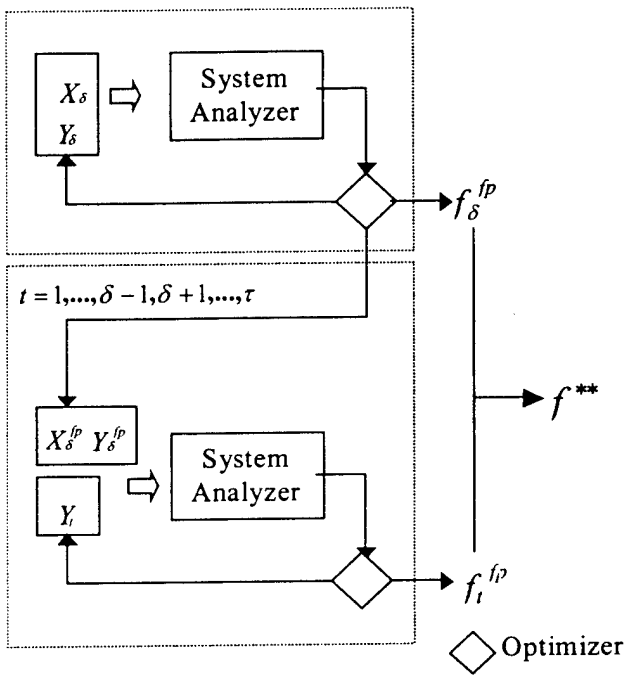

Figure 2.3. Synthesis/Design and Off-design time decomposition scheme.

The result obtained from solving equation (2.8) for a single synthesis / design is a set of feasible solutions[6] (one optimal with respect to equation (2.8) and the others near-optimal) that satisfies the constraints given by equations (2.8.1). These solutions have a corresponding set of vectors $\vec{X}_\delta$ and $\vec{Y}_\delta$. The most promising of these feasible solutions (indicated in Figure 2.3 for each feasible solution having decision variables $\vec{X}_\delta^{fp}$ and $\vec{Y}_\delta^{fp}$ and corresponding objective function value f_δ^{fp}) are then used to minimize the total cost over the entire load/environmental profile for each of these feasible solutions, i.e.

[6] This presupposes a means for generating these feasible solutions, which can be done with a heuristic approach such as a genetic algorithm or conventional gradient-based method.

$$\text{Minimize } f = \left[\left(\sum_{i=1}^{m} \dot{f}_i\right)\cdot \Delta t\right]_{\delta}^{fp} + \sum_{t=1}^{\tau-1}\left(\sum_{i=1}^{m} \dot{f}_i\right)\Delta t_t \tag{2.9}$$

$$\text{w.r.t.} \quad \vec{Y}^T = \left\{\vec{Y}_t\right\}^T = \left\{\vec{y}_{1t}, \vec{y}_{2t}, \cdots, \vec{y}_{mt}\right\} \qquad t = 1,...,\delta-1,\delta+1,...,\tau \tag{2.9.1}$$

subject to

$$\vec{H} = \left\{\vec{H}_t\right\} = \begin{Bmatrix} \vec{h}_{1t} \\ \vdots \\ \vec{h}_{mt} \end{Bmatrix} = \vec{0} \qquad t = 1,...,\delta-1,\delta+1,...,\tau \tag{2.9.2}$$

$$\vec{\Gamma} = \left\{\vec{G}_t\right\} = \begin{Bmatrix} \vec{g}_{1t} \\ \vdots \\ \vec{g}_{mt} \end{Bmatrix} \le \vec{0} \qquad t = 1,...,\delta-1,\delta+1,...,\tau$$

$$\text{and} \quad \vec{X} - \vec{X}_{\delta}^{fp} = \vec{0} \tag{2.9.3}$$

This type of decomposition uses the implicit assumption that only a relatively few number of sets of values of synthesis / design variables $\vec{X}$ are likely to lead to an optimum solution when the entire load profile is included. The first term on the right of equation (2.9) is known from solutions to equation (2.8). It is furthermore assumed that the best solution(s) for the reference (synthesis / design) point used with equation (2.8) is not necessarily the best when integrated over the various off-design conditions. To this end, as indicated by constraint (2.9.3), the values of the synthesis / design variables are set equal to the various synthesis / design variable values associated with the promising feasible solutions obtained from solving problem (2.8).

This type of time decomposition effectively transforms a problem with $d+o\tau$ variables into two problems (one of synthesis / design and the other of operation), the latter of which can be divided further into τ-1 problems since one can define τ-1 off-design optimization problems (implemented in parallel) with respect to the instantaneous operational decision variables ($\vec{Y}$). The synthesis / design problem will, thus, have $d+o$ decision variables while each of the operational or off-design problems will have o decision variables. The reduced number of variables for the decomposed problem, however, comes at the expense of possibly having to carry out the optimization problem given by problem (2.9) for several possible feasible (but promising) solutions found by solving the reduced problem given by problem (2.8). An obvious advantage over the nested time decomposition schemes described earlier (Figure 2.2) is that no time is spent on solutions that i) are infeasible or ii) do not meet the most stringent demand and operating conditions.

The solution of the synthesis / design problem (2.8) may be problematic, however, if the number of variables $d+o$ is still very large. In this case, time decomposition reduces the number of variables for each decomposed operational problem but does not completely facilitate the solution of the overall problem. Thus, an additional decomposition is necessary.

2.2 Physical (Unit) Decomposition

Physical decomposition relies on the premise that systems in general and energy systems in particular can be divided into components or sub-systems with clearly defined coupling functions which in energy systems, for example, can be considered as products, resources, or feedback functions. Under certain conditions, the resulting units could then be optimized independently while maintaining the resource and cost flow connections (couplings functions) between them. The resulting set of decomposed problems would, as with time decomposition, have a much smaller size than the overall problem making it possible to take into account a large number of variables. Depending on the size of the problem (number of units, number of inputs/outputs of each unit, number and nature of the independent variables), the two approaches presented in Muñoz (2000) and Muñoz and von Spakovsky (2000a, b, c; 2001a, b) can be used for solving the overall problem using physical decomposition. The first is Local-Global Optimization (LGO) and the second Iterative Local-Global Optimization (ILGO) applied to energy systems. The latter approach in particular use certain desirable properties of the shadow prices (a type of marginal costs) associated with the resource and cost flow couplings between units to facilitate the optimization and the convergence of the process. In order to apply either of these methods, let us consider the three-unit energy system of Figure 2.4. Three is considered a small enough number to understand the features of the methods yet large enough to reveal patterns and facilitate the use of compact mathematics.

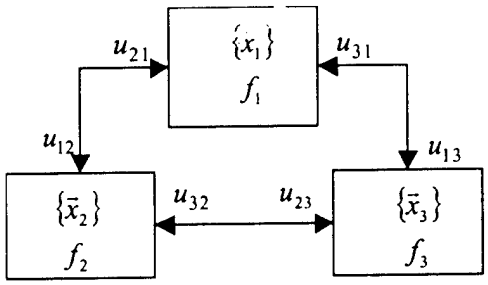

Figure 2.4. A highly coupled three-unit energy system.

The synthesis / design problem for this system is to

$$\text{Minimize } f = \sum_{t=1}^{\tau}\left[\begin{array}{c}\dot{f}_1\left(\vec{x}_1, \vec{y}_{1_t}, \left(u_{21}, u_{31}, u_{12}, u_{13}\right)_t\right)\Delta t_t + \dot{f}_2\left(\vec{x}_2, \vec{y}_{3_t}, \left(u_{12}, u_{32}, u_{21}, u_{23}\right)_t\right)\Delta t_t \\ + \dot{f}_3\left(\vec{x}_3, \vec{y}_{3_t}, \left(u_{13}, u_{23}, u_{31}, u_{32}\right)_t\right)\Delta t_t\end{array}\right] \quad (2.10)$$

w.r.t. $\vec{X}^T = \{\vec{x}_1, \vec{x}_2, \vec{x}_3\}$ $\vec{Y}^T = \{\vec{Y}_t\}^T = \{\vec{y}_{1t}, \vec{y}_{2t}, \vec{y}_{3t}\}$ $t = 1,...,\delta,...,\tau$

subject to the primary constraints

$$\vec{H} = \{\vec{H}_t\} = \begin{Bmatrix} \vec{h}_{1t} \\ \vec{h}_{2t} \\ \vec{h}_{3t} \end{Bmatrix} = \vec{0} \qquad t = 1,...,\delta,...,\tau$$

$$\vec{\Gamma} = \{\vec{G}_t\} = \begin{Bmatrix} \vec{g}_{1t} \\ \vec{g}_{2t} \\ \vec{g}_{3t} \end{Bmatrix} \leq \vec{0} \qquad t = 1,...,\delta,...,\tau \tag{2.10.1}$$

2.3 Local-Global Optimization (LGO) Applied to Energy Systems

In order to apply the LGO approach to the synthesis / design optimization of the energy system of Figure 2.4, it is assumed that each coupling functions u_i i.e. an intermediate product, feedbacks, is kept at a constant value ξ_{ij} at each instant of time, i.e.

$$\{u_{ij}\}_t = \{\xi_{ij}\}_t \qquad t = 1,...,\delta,...,\tau \tag{2.11}$$

Given the functional relationships for the coupling functions given by equations (2.5), it is clear that decision variable vectors $\vec{x}_i$ and $\vec{y}_i$ are strictly local and that the u_{ij} are the only link between unit i and the rest of the system. The fact that the u_{ij} (at the unit level) are kept fixed allows one to define a local optimization problem for unit 1 and a different one for units 2 and 3 combined or two different ones for units 2 and 3 as separate entities[7]. For example, as mentioned above, the following local (unit-level) synthesis / design problem for unit 1 could be defined:

$$\text{Minimize } f_1 = \sum_{t=1}^{\tau} f_1\left(\vec{x}_1, \vec{y}_{1t}, \left(\xi_{21}, \xi_{31}, \xi_{12}, \xi_{13}\right)_t\right) \Delta t_t \tag{2.12}$$

w.r.t. $\vec{x}_1$, $\vec{y}_{1t}$ $\qquad t = 1,...,\delta,...,\tau$

subject to

$$\vec{h}_{1t} = \vec{0} \qquad t = 1,...,\delta,...,\tau \tag{2.12.1}$$

$$\vec{g}_{1t} \leq \vec{0} \qquad t = 1,...,\delta,...,\tau \tag{2.12.2}$$

---

[7] Further decompositions of each of the units are also possible.

The requirement imposed by equation (2.11) on the values for the coupling functions may be overly restrictive, particularly if the values of the coupling functions at different instants are dependent on each other. In such cases, it is advisable to use the time decomposition scheme proposed above and solve the problem in two sequential steps. In the first step, problem (2.12) and the corresponding ones for units 2 and 3 are solved at one load/environmental condition, δ, judged to be the most critical so that it becomes the synthesis / design condition. The most promising solutions from these problems are then used to minimize the sum of the local (unit-level) rate forms of the objective functions at all the other (off-design) conditions.

The solutions obtained from solving problem (2.12) and similar problems defined for units 2 and 3 are the restricted local (unit-based) optimum cost rates at different times $\{\dot{f}_{i\,t}^{\bullet}\}$ and their corresponding restricted total values $f_i^{\bullet}$ as well as the optimum operational decision variables at all instants of time $\{\vec{y}_{i\,t}^{\bullet}\}$ and the optimum synthesis / design variables $\vec{x}_i^{\bullet}$. The sum of the restricted optimum values for the unit-level objective functions along with their corresponding coupling function values constitute a point on the system-level Optimum Response Surface (ORS) for the overall problem. The entire system-level ORS can then be created by varying the values of ξ_{ij} within specified ranges and solving the local (unit-level) problems for those values.

In addition to the unit-level sub-problems, the system-level problem is to

$$\text{Minimize } f = \sum_{t=1}^{\tau}\left(\dot{f}_1^{\bullet} + \dot{f}_2^{\bullet} + \dot{f}_3^{\bullet}\right)\Delta t_t \tag{2.13}$$

w.r.t. $\xi_{ij_t} \qquad t = 1,\ldots,\delta,\ldots,\tau$

subject to

$$\vec{H}_t = \begin{bmatrix} \xi_{ij} - \xi_{ij\,\max} \\ -\xi_{ij} + \xi_{ij\,\min} \end{bmatrix}_t \le \vec{0} \qquad t = 1,\ldots,\delta,\ldots,\tau \tag{2.13.1}$$

The local (unit-level) optimizations (e.g., problem (2.12)) can be performed at the time the system-level problem is solved (Real Time LGO (RT-LGO) approach). A second alternative is to store the results from the sub-problems and use them later in the system-level optimizer (Off-line LGO (OL-LGO) approach). In both cases, the optimum results for the unit syntheses / designs form the system-level ORS for the system.

It should be pointed out that the coupling function u_{ij} going from unit i to unit j may in fact be a vector of multiple products (e.g., electricity, steam, compressed air). It is clear then that a multi-unit, multi-product system may require a very large number of optimization runs (i.e. problems such as problem (2.12) would need to be solved innumerable times for many different combinations of the elements of the vectors u_{ij}). The potential problem caused by the large amount of computational and analysis time, which would be involved, is exacerbated by two facts:

- Each unit may need to be optimized using time decomposition (as described above).
- The synthesis / design problem in its entirety requires the use of binary, discrete, and continuous variables. The optimization algorithms needed to deal with the resulting mixed-integer, non-linear programming (MINLP) problems are usually of the artificial intelligence type (e.g., genetic algorithm and simulated annealing). Although these algorithms are effective when properly developed and conditioned, they impose a serious computational burden on finding the solution.

Thus, the application of the LGO approach for complex highly integrated, highly dynamic energy system synthesis / design may require a large number of optimizations to create the system-level optimum response surface. The amount of computational time required to do this may simply be impractical. A possible solution to these difficulties is the use of the ILGO approach mentioned at the beginning of section 2..2.

2.4 Iterative Local-Global Optimization (ILGO) Applied to Energy Systems

The ILGO approach uses the shadow prices associated with the coupling functions to guide the selection of values for the coupling functions that makes the system-level cost lower than that of some reference solution. Versions A and B of ILGO start with finding an arbitrary initial point on the system-level optimum response surface. This initial or reference solution is obtained by setting $u_{ij_t} = \xi^o_{ij_t}$ and solving a set of unit-level problems, which for unit 1 take the form

$$\text{Minimize } f_1 = \sum_{t=1}^{\tau} \dot{f}_1\left(\vec{x}_1, \vec{y}_{1_t}, \left(\xi^o_{21}, \xi^o_{31}, \xi^o_{12}, \xi^o_{13}\right)_t\right) \cdot \Delta t_t \tag{2.14}$$

$$\text{w.r.t. } \vec{x}_1,\ \vec{y}_{1_t} \qquad t = 1,\ldots,\delta,\ldots,\tau$$

subject to

$$\vec{h}_{1_t} = \vec{0} \qquad t = 1,\ldots,\delta,\ldots,\tau \tag{2.14.1}$$

$$\vec{g}_{1_t} \le \vec{0} \qquad t = 1,\ldots,\delta,\ldots,\tau \tag{2.14.2}$$

As before, time decomposition may be needed to solve the above problem. The solutions to the unit-level sub-problems are the restricted local (unit-level) optimum cost rates at different times $\left(\dot{f}_i^*\right)^o_t$ and their corresponding restricted total values $\left(f_i^*\right)^o$ as well as the optimum operational decision variables at various instants in time $\left(\vec{y}^*_{i_t}\right)^o$ and the optimum synthesis / design variables $\left(\vec{x}_i^*\right)^o$ at the initial or reference point.

The initial value selection for the coupling functions can be made by different means. For example a largely simplified model of the system can be used to find a near optimum solution, which could then be used as the ORS reference point. Another possibility is to use any of the analysis techniques described in previous chapters to find the coupling functions that cause the system to have a high Second Law efficiency, for example.

One of the most appealing features of ILGO is its ability to provide the information necessary to improve an existing synthesis / design. In fact, in engineering practice, the word optimization is often used not to indicate the search for an absolute global optimum but rather to find a solution which is *better* than some existing system. Any of the versions of ILGO excels at this task since one could use the existing synthesis / design (which is assumed to be "optimized") as the reference condition and start the iterative process from there.

Once a suitable initial or reference point on the system-level ORS is found, a Taylor series expansion is performed about that point. After taking the linear terms, the local (unit-level) cost rate at an instant t can then be written for unit 1 as

$$\dot{f}_{1_t} = (\dot{f}_1^\bullet)_t^o + \left(\frac{\partial \dot{f}_1^\bullet}{\partial u_{12}}\right)_t^o \Delta u_{12_t} + \left(\frac{\partial \dot{f}_1^\bullet}{\partial u_{13}}\right)_t^o \Delta u_{13_t} + \left(\frac{\partial \dot{f}_1^\bullet}{\partial u_{21}}\right)_t^o \Delta u_{21_t} + \left(\frac{\partial \dot{f}_1^\bullet}{\partial u_{31}}\right)_t^o \Delta u_{31_t} \qquad (2.15)$$

The partial derivatives above are by definition the shadow prices (type of marginal costs) of the coupling functions. Similar quantities, which have been defined in the past (e.g. von Spakovsky and Evans, 1993) form the basis of the calculus methods of thermoeconomics such as Thermoeconomic Functional Analysis (Frangopoulos, 1984, 1994), Engineering Functional Analysis (von Spakovsky and Evans, 1993; Evans and von Spakovsky, 1993; von Spakovsky, 1994) and the approach of El-Sayed (1989, 1996). The shadow prices used here are more general in that they are defined for arbitrary coupling functions, whether energy-based, exergy-based or not. Furthermore, the shadow prices in equation (2.15) are instantaneous and, thus, are allowed to take substantially different values at different instants in time.

Using the notation commonly found in the thermoeconomics literature, equation (2.15) is rewritten for units 1, 2, and 3 as

$$\dot{f}_{1_t} = (\dot{f}_1^\bullet)_t^o + \lambda_{12_t}^1 \Delta u_{12_t} + \lambda_{13_t}^1 \Delta u_{13_t} + \lambda_{21_t}^1 \Delta u_{21_t} + \lambda_{31_t}^1 \Delta u_{31_t} \qquad (2.16)$$

$$\dot{f}_{2_t} = (\dot{f}_2^\bullet)_t^o + \lambda_{21_t}^2 \Delta u_{21_t} + \lambda_{23_t}^2 \Delta u_{23_t} + \lambda_{12_t}^2 \Delta u_{12_t} + \lambda_{32_t}^2 \Delta u_{32_t} \qquad (2.17)$$

$$\dot{f}_{3_t} = (\dot{f}_3^\bullet)_t^o + \lambda_{31_t}^3 \Delta u_{31_t} + \lambda_{32_t}^3 \Delta u_{32_t} + \lambda_{13_t}^3 \Delta u_{13_t} + \lambda_{23_t}^3 \Delta u_{23_t} \qquad (2.18)$$

where the marginal costs based on the restricted local (unit-level) optimum cost rate at an instant of time t are defined as

$$\lambda_{ij}^i = \left(\frac{\partial \dot{f}_i^\bullet}{\partial u_{ij}}\right)_t^o \qquad (2.19)$$

Naturally "design" and "off-design" marginal costs are defined. The former are those with $t = \delta$ and the latter those with $t \neq \delta$.

The equations presented above contain a wealth of information that can be exploited for the purpose of improving the initial or reference synthesis / design. They provide a means of moving in the optimum system cost vs. coupling functions (intermediate products/feedbacks) space, i.e. on the system-level optimum response surface.

The first feature of these equations is that they show the trade-off between the costs that are purely local and those, which are affected by synthesis / design and operational considerations in the rest of the system. The comparative magnitude of the λ's will indicate whether a decrease in intermediate coupling functions coming from unit i and the (likely) resulting increase in local cost of unit j will reduce the system-level cost. These shadow prices will, provided that they are not identically equal to zero[8], suggest synthesis / design changes that will make the system as a whole better from the standpoint of the cost objective. Thus, for example, negative shadow prices will point towards the need for higher values for the coupling functions (e.g., more intermediate products/feedbacks) and vice versa. Therefore, the optimizer would tend to favor syntheses / designs with greater values of the coupling functions with associated lower shadow prices.

In addition, the off-design shadow prices become a measure of how important the entire load/environmental profile is when compared to the most critical point in the load/environmental profile, i.e. the synthesis / design point. The shadow prices will help pinpoint syntheses / designs that may have a relatively poor performance at the design point but may perform better than the best solution at the design point when combined with all of the off-design conditions.

The step that follows the calculation of the shadow prices is problem dependent. In both versions of ILGO (A and B), the shadow prices indicate the changes in the coupling functions that need to be made in order to improve the reference solution. In ILGO-A, a new set of values for the coupling functions is chosen according to the descent algorithm

$$\left(\xi^{o}_{ij\,t}\right)_{new} = \left(\xi^{o}_{ij\,t}\right)_{old} - \alpha_o \left(\frac{\partial \dot{f}^{\bullet}_{m\,t}}{\partial u_{ij}}\right)^{o} = \left(\xi^{o}_{ij\,t}\right)_{old} - \alpha_o \lambda^{m}_{ij\,t} \tag{2.21}$$

where the shadow prices used in the above equation is such that the greatest improvement in the overall objective function is achieved. The step size is chosen to ensure the descent properties of the algorithm.

The importance of equation (2.21) is that it shows the required changes in the coupling functions at all time steps so that both synthesis / design and operational variables can be adjusted accordingly. It may be necessary, particularly for large problems, to perform the changes sequentially by using time decomposition. Using ILGO-A, for example, a new set of values for the coupling functions at the synthesis / design point, i.e. $\left(\xi^{o}_{ij\,\delta}\right)_{new}$, can be chosen according to (2.21). An improved solution at the synthesis / design point can be found by solving the decomposed local (or unit-level) optimization problems.

[8] This would indicate that the reference point is in fact already the optimum for the objective consistent with the optimum for the system as a whole.

The resulting set of most feasible solutions are then fed into the off-design problems to find the optimum operational variables. It is apparent that an implicit assumption in the use of ILGO-A is that there is enough confidence that an optimum solution can be obtained for the new values of the coupling functions $\left(\xi^{o}_{ij\,t}\right)_{new}$, which may require some prior knowledge about the system's behavior. If this assumption does not hold, ILGO-B instead of ILGO-A must be applied.

In the second version of the ILGO approach, i.e. ILGO-B, the coupling functions are allowed to fluctuate within limits to preserve the validity of the Taylor series expansion (as opposed to forcing them to take fixed values $\left(\xi^{o}_{ij\,t}\right)_{new}$). ILGO-B improves upon the initial solution by solving a set of unit-based system-level sub-problems, which for unit 1 takes the form[9].

Minimize

$$f^{(1)} = \sum_{t=1}^{\tau} \begin{pmatrix} \left(\dot{f}_1^*\right)_t^0 + \lambda^1_{12_t}\Delta u^{(1)}_{12\,t} + \lambda^1_{13_t}\Delta u^{(1)}_{12\,t} + \lambda^1_{21_t}\Delta u^{(1)}_{21\,t} + \lambda^1_{31_t}\Delta u^{(1)}_{31\,t} \\ \dot{f}_2^* + \dot{f}_3^* + \lambda^2_{12_t}\Delta u^{(1)}_{12\,t} + \lambda^3_{13_t}\Delta u^{(1)}_{12\,t} + \lambda^2_{21_t}\Delta u^{(1)}_{21\,t} + \lambda^3_{31_t}\Delta u^{(1)}_{31\,t} \end{pmatrix} \Delta t_t \qquad (2.22)$$

or

Minimize

$$f^{(1)} = \sum_{t=1}^{\tau} \left(\dot{f}_1 + \dot{f}_2^* + \dot{f}_3^* + \lambda^2_{12_t}\Delta u^{(1)}_{12\,t} + \lambda^3_{13_t}\Delta u^{(1)}_{12\,t} + \lambda^2_{21_t}\Delta u^{(1)}_{21\,t} + \lambda^3_{31_t}\Delta u^{(1)}_{31\,t} \right) \Delta t_t \qquad (2.22.1)$$

w.r.t. $\vec{x}_1, \vec{y}_{1_t} \qquad t = 1,\ldots,\delta,\ldots,\tau$

subject to

$$\vec{h}_{1_t} = \vec{0} \qquad t = 1,\ldots,\delta,\ldots,\tau \qquad (2.22.2)$$

$$\vec{g}_{1_t} \le \vec{0} \qquad t = 1,\ldots,\delta,\ldots,\tau \qquad (2.22.3)$$

where for example

$$\Delta u^{(1)}_{12\,t} = \nabla_{x_1}\left(u_{12_t}\right)^T \Delta\vec{x}_1 + \nabla_{y_1}\left(u_{12_t}\right)^T \Delta\vec{y}_{1_t} \qquad (2.23)$$

In general the effect of the decision variables on the coupling functions is given by

$$\Delta u^{(i)}_{ij\,t} = \nabla_{x_i}\left(u_{ij_t}\right)^T \Delta\vec{x}_i + \nabla_{y_i}\left(u_{ij_t}\right)^T \Delta\vec{y}_{i_t} \qquad (2.24)$$

In addition to the above constraints, the additional constraints

---

[9] Note that for convenience the subscript t and the superscript o have been dropped from the functions $\dot{f}_i$ and $\dot{f}_i^*$ in equations (2.22) and (2.22.1)

$$\Delta u_{ij_t} - \varepsilon \, \Delta u_{ij_{t\max}} \leq 0 \tag{2.25}$$

are imposed upon the problem. In expression (2.25), the $\Delta u_{ij_{t\max}}$ are the maximum allowable values for the coupling functions and the factor ε is added to ensure that the linear Taylor series expansions are a good local representation of the system-level ORS. It is readily seen that one of the advantages of ILGO-B over ILGO-A is that $\vec{x}_1$ *and* $\vec{y}_{1_t}$ may be chosen so that the internal constraints (both the analysis system of equations and the desired unit's products or tasks) are met.

Problem (2.22) represents the minimization of the system-level objective function by varying the local (unit 1) decision variables only. The function to be minimized is composed of the local contribution (in this case f_1) to the overall objective *plus* the impact that the local decision variables ($\vec{x}_1, \vec{y}_{1_t}$) have on the local objectives of the other units (2 and 3). This impact is made via the coupling functions.

2.5 Additional Comments

As discussed above, in energy systems, the coupling functions can be regarded as intermediate products/resources and/or feedbacks going to or coming from the units. Typically these functions can be expressed in terms of thermodynamic or flow variables. In this work, however, non-energy functions are permitted.

As to purely thermodynamic and flow connections between units, the previous discussion allows one to tackle in an informed way the question of what thermodynamic property should be used as the linking or coupling variable between sub-problems (i.e. sub-systems or components) when physical decomposition is used for optimization purposes. Thus, the decomposition optimization methods presented above shed some light on the on-going debate (e.g. Newberry, 2000; Paulus and Gaggioli, 2000; Bejan 2000; Muñoz and von Spakovsky, 2000a,b,c) as to the property of choice for representing energy-based coupling functions. The answer depends on how the system-level objective behaves with respect to the system's coupling functions (i.e. how the system-level ORS behaves) when represented in terms of any of the candidate quantities (e.g., energy, exergy, thrust, negentropy, etc.)[10]. In fact, Gaggioli and El-Sayed, two of the biggest proponents of exergy and Second Law analysis, state in their landmark 1989 article (Gaggioli and El-Sayed, 1989) that for optimization, which quantity (ies) is (are) best is an open question and will more than likely depend on the case at hand. Of course, in the past, a number of authors have observed advantages to using exergy as opposed to energy, advantages, which they believed, simplified decomposition and speeded up and possibly even ensured convergence (Frangoupolos and Evans, 1984; Frangopoulos, 1984; Gaggioli and El-Sayed, 1989; von Spakovsky and Evans, 1993; Evans and von Spakovsky, 1993; El-Sayed, 1989, 1996).

[10] This has direct bearing on the associated shadow prices and their behavior.

These results cannot be directly compared to those for the ILGO approach presented here since they were obtained with the Evans and El-Sayed formalism or one of its derivatives. However, with respect to ILGO, exergy as the basis for the coupling functions between unit sub-problems is only justified[11] on the basis of how, as stated above, the system-level cost function behaves with respect to the system's coupling functions and, thus, aids in decomposition and, in turn, in the optimization of the system as a whole.

In certain cases, it will be the quantity of choice. In others, as has been shown (Muñoz and von Spakovsky, 1999, 2000a; Frangopoulos, 1994; von Spakovsky, 1994), energy or some other quantity (e.g., thrust, negentropy, etc.) may work very well and be a better choice for any number of practical reasons.

Based on recent and past work by Muñoz and von Spakovsky (1999; 2000a,b,c) and by others, the conditions sufficient for the successful application of ILGO as a decomposition technique for optimizing complex systems are:

- that the system-level ORS be smoothly convex (or concave) with respect to the coupling functions; this will ensure that the ILGO approach leads to the global optimum;

- that ideally the system-level objective be linear or nearly so with respect to these coupling functions; this will increase the convergence speed of the algorithm; obviously since the system-level objective may, for example, the sum of resources (usually fuel) and capital, there is always the alternative of manipulating the latter to make this objective linear or piecewise linear, a technique which has been used by a number of researchers (e.g., Frangopoulos, 1984, von Spakovsky, 1986). A linear objective with respect to the coupling functions would produce a hyper-plane and the optimum solution would be expected to be at or close to one of the corners of that plane.

Finally, some additional observations as to the best choice of thermodynamic quantities for describing the coupling functions of a system can be made:

- Consider a single unit that uses a single resource R_I to produce a single product P_I. The synthesis / design optimization will find the optimum vector of decision variables $\vec{x}_1^*$ and $\vec{y}_1^*$ that minimize the sum $k_1 R_1 + Z_1$ for a given value of P_I. Typically, if the quantity or quality of product P_I increases, the best design will tend to have a higher value for the total cost function than that of a synthesis / design with a lower required P_I. This is valid regardless of the choice of thermodynamic property used to describe the product. The implication is that overall (total) cost functions have the tendency to be *monotonic* with respect to their pro-

[11] Of course, using exergy may add information which otherwise would not be there and could eventually aid in an interpretation of the optimization results. The argument made here, however, is simply that exergy is not necessarily required in order to obtain these results using decomposition.

ducts. This type of behavior will favor the convexity of the cost function, i.e. of the system-level objective[12]. Problems arise, however, when the need to have a larger product forces changes in the technology being employed. In this case the tendency may be inverted and even make the total cost function discontinuous. This obviously can occur when the overall optimization problem uses a discrete variable that represents various possible types of units (a vapor compression cycle vs. an absorption cycle, for example). Note, however, that discrete variables present in the local (unit-level) optimization problem (e.g., representing different types of material for a given component) do not pose this problem.

- Exergy has the important mathematical characteristic of combining temperature, pressure, chemical composition, velocity, mass flow rate, etc. in a single function. This conceptually poses an advantage for the calculation of the shadow prices. A fair amount of work has been devoted to the study of exergy-based shadow prices in stationary applications (Serra, 1994; Frangopoulos, 1994; von Spakovsky, 1994; Lazzaretto and Andreatto, 1995; etc.). However, there are practical difficulties for calculating them when models of real systems are used. For example, take the case of the design of a gas turbine, which in addition to shaft work produces compressed air for a process. The air is to be taken, say, from the last compressor stage. It is much easier to design the system for a given value of the air mass flow rate to be taken from the compressor than for a given exergy value. This is because the pressure and temperature of the air depend on a number of factors that are not easily controllable, including, among others, the position of the design point on the gas turbine maps, the maximum allowable temperature in the combustor, the technology used and some stability considerations.

- There is a need to remain open-minded to the possibility of using shadow prices based on commodities other than exergy or energy[13]. In some applications, the use of non-energy values may be necessary. For example, size (volume and mass) and thrust (force) are critical factors in aircraft design. Although some authors (Frangopoulos and von Spakovsky, 1993; von Spakovsky and Frangopoulos, 1994; Sciubba, 1999) may argue that one could relate exergy to a unit's mass via the manufacturing process, that option is replete with difficulties and pitfalls (Curti, von Spakovsky, Favrat., 2000a,b) and will simply not be considered here.

---

[12] Of course, the system-level objective might not be cost but gross takeoff weight instead. However, this objective has the same tendencies since weight translates directly into fuel, which in turn translates directly into cost. Nonetheless, objectives are possible which do not have these tendencies.

[13] Other functions have been proposed and used in the past. For example, Valero et al. (1993) proposed the use of the relative free energy.

CHAPTER 3

3. SYSTEM SYNTHESIS / DESIGN OPTIMIZATION

The synthesis / design task at hand is to perform the integrated optimization of four sub-systems, which are part of an advanced military aircraft. The problem is to carry out the conceptual design of a low-bypass turbofan engine with afterburning (Propulsion Sub-system - PS), the full synthesis / design optimization of an air-cycle Environmental Control Sub-system (ECS) and a Thermal Management Sub-system (TMS), and the design optimization of a Structural Sub-system (SS). Note that the TMS is actually comprise of two subsystems: a vapor compression / PAO sub-system and a fuel loop sub-system.

The PS provides the necessary thrust, while the SS provides the necessary lift for the vehicle to carry out the desired mission. The mission[1] is the set of conditions under which the aircraft must be synthesized / designed. Here, the mission defined by the Request for Proposal for an Air-to-Air Fighter (AAF) given by Mattingly et al. (1987) is used. The mission has 14 different phases or legs. A general description of the mission is given in Figure 3.1. and Tables 3.1 & 3.2. In addition to providing the required rates of climb and acceleration and overcoming the aircraft's drag, the PS must provide the power required to operate all the remaining sub-systems.

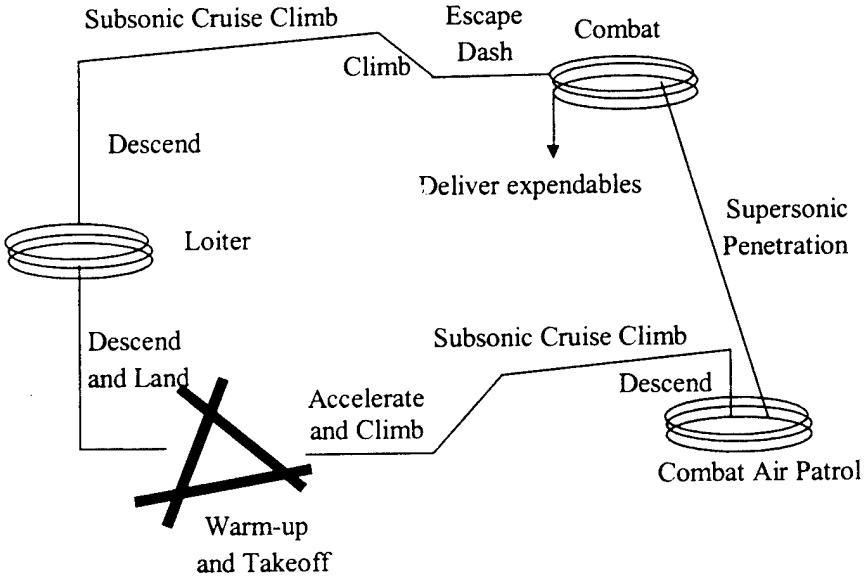

Figure 3.1. Mission profile by phase or leg (Mattingly et. al., 1987).

[1] The mission is equivalent to the load profile and set of environmental conditions in a stationary application.

Table 3.1. Mission Specifications.

Phase	Description
1	Warm-up and take-off, field is at 600 m pressure altitude with T=310 K. Fuel allowance is 5 min at idle power for taxi and 1 min at military power for warm-up. Take-off roll plus rotation must be $\leq$ 450 m on surface with a friction coefficient = 0.05. $V_{TO} = 1.2V_{STALL}$
2	Accelerate to climb speed and perform a minimum time climb in military power to best cruise mach number and best cruise altitude conditions (BCM/BCA)
3	Subsonic Cruise Climb at BCM/BCA until total range for climb and cruise climb is 280 km
4	Descend to 9150 m
5	Perform combat air patrol loiter for 20 min at 9150 m and a Mach number for best endurance.
6	Supersonic penetration at 9150 m and M=1.5. Range=185 km
7	Combat is modeled by the following: • Fire 2 AMRAAM missiles • Perform one 360 deg., 5g sustained turn at 9150 m, M=0.9 • Accelerate from M=0.8 to M=1.6 at 9150 m at max. power • Fire 2 AIM-9Ls and ½ ammo. Conditions at end of combat are M=1.5 at 9150 m
8	Escape dash, at M=1.5 and 9150 m for 46 km.
9	Using military power, do a minimum time climb to BCM/BCA
10	Subsonic cruise climb to BCM/BCA
11	Subsonic cruise climb at BCA/BCM until total range from the end of combat equals 278 km
12	Descend to 3000 m
13	Loiter 20 min at 3000 m and a Mach number for best endurance
14	Descend and land, field is at 600 m pressure altitude with T=310 K. A 2 s free roll plus breaking distance must be $\leq$ 450 m. Runway has a friction coefficient = 0.18. $V_{TD} = 1.15V_{STALL}$

The ECS and TMS provide the cooling necessary for dissipating the heat generated in the aircraft. A set of cooling requirements has been added to the mission according to design specifications given by Muñoz and von Spakovsky (1999). These requirements are shown in Table 3.2. Overall aircraft performance is significantly affected by the thermodynamic performance of on board sub-systems. The major factor affecting the thermodynamic performance of these sub-systems are heat sources. These heat sources can be separated in two categories, internal and external. Internal sources are comprised of avionics, hydraulics, generators, fuel pumps, people, engine, gearbox; etc. External sources include kinetic (friction) and solar.

The most commonly used cooling methods are the ECS and the TMS. Modern aircraft cooling sub-systems face a number of challenges that are produced by higher speed flight conditions and increasing internal heat loads such as those due to avionics and those coming from the propulsion sub-system. Heat is transferred from heat sources to heat sinks outside or within the aircraft. The available heat sinks are ambient air, bleed air, and fuel.

Table 3.2. Performance Requirements / Constraints.

Item	Requirement
Payload	• 2 AMRAAM missiles (148 kg each) • 2 AIM-9L missiles (87 kg each) • 500 rounds of 25 mm ammo (522 fixed weight (cannon, ammo casings, etc), 125 kg spent ammunition)
Max. Mach Number	2.0 @ 12200 m
Acceleration	$0.8 \rightarrow 1.6$ M/9150 m $t \leq 5$ s
Sustained g level	$n \geq 5$ at 0.9 M/9150 m, $n \geq 5$ at 1.6 M/9150 m
Crew	One (90 kg pilot plus equipment)
Fuel	JP-4
Cooling	Requirements as per cooling, temperature and pressure schedules given by Muñoz and von Spakovsky (1999)
Jet Engines	One or two engines. Bleed air flow rate and bleed port depend on ECS design.

3.1 System-level Optimization Problem Definitions

The sub-systems considered her that make up the aircraft as well as their coupling functions are shown in Figure 3.2. As explained above, the interdependence between the four units being synthesized / designed (PS, TMS, ECS and SS) is quite tight. Although the other units, namely the payload sub-systems (EPAYS and PPAYS), are not synthesized / designed, i.e. they do not have decision parameters which are optimized, their role is not strictly passive. Thus, for example, the SS sub-system's optimal design is affected by the optimal synthesis / design decisions made in the PS, ECS and TMS as well as by the mission requirements dictated for the EPAYS and PPAYS. The result is that the aircraft system at hand constitutes the typical case of a system in which "everything influences everything else".

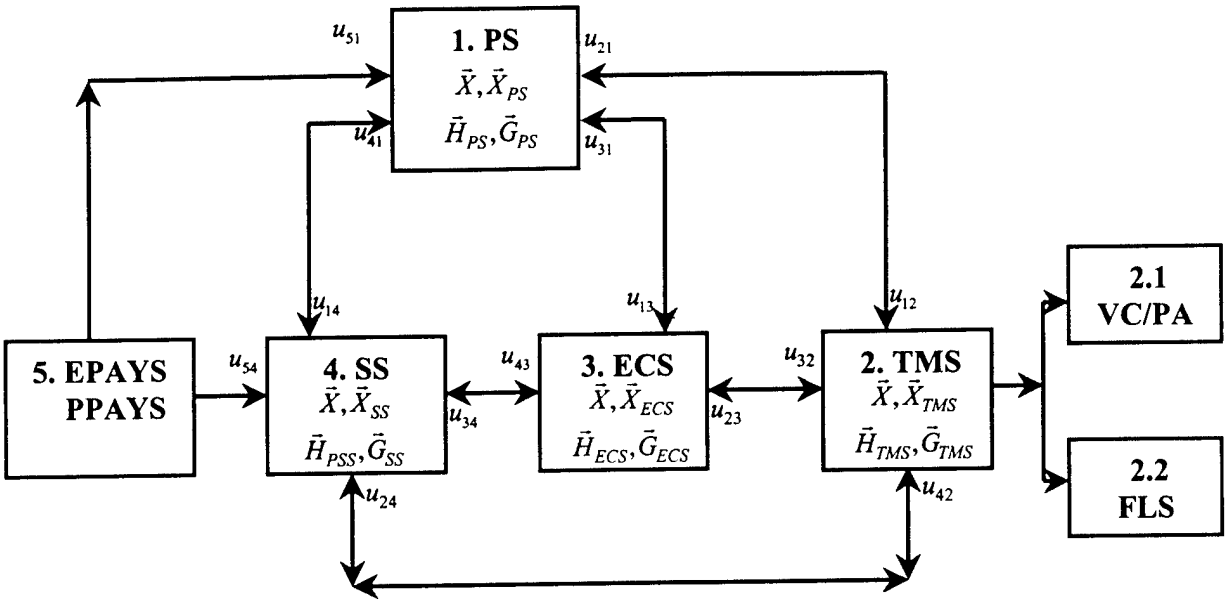

u_{12}	Extracted power
$\vec{u}_{21}$	Ram air momentum drag, ECS weight, power requirement
$\vec{u}_{13}$	Bleed air temperature and pressure
$\vec{u}_{31}$	Ram air momentum drag, ECS weight, bleed air requirement
u_{14}	Weight of the PS
$\vec{u}_{41}$	Drag and lift coefficients at different Mach numbers, weight of the structures
$\vec{u}_{51}$	Weight of the permanent and expendable payload
$\vec{u}_{23}$	Hot PAO temperature and flow, PAO heat exchanger geometry
$\vec{u}_{32}$	Bleed air temperature and flow, ram air inlet conditions
$\vec{u}_{24}$	TMS weight and drag
$\vec{u}_{34}$	ECS weight and drag

Figure 3.2. Sub-systems and sub-system coupling functions.

Thus, determining the optimal synthesis / design of the aircraft system required that the optimal synthesis / design of each of the aircraft sub-systems (e.g. PS, TMS, ECS, and SS[2]) be carried out in an integrated fashion. Individually optimizing each without consideration for their integration as a whole will not lead to the optimum for the system as a whole. The decomposition approach (LGO and ILGO) described in chapter 2 are two means by which each sub-system can be individually optimized consistent with their integration into the overall system.

The latter of these two approaches (i.e. ILGO) is in the process of being applied to the synthesis / design optimization. How the ILGO is applied is discussed in chapter 4, the aircraft system describes in this chapter and, thus, only some preliminary results for this system-wide optimization are presented in chapter 7 of this report. However, we first begin with a description of the overall (system) synthesis / design optimization problem and then complete chapter 3 with description of each of each of the sub-system optimization problems as well as of each sub-system. More detailed description of the PS and ECS can be found in Muñoz (2000) and Muñoz and von Spakovsky (2000a, b ; 2001a,b,c) while those for the TMS and SS are found in chapter 5 and 6 of this report. Respectively.

3.1.1 Gross Take-Off Weight System-Level Optimization Problem Definition[3]

The first system-level optimization problem formulated for the military AAF and mission given in Section 3.1 uses gross take-off weight as figure of merit. Thus, the problem statement is as follow:

$$\text{Minimize} \qquad W_{TO} = W_{SS} + W_{PS} + W_{ECS} + W_{TMS} + W_{FUEL} + W_{PPAY} + W_{EPAY} \tag{3.1}$$

$$\text{w.r.t.} \quad \left\{\vec{X}_{PS}, \vec{Y}_{PS}\right\}, \quad \left\{\vec{X}_{ECS}, \vec{Y}_{ECS}\right\}, \quad \left\{\vec{X}_{TMS}, \vec{Y}_{TMS}\right\}, \quad \left\{\vec{X}_{SS}, \vec{Y}_{SS}\right\}$$

subject to

$$\vec{H}_{PS} = \vec{0}, \quad \vec{G}_{PS} \le \vec{0} \tag{3.2}$$

$$\vec{H}_{ECS} = \vec{0}, \quad \vec{G}_{ECS} \le \vec{0} \tag{3.3}$$

$$\vec{H}_{TMS} = \vec{0}, \quad \vec{G}_{TMS} \le \vec{0} \tag{3.4}$$

$$\text{and } \vec{H}_{SS} = \vec{0}, \quad \vec{G}_{SS} \le \vec{0} \tag{3.5}$$

---

[2] Of course these sub-systems do not comprise all of the aircraft sub-systems but do nonetheless represent a large number of its principal ones.

[3] W_{TO} is a figure of merit commonly used by the aircraft/aerospace community.

where the vectors of equally constraints $\vec{H}$ represent the thermodynamic and physical models (weight and volume) for each of the sub-systems. The vectors of inequality constraints $\vec{G}$ represent the physical limits placed on independent and dependent variables or other physical quantities. Also note that the weight W_{PPAY} and the W_{EPAY} are fixed by the mission and, thus, are not minimized along with the remaining terms in the objective, which consist of the weight of each of the sub-systems plus the weight of the fuel.

It is important to observe that although the minimization of weight is not a thermoeconomic problem, it shares many of its characteristics. For example, the synthesis / design and operation of any given sub-system forces the sub-systems with which it interacts to change their size. In the present problem, that change is reflected in different weights and in a thermoeconomic problem in different costs.

3.1.2 Fuel Consumption System-Level Optimization Problem Definition

The minimization of total fuel consumption is also a problem of great interest. This system-level optimization is defined as

$$\text{Minimize } W_{FUEL} = w_{fuel}(W_{TO}, \vec{X}_{PS}, \vec{Y}_{PS}, \vec{X}_{TMS}, \vec{Y}_{TMS}, \vec{X}_{ECS}, \vec{Y}_{ECS}, \vec{X}_{SS}, \vec{Y}_{SS}, mission) \quad (3.6)$$

$$\text{w.r.t. } \{\vec{X}_{PS}, \vec{Y}_{PS}\} \;,\; \{\vec{X}_{ECS}, \vec{Y}_{ECS}\} \;,\; \{\vec{X}_{TMS}, \vec{Y}_{TMS}\} \;,\; \{\vec{X}_{SS}, \vec{Y}_{SS}\}$$

subject to

$$\vec{H}_{PS} = \vec{0}, \quad \vec{G}_{PS} \le \vec{0} \quad (3.7)$$

$$\vec{H}_{ECS} = \vec{0}, \quad \vec{G}_{ECS} \le \vec{0} \quad (3.8)$$

$$\vec{H}_{TMS} = \vec{0}, \quad \vec{G}_{TMS} \le \vec{0} \quad (3.9)$$

$$\text{and } \vec{H}_{SS} = \vec{0}, \quad \vec{G}_{SS} \le \vec{0} \quad (3.10)$$

3.1.3 Total Cost System-Level Optimization Problem Definition

Future air vehicles present a unique set of requirements not previously addressed. For example, future Uninhabited Air Vehicles (UAVs) must be substantially more affordable than comparable manned systems both in terms of acquisition and operational costs. Future UAVs will likely be high Mach, high performance vehicles. To permit an integrated approach to their and other aerospace vehicles optimal synthesis and design, it will be necessary to combine into a single comprehensive model thermodynamic as well as cost functions so that a large number of independent variables related to how different technologies optimally accommodate limited

payload spaces can be investigated (Brown, 1999).Thus the system-level optimization problem would be that of minimizing the total cost . It is formulated as follow:

$$\text{Minimize} \quad C_T = C_{SS} + C_{PS} + C_{ECS} + C_{TMS} + C_{FUEL} + C_{PPAYS} + C_{EPAYS} \tag{3.11}$$

$$\text{w.r.t.} \ \{\vec{X}_{PS}, \vec{Y}_{PS}\} \ , \ \{\vec{X}_{ECS}, \vec{Y}_{ECS}\} \ , \ \{\vec{X}_{TMS}, \vec{Y}_{TMS}\} \ , \ \{\vec{X}_{SS}, \vec{Y}_{SS}\}$$

subject to

$$\vec{H}_{PS} = \vec{0}, \quad \vec{G}_{PS} \le \vec{0} \tag{3.12}$$

$$\vec{H}_{ECS} = \vec{0}, \quad \vec{G}_{ECS} \le \vec{0} \tag{3.13}$$

$$\vec{H}_{TMS} = \vec{0}, \quad \vec{G}_{TMS} \le \vec{0} \tag{3.14}$$

$$\text{and} \ \vec{H}_{SS} = \vec{0}, \quad \vec{G}_{SS} \le \vec{0} \tag{3.15}$$

Noted that both the C_{PPAYS} and C_{EPAYS} are fixed cost and are thus not minimized along with the rest of the objective, which consists of the total cost of each sub-system and its associated fuel cost penalties.

Having stated three likely system –level optimization problems, we now turn to those for each sub-system, describing them in terms of total cost only since the analogs for weight and fuel follow straight forwardly from those for cost.

3.2 Structural Sub-system (SS) Design Unit-level Optimization Problem

3.2.1 General Description of the SS

The relationship between the different sub-systems that make up an aircraft is very complex. Before attempting to understand all of the factors involved in the problem, consider an aircraft system such as the one shown in Figure 3.3. An energy balance on the aircraft leads to the following expression:

$$\{T - (D + R)\} V = W \frac{dh}{dt} + W \frac{d}{dt}\left\{\frac{V^2}{2g}\right\} \tag{3.16}$$

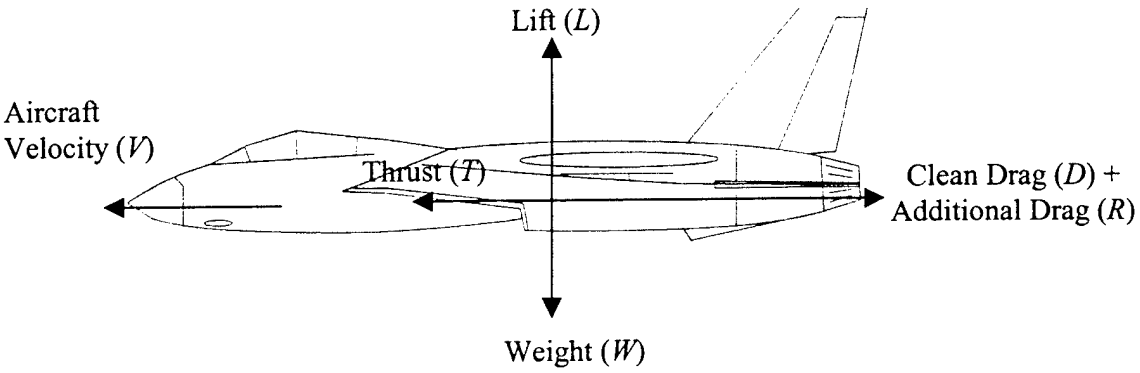

Figure 3.3. Force balance on an aircraft.

The term on the left-hand-side of equation (3.16) is the net rate of mechanical energy input. The first and second terms on the right-hand-side represent the storage of potential and kinetic energy, respectively. Here the traditional aircraft lift and drag relationships.

$$L = nW = qC_L S \tag{3.17}$$

and $$D = qC_D S \tag{3.18}$$

are used where n is the load factor, which is equal to the number of g's perpendicular to the direction of the velocity. A lift-drag polar relationship of the form (Mattingly et al., 1987)

$$C_D = K_1 C_L^{\,2} + K_2 C_L + C_{D_0} \tag{3.19}$$

is assumed.

Equations (3.16) through (3.19) can be manipulated to produce the thrust equation for the i_{th} mission leg, namely,

$$\frac{T_i}{W_i} = \frac{q_i S}{W_i}\left[K_1\left(\frac{n_i}{q_i}\frac{W_i}{S}\right)^2 + C_{D_0} + \frac{D_{ECS_i} + D_{TMS_i}}{q_i S}\right] + \frac{1}{V_i}\frac{d}{dt}\left(h_i + \frac{V_i^2}{2g}\right) \tag{3.20}$$

where the fact that $K_2 \approx 0$ for high performance aircraft (Mattingly et al. 1987) has been used, and where the drag-polar behavior associated with the coefficient Ki is similar to that of the current military aircraft. The only additional drag, R, which considered is the momentum drag created by the ECS and the TMS (i.e. $R_i = D_{ECS_i} + D_{TMS_i}$).

In equation (3.20), the velocity (Vi) and the rates of climb (dh_i/dt) and acceleration (dV_i/dt) are directly or indirectly given by the mission specifications (Table 3.1). The drag created by the ECS is also leg-dependent as will be discussed below.

An alternative version of equation (3.20) can be given as a function of the thrust at sea level take-off (T_{SL}) and the gross take-off weight (W_{TO}), i.e.

$$T_i = \alpha T_{SL} = q_i S\left[K_1\left(\frac{n_i}{q_i}\frac{\beta_i W_{TO}}{S}\right)^2 + C_{D_0} + \frac{D_{ECS_i} + D_{TMS_i}}{q_i S}\right] + \frac{\beta_i W_{TO}}{V_i}\frac{d}{dt}\left(h_i + \frac{V_i^2}{2g}\right) \quad (3.21)$$

where β_i is the fraction of the take-off weight at leg i and α is the fraction of the sea level take-off thrust. The take-off gross weight is given by

$$W_{TO} = W_{SS} + W_{PS} + W_{ECS} + W_{TMS} + W_{FUEL} + W_{PPAYS} + W_{EPAYS} \quad (3.22)$$

An analysis of the constraints of the RFP will show a functional relationship between the minimum thrust-to-weight ratio or thrust loading at sea-level takeoff (T_{SL}/W_{TO}) and wing loading at take-off (W_{TO}/S). The construction of the resulting constraint diagram is showed in Chapter 6. The following values for the thrust to weight ratio and thrust to wing area were selected according to data from Mattingly et. al.(1987)

$$\frac{T_{SL}}{W_{TO}} = 1.20 \quad (3.23)$$

and

$$\frac{T_{SL}}{S} = 3065 \text{ N/m}^2 \quad (3.24)$$

Equations (3.21) through (3.24) hint at the tight integration issues associated with the synthesis / design of an aircraft. The synthesis / design and operation of any given sub-system is highly influenced by and in turn influences the synthesis / design and operation of all the others. Take the case of the TMS, for example. The TMS's weight and energy and extra thrust requirements affect the required total thrust which leads to higher fuel consumption and higher take-off gross weight. Equation (3.23) clearly shows that an increase in W_{TO} is associated with higher thrust, which in turns affects the size of the PS. The weight of the structures is also affected as indicated by equation (3.24). Thus, one can conclude that, in general, when any sub-system is installed in an aircraft, additional fuel (with the consequent effect on system weight) is required to:

- provide the additional thrust associated with carrying the increased system mass
- overcome any additional drag, which may result from installing the sub-system in the aircraft
- carry the quantity of fuel required for the previous items

- produce the power that some sub-systems may require, power extractions from the PS cause increased fuel consumption and the associated larger weight discussed above.

Now returning equation (3.22), the fuel weight is calculated based on engine performance and mission requirements and depends on the system synthesis / design and mission requirements. The weight of the ECS, the TMS, the SS and the PS result from the sub-system optimization problems. The weight of the structures in particular depends on a number of design considerations such as materials used, aerodynamic performance, durability, strength, and stability among many others. For the case where the weight of the SS is not determined by its sub-optimization problem as will be the case for the preliminary results presented in *Chapter 7* of this report[4], the weight of the structures can be determined from values in agreement with existing design practices. Data given in Muñoz (2000) show the empty weight (structures plus PS plus ECS) for a number of high performance jet aircraft. From this information, it is possible to obtain the weight of the SS for a given value of the take-off weight. Thus, the weight of the SS sub-system is the empty weight minus the engine weight multiplied by a factor, $k_{ecs/tms}$, to reflect the fact that the empty weight also includes the weight of the ECS and TMS. Based on the work of Muñoz and von Spakovsky (1999), $k_{ecs} = 0.975$ and $k_{tms} = 0.97$ are used (i.e. the ECS mass is assumed to be 2.5 % of the structures mass and the TMS is assumed to be 3% of the structure mass).

As to the fuel weight in equation (3.22), it is a complex function of the thermodynamic performance of the engine, the mission requirements, the technology used, and some stability considerations. In general, it is given by

$$W_{FUEL} = g \sum_{mission} \dot{m}_i \Delta t_i = g \sum_{mission} TSFC \cdot T \cdot \Delta t_i \qquad (3.25.a)$$

or

$$W_{FUEL} = w_{fuel}(W_{TO}, \vec{X}_{PS}, \vec{Y}_{PS}, \vec{X}_{TMS}, \vec{Y}_{TMS}, \vec{X}_{ECS}, \vec{Y}_{ECS}, \vec{X}_{SS}, \vec{Y}_{SS}, mission) \qquad (3.21.b)$$

where the rate of fuel consumption has been written in terms of the thrust specific fuel consumption (*TSFC*). Equation (3.21), however, is fairly inconvenient due to the fact that the specifications of each of the mission legs are given in terms of different parameters. As seen in Table 3.1, some of the legs have a specified range, others specified duration, while still others have specific maneuvers to be carried out. In addition, the duration of some of the legs changes as the decision variables are varied. Therefore, it is useful to employ a transformation, which puts all mission segments

---

[4] Note that in the no-cost extension of this project for another 12 months, it is our intention to determine the SS weight from its sub-optimization problem.

under a unified measure. Fuel consumed in each leg written in terms of the weight ratio is such a measure. The ratio of the final to the initial weight for leg i is defined as

$$\pi_i = W_{final} / W_{initial} \tag{3.26}$$

In order to proceed with the calculation of the weight ratios, consider the rate at which aircraft weight diminishes due to the consumption of fuel, namely,

$$\frac{dW}{dt} = -TFSFC \cdot T \tag{3.27}$$

$$\text{or} \quad \frac{dW}{W} = -TSFC \frac{T}{W} dt = -TSFC \frac{T}{W} \frac{dt}{ds} ds = -TSFC \frac{T}{W} \frac{ds}{V} \tag{3.28}$$

Equation (3.28) represents the weight-time and weight-velocity transformation that is used to unify the different requirements of the mission. The integration of equation (3.28) is done by breaking each mission segment into several (typically 5) intervals. The flight and operating conditions for each interval or sub-segment are assumed to be constant at some representative value so that the integration can be accomplished explicitly. It was found that in most cases, five intervals are sufficient to ensure excellent accuracy. The resulting weight ratio relations for different cases are given in Table 6.4. *Chapter 6.* There is a special case, however, which deviates from the above calculations and corresponds to the mission segment where the expendable payload is delivered. If it is assumed that the delivery is done at some point j in the mission then

$$\frac{W_j - W_{EPAYS}}{W_j} = 1 - \frac{W_{EPAYS}}{W_j} \tag{3.29}$$

With equation (3.25) and the weight ratios and after some manipulation, the fuel consumption can be written as

$$W_{FUEL} = W_{TO}(1 - \prod_{i=1}^{n} \pi_i) - W_{EPAYS}(1 - \prod_{i=j} \pi_i) \tag{3.30}$$

where n is the number of legs being considered.

The weight fractions (π_i) depend on the design of the PS and other sub-systems, the thrust required, the afterburner setting, the power requirements of the other sub-systems, ambient conditions, and a number of other factors. These complex set of factors are addressed by means of solving Equation. (3.21) for each leg. A computer code was written to solve the resulting set of equations. The resulting values for thrust for each of the legs is then used with the engine simulation code to estimate the fuel consumed in each of the mission legs.

3.2.2 SS Unit-level Optimization Problem Definition

Now having fairly briefly outlined the general characteristics of the SS performance and weight models (more detailed description is given in *Chapter 6*) and the effects of interactions with other sub-system, we now define on a cost basis the SS unit-level optimization problem in general terms. In order to generate a suitable optimization problem, the energy (fuel) requirements of the SS must be added to the capital costs of the components. The unit-level problem can be written as

$$\text{Minimize} \quad C_{SS} = \int_{time} c_f (\dot{m}_f^w + \dot{m}_f^D + \dot{m}_f^{DL} + \dot{m}_f^f)\, dt + \sum_n C_n^P \tag{3.31}$$

w.r.t. $\{\vec{X}_{SS}, \vec{Y}_{SS}\}$

subject to

$$\vec{H}_{SS} = \vec{0}, \quad \vec{G}_{SS} \le \vec{0} \tag{3.32a}$$

$$C_n^P = C_n^P(\vec{X}_{SS}, \vec{Y}_{SS}) \tag{3.32b}$$

where C_{SS} is the total cost of the SS (first term on the right in Equation (3.11)), c_f is the unit cost of fuel, $\dot{m}_f^w$ is the rate of fuel needed to carry the total weight of the SS, $\dot{m}_f^D$ is the rate of fuel necessary to overcome the drag penalty created by the interaction between the SS and the air, $\dot{m}_f^{DL}$ is the rate of fuel necessary to overcome the drag penalty due to lift, and $\dot{m}_f^f$ is the fuel needed to carry the fuel itself. C_n^p is the capital and capital related costs[5] such as those for purchase, research and development, maintenance, etc. which are associated with the different components that comprise the SS

Optimization of the objective problem in equation (3.31) is constrained by the drag polar relation and equation (3.32). The drag due to the lift and any additional drag depend not only on the flight conditions and requirements (e.g. Mach number) but also on geometry and weight of the SS. The weight in turn depends on the SS's (e.g. Aspect ratio, angle of attack).

---

[5] Note that writing the optimization problem on a cost basis is more general that writing it on a gross takeoff weight or fuel weight basis since the latter two are in effect special cases or subsets of the cost problem.

3.3 Thermal Management System (TMS) Synthesis / Design Unit-Level Optimization Problem

3.3.1 General Description of the TMS

Figure 3.4. shows a TMS using a basic vapor compressor cycle. The TMS interacts with a bootstrap ECS, this combination represents a highly complex cooling system, similar to the ones used by advanced fighter aircrafts and uninhabited combat air craft vehicles (UCAV's), which have two avionics boxes. The TMS has a number of sub-systems including two Polyalphaolefin (PAO) loops, a vapor compressor cycle and a fuel loop. In contrast to the ECS supplies conditioned air for the cockpit and the low heat generation avionics, the TMS provides conditioned air for the high heat generation avionics.

The TMS removes heat from the high heat generation avionics via the cold PAO[6] loop. The pump power required to drive the coolant through the loop is calculated from the pressured drops in the liquid line as well as the avionics box and evaporator.

The vapor compression (VC) cycle transfer heat from the cold PAO loop to one at a higher temperature (the hot PAO[7] loop). The basic VC cycles shown in Figure 3.5. is the one chosen for this study. Evaporation of the liquid refrigerant in the evaporator absorbs energy from the heat source fluid, the cold PAO fluid, which in turn takes energy from the avionics. The refrigerant is compressed to a higher pressure and temperature and then cooled in a condenser where the acquired heat is rejected to a heat sink, the hot PAO fluid. The refrigerant liquid leaving the condenser flows again to the evaporator through a throttling (expansion) valve, closing the loop.

Variants on the basic VC which are not included here multiple evaporator operation cycle and the subcooler-superheater cycle in which more than two heat exchangers are allocated to handle separate cooling loads or to improve the COP. Detailed analysis of different configurations is presented in *SAE Aerothermodynamic System Engineering and Design* (1990). In general, since the open air cycles used in ECSs are limited by a relatively small temperature difference between heat sources and sinks, a closed VC cycle may be combined with the air cycle in order to increase the effective temperature range of the cooling system. With moderate temperature differences, one VC cycle may suffice. With larger temperature differences, a cascade VC cycle may be required.

---

[6] The cold Polyalphaolefin (PAO) is the fluid used as a heat source for the vapor compressor cycle.

[7] The hot Polyalphaolefin (PAO) is the fluid used as the intermediated heat sink between the vapor compressor cycle and the fuel loop.

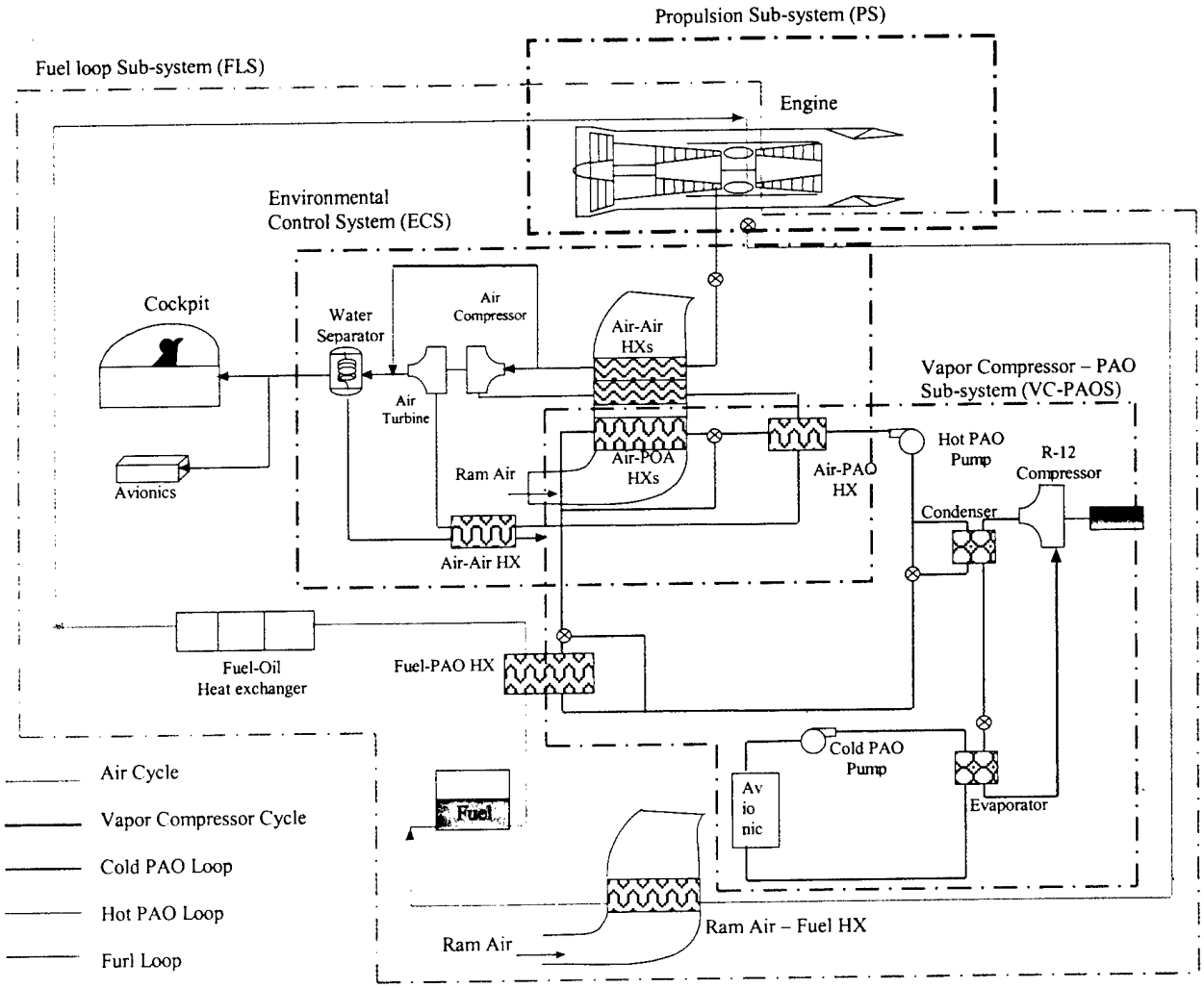

Figure 3.4. Thermal Management Sub-system (TMS) and associated subsystems of an advanced military aircraft.

The hot PAO loop is highly coupled to other sub-systems, i.e. the ECS, the fuel loop sub-system and the VC cycle. This PAO loop receives heat from the VC cycle through the condenser. Flow on the PAO side of the condenser is controlled through a valve. Following the condenser, the PAO is pumped toward a bleed air-PAO heat exchanger where it receives heat from the bleed air, which comes from the ECS secondary heat exchanger. The PAO, at high temperature, is then cooled using ram air at the same scoop inlet as that used for the ECS. Before the PAO returns to the condenser, it is cooled using the aircraft fuel as a heat sink. The fuel in the fuel loop also receives heat from the oil sub-system and the PS. The cooling loads from these sub-systems depend on the specific fuel consumption, which is constant for a specific mission segment. After the fuel required by PS is taken from the fuel stream, the remaining fuel is cooled in a counter-flow heat exchanger using ram air from a separate ram air scoop inlet. Although the fuel returning to the main fuel tank is cooled, the inlet temperature is higher than the outlet one, resulting in thermal storage within the tank. Thus , the fuel loop must be solved as a transient problem. This is detailed *Chapter 5.*

The TMS, in general is highly affected by the aircraft flight conditions, since it is highly coupled to the PS and engine heat load depends on engine setting, producing a change of conditions in the fuel loop. Moreover, TMS performance depends on the bleed air temperature which depends on the engine setting, and on the Mach number which determines the ram air inlet pressure and temperature. In addition the TMS pumps and compressor, and the drag produced by the ram air inlets, impose a power load on the PS.

Thus , in summary, the TMS introduces the following additional fuel requirements to:

- Provide the additional thrust needed for carrying the mass of the TMS.
- Supply power to the TMS; this can be expressed as the amount of power required to meet the TMS requirements, while maintaining constant net thrust.
- Overcome any additional drag, resulting from the installation of an additional sub-system.
- Compensate for an increased drag profile due to the installation of ram air scoop inlets for cooling purposes.
- Carry the amount of fuel required to by the previous tasks.

3.3.2 TMS Unit-level Optimization Problem Definition

Now in order to generate a suitable unit-level optimization problem for the TMS, the energy (fuel) requirements of the sub-system must be added to the capital cost of the components as was done with the SS[8], i.e.

$$\text{Minimize} \quad C_{TMS} = \int_{time} c_f (\dot{m}_f^P + \dot{m}_f^r + \dot{m}_f^w + \dot{m}_f^v + \dot{m}_f^f)\, dt + \sum_n C_n^P \tag{3.33}$$

$$\text{w.r.t.} \quad \{\vec{X}_{TMS}, \vec{Y}_{TMS}\}$$

subject to

$$\vec{H}_{TMS} = \vec{0}, \quad \vec{G}_{TMS} \le \vec{0} \tag{3.34a}$$

$$C_n^P = C_n^P(\vec{X}_{TMS}, \vec{Y}_{TMS}) \tag{3.34b}$$

---

[8] Note that writing the optimization problem on a cost basis is more general that writing it on a gross takeoff weight or fuel weight basis since the latter two are in effect special cases or subsets of the cost problem.

where C_{TMS} is the total cost of the TMS, c_f is the unit cost of fuel, $\dot{m}_f^P$ is the rate of required fuel to generate the power required by the compressor and pumps, $\dot{m}_f^r$ is the rate of fuel necessary for overcoming the drag penalty created by the ram air, $\dot{m}_f^w$ and $\dot{m}_f^v$ are the rates of fuel needed to carry the total weight and volume of the TMS, respectively, $\dot{m}_f^f$ is the rate of fuel required for carrying the fuel itself. C_n^p is the capital cost (purchase, research and development, maintainability, etc.) of the component or sub-system *n*.

3.4 Environmental Control Sub-system (ECS) Synthesis / Design Unit-Level Optimization Problem

3.4.1 General Description of the ECS

The air cycle of the ECS dissipates heat by transforming it into work. Two types of air cycles are possible:

- Open Cycles: Those in which the air is taken from the outside the aircraft and rejected after being used in the cycle.
- Closed Cycles: Those in which air is re-circulated continuously through the cycle.

A survey of the many possible different configurations is given in the *SAE Aerospace Applied Thermodynamics Manual* (1969). Of these the bootstrap system, is by far the most widely used, due to its higher efficiency when compared to a simple air cycle. In the bootstrap system, performance is improved by using the air turbine work output for increased compression of the air upstream of the turbine. Thus, a higher compression ratio is achieved with a correspondingly higher temperature drop across the turbine.

The conventional bootstrap system shown in Figure 3.5. is similar to the one used by the F-16 fighter. It provides conditioned air to the cockpit and avionics. Airflow to the ECS is from pre-conditioned bleed air. Flow into the ECS is varied by a pressure-modulating valve at the ECS inlet. This valve also limits maximum inlet pressure to the ECS's primary heat exchanger and bootstrap compressor. Air is compressed and cooled in the bootstrap ECS. After compression, the air is cooled in a counter-flow, secondary heat exchanger using ram air from ram air scoop inlets. Air from the secondary heat exchanger is then cooled in the regenerative heat exchanger, before it is cooled further by expansion in the bootstrap turbine. Most of the water condensed during cooling of the air in the air turbine is removed in a low-pressure water separator.

Of course, ECS performance is closely coupled with the PS and aircraft flight conditions. Changes in engine power settings cause changes in bleed air pressures and temperatures, which in turn affect the performance of the ECS.

Furthermore, the mass flow rate and pressure of the bleed air will in general depend on the pressure and temperature at which the cold air must be delivered to the cockpit and avionics and the design of the ECS. Quite obviously, the energy or exergy of the air that can then be had from the main engine compressor is not a continuous function but rather is limited by the fact that it can only be extracted from the discrete stages of the compressor. Typically, modern ECSs have a bleed port at a low and one at a high-pressure stage. Once the amount of bleed air needed (usually a unique value calculated from the allowed inlet and outlet temperatures of the load (cabin and avionics) and the cooling load itself) and the stage at which air is bled are fixed, the energy of the bleed air can be calculated. It is then possible to estimate the amount of fuel required to produce the compressed air by means of, for example, an engine simulator.

As to the ram air inlet, it will create a penalty in the system, which is proportional to the drag force created by it. The basic principle is to decelerate the cooling airflow, pass it through the heat exchanger at low speed, and then accelerate it back to ambient pressure. Quantitatively, the drag force created by the inlet-heat exchanger-exit assembly is defined as the cooling airflow's rate of momentum change. The greater the pressure drop in the heat exchanger and ducts, the higher the associated momentum drag will be. Increasing the heat transfer rate in the heat exchanger has the opposite effect. In addition there will be a profile drag of the inlet and exit and perhaps some 'interference' drag due to unfavorable interactions.

Now as to the mass of the ECS, the amount of fuel required to carry this mass and the fuel itself is a function of a number of factors including the flight conditions (altitude, Mach number, angle of attack, etc.) and the relative location of the ECS with respect to the center of gravity of the aircraft. Therefore, the fuel penalty due to weight is highly dependent on the aircraft being analyzed. This weight is affected by the independent variable set which minimizes the objective (i.e., Equation (3.35) below) and includes among others the pressure setting in the regulating valve, the mass flow rate of cooling air in the regenerative heat exchanger and the mass flow rate of bypass warm air necessary to obtain the pressure, temperature and mass flow rate schedules in the cabin and avionics. The available pressure of the bleed air is dependent on the altitude and Mach number of the aircraft. It is assumed that the bleed air is extracted from a fixed, high-pressure compressor stage. The energy (or exergy) of the bleed air is calculated along with the drag created by the ram air. The weight of each component is also calculated according to the physical models given in Muñoz and von Spakovsky (1999).

Thus, as with the TMS the ECS introduces the following additional fuel requirements to:

- Provide the additional thrust needed for carrying the mass of the ECS

- Supply power to the ECS; this can be expressed as the amount of fuel required to meet ECS requirements while maintaining constant net thrust. The energy extracted can be in the form of compressed (bleed) air or shaft power.
- Overcome any additional drag, which may result from installing a subsystem in the aircraft due to increases in profile and momentum drag caused by ram air induction for cooling purposes.
- Carry the quantity of fuel required by the previous items.

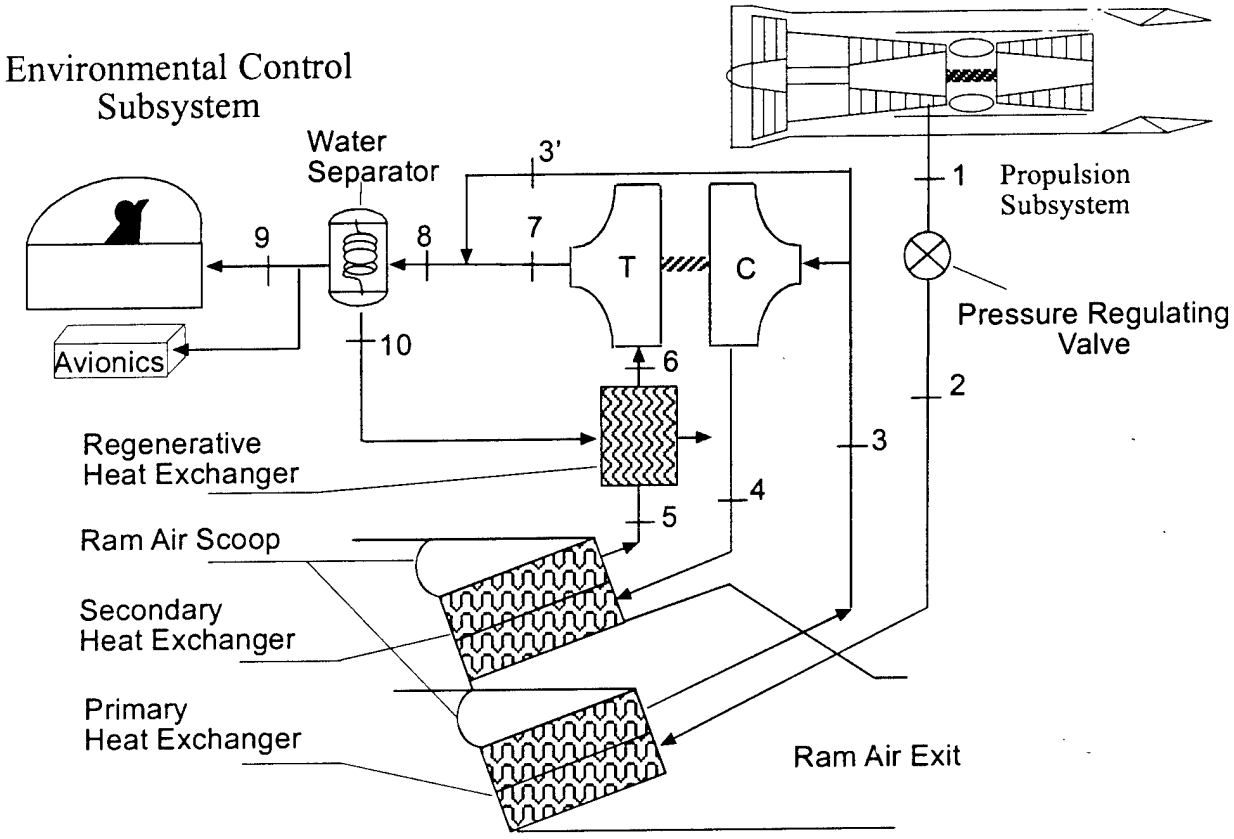

Figure 3.5. Schematic diagram of an ECS.

3.4.2 ECS Unit-level Optimization Problem Definition

Now in order to generate an appropriate unit-level optimization problem for the ECS, the fuel consumptions outlined above must be added to the capital cost of the components such that[9]

[9] Note that writing the optimization problem on a cost basis is more general that writing it on a gross takeoff weight or fuel weight basis since the latter two are in effect special cases or subsets of the cost problem.

$$\text{Minimize} \quad C_{ECS} = \int_{time} c_f (\dot{m}_f^b + \dot{m}_f^r + \dot{m}_f^w + \dot{m}_f^v + \dot{m}_f^f)\, dt + \sum_n C_n^p \tag{3.35}$$

$$\text{w.r.t.} \quad \left\{\vec{X}_{ECS}, \vec{Y}_{ECS}\right\}$$

subject to

$$\vec{H}_{ECS} = \vec{0}, \quad \vec{G}_{ECS} \le \vec{0} \tag{3.35.a}$$

$$C_n^P = C_n^P(\vec{X}_{ECS}, \vec{Y}_{ECS}) \tag{3.35.b}$$

where C_{ECS} is the total cost of the ECS, c_f is the unit cost of fuel, $\dot{m}_f^b$ is the rate of fuel needed to produce the bleed air at the desired pressure, $\dot{m}_f^r$ is the rate of fuel necessary for overcoming the drag penalty created by the ram air, $\dot{m}_f^w$ and $\dot{m}_f^v$ are the rates of fuel required for carrying the total weight and volume of the ECS, respectively, and $\dot{m}_f^f$ is the rate of fuel needed to carry the fuel itself. C_n^p is the capital and other (purchase, research and development, maintainability, etc.) costs.

3.5 Propulsion Sub-system (PS) Unit-Level Optimization Problem

3.5.1 General Description of the PS

The PS has eighteen components as indicated in Figure 3.6. The sub-system is a low-bypass turbofan engine with afterburning. The on and off-design behavior of the engine is simulated using a modern performance code developed by an engine manufacturer for modeling any type of aircraft engine system. The model of the engine uses typical component maps (e.g., compressor, fan hub, fan tip, turbine, burner, and compressor maps) and functional relationships and numerical constants that modify the maps to make the simulation as realistic as possible. The component maps are chosen from several alternatives depending on the design pressure ratio. The computer program has its own set of solvers to carry out the mass, momentum, energy and shaft speed balances. Results from the simulation are the thermodynamic properties at each of the engine stations (pressure, temperature, Mach number, etc.), the inlet air flow rate, nozzle areas, and the fuel consumed in the combustor and afterburner adjusted to provide the thrust required by the mission during the different segments of the mission.

The thrust provided by the engine simulator does not account for the drag created by the installation of the engine. This "uninstalled" thrust (F) must be adjusted for the drag created by the engine inlet and nozzle. Thus,

$$T = F - \phi_{inlet}F - \phi_{nozzle}F \tag{3.36}$$

The drag created by the inlet at subsonic conditions is approximated as the momentum drag created by the isentropic, one-dimensional flow of a perfect gas. Assuming massive separation and no recovery of the additional drag (i.e. the worst case scenario), the conservation of mass and perfect gas relationships lead to

$$\phi_{inlet} = \frac{\frac{M_0}{M_1}\sqrt{\frac{T_1}{T_0}}\left(1+\gamma M_1^2\right)-\left(\frac{A_1}{A_0}+\gamma M_0^2\right)}{\left(\frac{F}{m_0}\right)\left(\frac{\gamma M_0}{a_0}\right)} \tag{3.37}$$

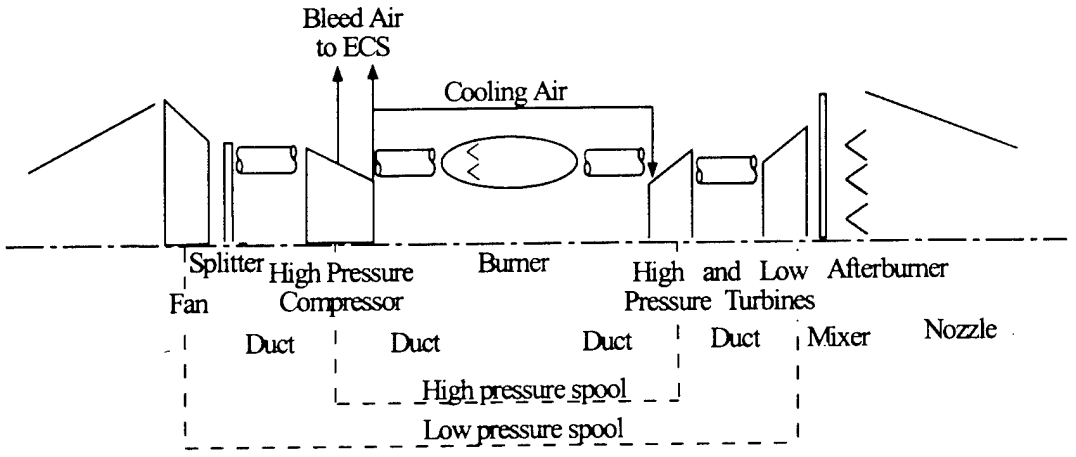

Figure 3.6. Turbofan engine components of the propulsion sub-system (PS).

For the supersonic case, a compressible model that uses a normal shock approximation and neglects internal friction and the disturbed pressure field on the cowl yields

$$\phi_{inlet} = \frac{\left(\frac{A_1}{A_0}-1\right)\left\{M_0-\left(\frac{2}{\gamma+1}+\frac{\gamma-1}{\gamma+1}M_0^2\right)^{1/2}\right\}}{\frac{F}{m_0 a_0}} \tag{3.38}$$

The computer program that simulates the PS cycle also provides the inlet and exit areas of the nozzle at various segments of the mission. The installation penalty due to the nozzle is given by

$$\phi_{nozzle} = \frac{M_0 \dfrac{C_{D_{nozzle}}}{2}\left(\dfrac{A_{exit} - A_{in}}{A_0}\right)}{\dfrac{F}{m_0 a_0}} \tag{3.39}$$

where the drag coefficient is a function of the Mach number as presented in Mattingly et al. (1987).

The weight and dimensions of the PS are calculated using the computer code *Weight Analysis of Turbine Engines (WATE) (WATE User's Guide,* 2000). WATE was originally developed by the Boeing Military Aircraft Company in 1979 and improved by NASA and the McDonnell Douglas Corporation. The original weight and dimensions were derived using a semi-empirical method obtained from analyzing a database of 29 engines. The improved code (used in this paper) is based on analytical and dimensional calculations (the primary method is to calculate material volume and then multiply by density). The new code also accounts for more of the individual parts that make up an engine component than the original empirical method.

3.5.2 PS Unit-level Optimization Problem Definition

The PS, i.e. power plant, unit-level design optimization problem is defined on a cost basis[10] as follow:

$$\text{Minimize} \quad C_{PS} = \int_{time} c_f (\dot{m}_f^w + \dot{m}_f^D + \dot{m}_f^f + \dot{m}_f^T)\, dt + \sum_n C_n^p \tag{3.40.a}$$

w.r.t. $\{\vec{X}_{PS}, \vec{Y}_{PS}\}$

subject to

$$\vec{H}_{PS} = \vec{0}, \quad \vec{G}_{PS} \le \vec{0} \tag{3.40.b}$$

$$C_n^P = C_n^P(\vec{X}_{PS}, \vec{Y}_{PS}) \tag{3.40.c}$$

---

[10] Note that writing the optimization problem on a cost basis is more general that writing it on a gross takeoff weight or fuel weight basis since the latter two are in effect special cases or subsets of the cost problem.

where C_{PS} is the total cost of the PS (first term on the right in Equation (3.11)), c_f is the unit cost of fuel, $\dot{m}_f^w$ is the rate of fuel needed to carry the total weight of the PS, $\dot{m}_f^D$ is the rate of fuel necessary to overcome the drag penalty created by PS nozzle, $\dot{m}_f^T$ is the fuel to produce the required thrust, and $\dot{m}_f^f$ is the fuel needed to carry the fuel itself. C_n^p is the capital and capital related costs such as those for purchase, research and development, maintenance, etc. which are associated with the different components that comprise the PS. In particular the $\vec{H}_{PS}$ includes

$$T_i = \alpha T_{SL} = q_i S\left[K_1\left(\frac{n_i}{q_i}\frac{\beta_i W_{TO}}{S}\right)^2 + C_{D_0} + \frac{D_{ECS_i}}{q_i S}\right] + \frac{\beta_i W_{TO}}{V_i}\frac{d}{dt}\left(h_i + \frac{V_i^2}{2g}\right) \tag{3.41}$$

as well as the system of equations generated by an engine simulator and where it should be pointed out that for the unit-level optimization (as opposed to the system-level optimization, equations (3.1)), W_{ECS} and W_{TMS} are held constant, i.e.

$$W_{ECS} - W_{ECS}^o = 0 \tag{3.42}$$

$$W_{TMS} - W_{TMS}^o = 0 \tag{3.43}$$

In addition, the following constraints are also imposed:

$$\dot{m}_{bleed\,i} - \dot{m}_{bleed\,i}^o = 0 \tag{3.44}$$

$$BP_{low_i} - BP_{low_i}^o = 0 \tag{3.45}$$

$$BP_{high_i} - BP_{high_i}^o = 0 \tag{3.46}$$

$$Power_{TMS} - Power_{TMS}^o = 0 \tag{3.47}$$

$$Drag_{SS} - Drag_{SS}^o = 0 \tag{3.48}$$

Constraints (3.42) through (3.48) indicate that the weight of the ECS, the bleed air flow rate, the bleed port from which it is taken, the TMS weight, power requirement, the SS weight and drag are set equal to the values indicated with the superscript *0*. These values are set externally.

CHAPTER 4

4. DECOMPOSITION: APPLYING ILGO TO THE AIRCRAFT SYSTEM SYNTHESIS / DESIGN OPTIMIZATION PROBLEM

In order to solve the system-level and unit-level optimization problem (i.e. Equations (3.1), (3.6), (3.11)) one can use the local-global optimization (LGO) decomposition technique presented by Muñoz and von Spakovsky (2000b). In order to do this, the design of the PS (problem (3.40)) would need to be carried out for multiple bleed air flow rates, ECS drags and ECS weights, bleed port selections, and TMS drag, weight, and power extraction. This would mean that a number of unit-level optimization runs with respect to the PS design and operational variables would have to be solved for innumerable combinations of values of the constraints related to the quantities listed in the previous sentence. A similar number of unit-level optimizations would have to be done for the ECS, TMS and SS. The results would then be used to generate the optimum response surface (ORS) of the system, which in this case would be in the WTO versus ECS drag, bleed, and weight domain, TMS drag, weight, and power domain, and SS drag and weight domain. If this off-line version of the method (OL-LGO; see Muñoz and von Spakovsky (2000b)) were used, the results would have to be stored for later use by the system-level optimization problem for the PS, ECS, TMS, and SS combined. The latter problem involves finding the combination of bleed air, ECS drag and weight, TMS drag, weight, and power, and SS drag and weight that minimize the system-level objective function.

From a practical viewpoint, the principal difficulty associated with the implementation of the OL-LGO technique (or for that matter RT-LGO) in its general form for this case is the computational burden which it entails. For example, for the PS the calculation of the take-off gross weight involves "flying" the engine on paper over the entire mission to obtain the fuel consumption. The process is repeated a number of times until convergence on the take-off weight is achieved. The resulting W_{TO} value can then be sent to the optimizer for analysis. The process just described requires different computer codes. First, there is a computer program that calculates the necessary thrust for each of the mission legs by solving the differential equation (3.28) (flight dynamics code). The thermodynamic engine simulation follows. This step is particularly slow due to the fact that the engine performance code in use is not 'persistent', i.e. it is necessary to launch the program every time the engine is 'flown' over the mission. The thrust obtained from the engine simulator is adjusted by a different computer code to account for inlet and nozzle losses, i.e. equations (3.36) to (3.39). Some of the outputs of the thermodynamic simulation added to aerodynamic, materials and other design variables are used by WATE (NASA's engine weight code) to calculate the weight of the engine. The final step before going to the optimizer is the post-processing of all of the codes' results. This entire process makes the simulation of the PS very expensive

computationally. For reference, the calculation of a single value of the gross takeoff weight takes on average about 55 seconds on a current dual processor PC workstation, a duration which can be prohibitive for large-scale optimization, especially since this duration accounts for only one of the four sub-systems being optimized here as part of the aircraft system.

Thus, another decomposition approach is needed which significantly lessens this prohibitive computational burden, i.e. ILGO, as discussed in *Chapter 2*[1]. Of the two versions of ILGO, version A requires that the PS, ECS, TMS, and SS be synthesized / designed for arbitrary values of the coupling functions (i.e. ECS bleed, drag, and weight, TMS drag, weight and power, and SS drag and weight). Such a constraint is easy to meet in the PS design. However, the ECS and TMS synthesis / design would unnecessarily be constrained by this requirement. In fact, arbitrary combinations of the coupling functions between the PS and ECS and TMS may not necessarily lead to feasible solutions for the ECS and TMS. Therefore, version B of ILGO, which does not have these shortcomings, is used for the ECS, SS and TMS synthesis / design optimization while version A is retained for the PS. Furthermore, in addition to these four sub-systems, an additional decomposition at the sub-system level of the TMS is performed, in order to effectively deal with the highly dynamic behavior of the fuel loop. The two additional sub-systems are the fuel loop subsystem (FLS) and the vapor compression / PAO loops sub-system (VC/PAOS). Details of the model developed for the TMS are given in *Chapter 5*.

In order to apply ILGO to the system-level optimization problem defined in *Chapter 3* for gross takeoff weight (Equations (3.1.) to (3.5.)) one unit-level optimization problem is defined (i.e. ILGO-A applied to the PS) and three system-level, unit based optimization problem are defined (i.e. ILGO-B applied to the ECS, TMS, and SS). The boundaries of each unit (sub-system), their associated local decision variables as well as the coupling functions connecting each unit to the rest are clearly seen in Figure 4.1. The resource used to produce the system-level product (thrust) is fuel. The coupling functions which along with their associated shadow prices[2]: are used in ILGO to eliminate the system level optimization problem by providing system –level information in the unit-level (ILGO-A) and system-level, unit-based (ILGO-B) problems include the power for the TMS, the bleed air for the ECS, the ECS and TMS drag penalties, the TMS and ECS mass, and the ECS bleed port selection. This figure illustrates the decomposition of the system-level problem for aircraft synthesis / design into four separate but integral sub-problems. It is our intention at the completion of this project to have solved this problem in its entirety, resulting in a Ph. D. dissertation already completed and submitted as our annual report in year one of this project and an

---

[1] Note that there are a number of other advantages that ILGO brings to the table (see Muñoz and von Spakovsky, 2001a, b) including the elimination of nested optimization and the ability to be used across geographically dispersed teams of design specialist.

[2] See discussion in the following sections

M.S. thesis the latter of which will serve as our final report for the final phase of this project to be complete next year[3]. In the meantime, however, for the purpose of this report, we will present some preliminary results showing the influence of the various coupling function on the unit-level and system-level, unit-based synthesis / design optimization of the PS, ECS, and TMS (i.e. FLS and VC/PAOS). Furthermore, for the time being, no decision variables are used for the SS, which is solved as an integral part of the PS by applying the procedure described by Mattingly (1999) and previously applied in Muñoz (2000) and Muñoz and von Spakovsky (2001a,b). Details of the SS optimization sub-problem and its associated model for the synthesis / design optimization of the airfoil are given in *Chapter 6*.

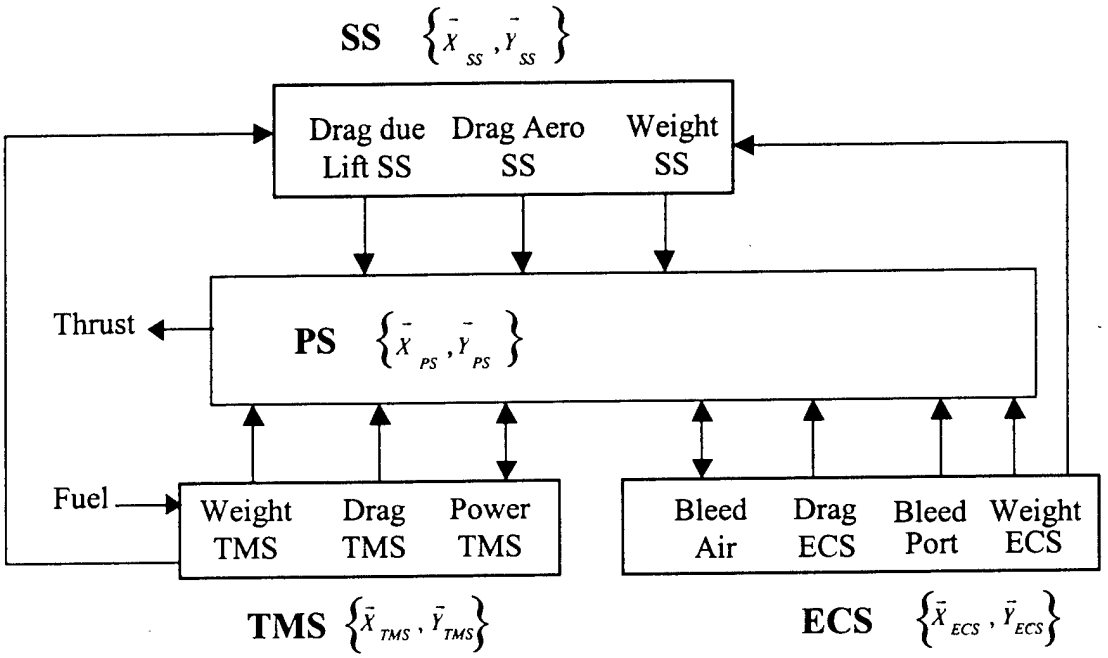

Figure 4.1. Schematic of sub-system boundaries, decision variables and coupling functions

Now, in order to define the optimization sub-problems for each of the three sub-systems, i.e. the PS, ECS, and TMS, it is necessary to first subdivide the mission of Figure 3.1. and Table 3.1 into segments (phases or legs). A preliminary analysis reveals that the mission segments given in Table 4.1 are the most critical ones, either because their fuel consumption is significant or the operating conditions are very stringent for the three (eventually four) sub-systems being synthesized / designed. Furthermore, given the relatively high fidelity of the simulations and the number and type of decision variables and constraints (see table 4.2 to 4.7), one can clearly see that one is confronted with a very complex, large-scale mixed integer non-linear

[3] We have received a 6 month no-cost extension (i.e. an extension of the funds originally allocated to this project through May of next year).

optimization problem. The difficulties associated with solving this problem are exacerbated by the following:

- There is a need to iterate the engine simulation until proper convergence of the take-off weight is achieved.
- The engine simulation tool was not specifically written for optimization purposes. Each time a simulation is run, it is necessary to launch the program and read the necessary software licenses. This difficulty added to the previous item makes the take-off weight calculation (for any given values of the decision variables) very expensive computationally. The ECS simulation code does not have this drawback since it was developed in-house.
- The presence of both binary and discrete variables makes it necessary to use a heuristic approach: either a genetic algorithm or a simulated annealing optimization algorithm. There are no general gradient-based methods able to solve this mixed integer non-linear programming (MINLP) problem. However, heuristic algorithms impose a significant time penalty in terms of solution time.

Table 4.1. AAF critical mission segments.

Mission segments		
No.	**Name**	
1	wup	Warm-up
2	tka	Take-off acceleration
3	tkr	Take-off rotation
4	clac	Climb/accelerate
5	scc	Subsonic cruise climb
6	cap	Combat air patrol
7	acc	Acceleration
8	pen	Penetration
9	ct1	Combat turn 1
10	ct2	Combat turn 2
11	cac	Combat acceleration
12	esc	Escape dash
13	scc_2	Subsonic cruise climb 2
14	loi	Loiter
15	mmn	Maximum Mach number

4.1 ECS System-Level, Unit-Based Synthesis / Design Optimization Problem Definition

The synthesis / design and operational decision variables for the ECS are given in Table 4.2. The ranges of the decision variables are based on existing designs and on the work of Muñoz and von Spakovsky (1999, 2000a).

Table 4.2a. ECS synthesis / design decision variables and inequality constraints.

Component	Synthesis / Design Decision Variable			Constraints
Primary and secondary heat exchangers	L_c	Cold side length (m)		$0.5<L_c<0.9$
	L_h	Hot side length (m)		$0.06<L_h<0.9$
	L_n	Non flow length (m)		$0.5<L_n<0.9$
Air cycle machine	PR_{cp}	Compressor design pressure ratio		$1.8<PR_{cp}<3.0$
	PR_{tb}	Turbine design pressure ratio		$PR_{tb}<12$
First and second regenerative heat exchangers	L_c	Cold side length (m)		$0.3<L_c<0.5$
	L_h	Hot side length (m)		$0.15<L_h<0.3$
	L_n	Non flow length (m)		$0.3<L_n<0.5$
	Reg_1 Reg_2	Existence-nonexistence of regenerative heat exchanger in configuration		$Reg_1,Reg_2=0,1$
				$Reg_1+Reg_2=1$
Ram air inlet, outlet	A_1,A_2	Areas of inlet, outlet (cm^2)		$120< A_1,A_2<220$
Primary and secondary heat exchanger fin type: hot and cold sides[4, 5]	Fin_{hot} Fin_{cold}	Fin No.	Surface designation[6]	R_{emax}
		1	¼(s)-11.1	8000
		2	1/8-15.2	6000
		3	1/8-13.95	6000
		4	1/8-15.61	6000
		5	1/8-19.86	5000
		6	1/9-22.68	5000
		7	1/9-25.01	4000
		8	1/9-24.12	4000
		9	1/10-27.03	4000
		10	1/10-19.35	4000

[4] Discrete variable.

[5] The plate thickness is 0.254 mm.

[6] See Kays and London (1998).

Table 4.2b. ECS operational decision variables and inequality constraints.

	Operational Decision Variables		
Pressure regulating valve	PR_{vv}	Pressure setting	$PR_{vv}<6.0$
Low pressure bleed port	BP_{low}	Low pressure bleed port[7]	$BP_{low}=0,1$
High pressure bleed port	BP_{high}	High pressure bleed port[5]	$BP_{high}=0,1$
Splitter	m_{byp}	Bypass air flow rate	$m_{byp}<0.2$ kg/s
Bleed port	m_{hot}	Hot air flow rate	$m_{hot}<0.2$ kg/s
Regenerative heat exchanger	m_{creg}	Cold air flow rate	$m_{creg}<0.2$ kg/s
	Dependent variables		
Cold and hot sides heat exchangers	Re_c[8]	Reynolds number, cold air side	$R_{ec}/ R_{emax} <1$
	Re_h[6]	Reynolds number, hot air side	$R_{eh}/ R_{emax} <1$
Cabin and avionics	T_{cold}[6]	Cooling air temperature	$\|T_{cold}-T_{sched}\|< 3$
	P_{cold}[6]	Cooling air pressure	$P_{cold} = P_{sched}$
	m_{cold}[6]	Cooling air flow rate	$m_{cold} = m_{sched}$
ACM	W_{cp}, W_{tb}[6]	Compressor and turbine work	$W_{cp}=W_{tb}$

Now as to the coupling functions Figure 3.2. in *Chapter 3* shows the coupling functions between the ECS and the PS (the bleed air mass flow, the ECS weight and drag), each of which demands additional thrust from the PS and in turn results in an increment in the fuel consumption. This tight dependence shows the effects that the coupling functions have on the total fuel consumption and thus , on the system-level objective function. Figure 3.2 also shows the coupling function between the ECS and the TMS (the rate of energy transferred between the two sub-systems). This coupling function as well affects the amount of fuel due to the ECS and the system-level objective. A measure of these effects is the shadow prices (Equation (2.19) *in Chapter 2*) which shows the relative importance of the coupling functions in terms of the overall system-level objective. In ILGO-B, these shadow prices (λ's) are used to define the system-level, unit-based objective functions. The shadow prices for the coupling functions of the ECS for a given selection of the bleed port, mission leg_i and optimum fuel weight for leg_i are given by

[7] Binary variable: *0* means no bleed air is taken from the bleed port.

[8] This variable takes different values at different mission segments.

$$\lambda_{\dot{m}\,Bleed_{ECS\,i}} = \frac{\partial W^{*}_{FUEL_i}}{\partial \dot{m}_{Bleed_{ECS}}} \tag{4.1}$$

$$\lambda_{Decs\,i} = \frac{\partial W^{*}_{FUEL_i}}{\partial D_{ECS}} \tag{4.2}$$

$$\lambda_{\dot{E}ecs-tms\,i} = \frac{\partial W^{*}_{FUEL_i}}{\partial \dot{E}_{ECS-TMS}} \tag{4.3}$$

and

$$\lambda_{Wecs\,i} = \frac{\partial W^{*}_{FUEL_i}}{\partial W_{ECS}} \tag{4.4}$$

where the $*$ indicates and optimal value and the weight of the fuel at the i_{th} leg (see *Chapter 3*)is given by

$$W_{FUEL_i} = W_{TO}\left(1-\pi_i\right)\cdot \overset{i-1}{\underset{1}{\pi}} \tag{4.5}$$

and the fuel consumed due to the ECS can then be written as

$$W_{FUEL_{ECS}} = \sum_{i=1}^{n}\left(\lambda_{\dot{m}\,Bleed_{ECS\,i}}\dot{m}_{Bleed_{ECS\,i}} + \lambda_{Decs\,i}D_{ECS\,i} + \lambda_{\dot{E}ecs-tms\,i}\dot{E}_{ECS-TMS\,i} + \lambda_{Wecs\,i}W_{ECS}\right) \tag{4.6}$$

It has been assumed in equation (4.6) that the shadow prices costs are constant over the range of bleed, drag, and weight and TMS energy of the ECS. Each term on the right of equation (4.6) can be written with respect to a reference fuel weight W^{o}_{FUEL} such that

$$W_{FUEL\,\dot{m}\,Bleed_{ECS}} = W^{o}_{FUEL} + \sum_{i=1}^{n}\left(\lambda_{\dot{m}\,Bleed_{ECS\,i}}\dot{m}_{Bleed_{ECS\,i}}\right) \tag{4.7}$$

$$W_{FUEL\,Decs} = W^{o}_{FUEL} + \sum_{i=1}^{n}\left(\lambda_{Decs\,i}D_{ECS_i}\right) \tag{4.8}$$

$$W_{FUEL\,\dot{E}ecs-tms} = W^{o}_{FUEL} + \sum_{i=1}^{n}\left(\lambda_{\dot{E}ecs-tms\,i}\dot{E}_{ECS-TMS_i}\right) \tag{4.9}$$

$$W_{FUEL\,Wecs} = W^{o}_{FUEL} + \sum_{i=1}^{n}\left(\lambda_{Wecs\,i}W_{ECS}\right) \tag{4.10}$$

The reference fuel weight W^{o}_{FUEL} has been set to correspond to the case with no bleed air, ECS drag or weight, and no energy transfer to the TMS.

To obtain the impact of these factors on the system-level objective function, for example, the gross take-off weight, problem (3.1) in *Chapter 3* is solved (i.e. iterated on W_{TO} until convergence is achieved) with the fuel weight values given by equations (4.7) to (4.10). Thus, the increase in the gross take-off weight due to the ECS Coupling functions are given by

$$\Delta W_{TO\,\dot{m}\,Bleed_{ECS}} = W_{TO}(W_{FUEL\,\dot{m}\,Bleed_{ECS}}) - W_{TO}(W^{o}_{FUEL}) \tag{4.11}$$

$$\Delta W_{TO\,Decs} = W_{TO}(W_{FUEL\,Decs}) - W_{TO}(W^{o}_{FUEL}) \tag{4.12}$$

$$\Delta W_{TO\,\dot{E}_{ecs-tms}} = W_{TO}(W_{FUEL\,\dot{E}_{ecs-tms}}) - W_{TO}(W^{o}_{FUEL}) \tag{4.13}$$

$$\Delta W_{TOWecs} = W_{TO}(W_{FUELWecs}) - W_{TO}(W^{o}_{FUEL}) \tag{4.14}$$

Note that both the bleed and drag have been represented in the above equations by the bleed air flow rate and drag force. In the case of bleed air, other options to use instead are energy, exergy or other thermodynamic properties. Drag can be represented as a force or a form of energy (i.e. propulsive power loss). The work of Muñoz and von Spakovsky (2000b) indicates that there is a mathematical advantage with the use of properties that make the shadow prices monotonic and, ideally, linear. In a different paper, the same authors (Muñoz and von Spakovsky, 2000a) found a linear relationship between fuel consumption and bleed air flow rate as well as between fuel consumption and drag force. Thus, these findings constitute a good choice for the properties to represent bleed and drag. In addition, there is an intrinsic practical advantage with the use of these two properties. The engine simulator can be easily adjusted to provide variable air flow rates at the high and low bleed ports. It is also easy to increase or decrease the necessary thrust according to the drag penalty created by the ECS.

One problem arising from the use of bleed air flow rate is the need for "matching" the bleed port temperatures and pressures in both sub-systems for all mission legs. The PS is designed with assumed values for the drag, bleed air flow rate, and weight of the ECS. If the overall system is optimized without decomposition, the values used by the PS and obtained from optimizing the ECS are identical. However, the iterative version of the decomposition approach used (ILGO) makes it necessary in the ECS synthesis / design to use the temperature and pressure of the bleed port obtained from running the PS in the previous iteration. Therefore, it is necessary to check that in addition to flow rate, the bleed thermodynamic conditions are consistent. Although this potentially poses a problem in terms of convergence, the expected low variability of the bleed port conditions after a few iterations should render this problem insignificant.

With the above comments and taking into account that there is no external resource being used by the ECS, the system-level, unit-based synthesis / design optimization problem is set up as follows:

ECS system-level, unit based Gross Takeoff Weight Problem

$$\text{Minimize} \quad \Delta W_{TO\,ECS} = \Delta W_{TO\,\dot{m}\,Bleed_{ECS}} + \Delta W_{TO\,Decs} + \Delta W_{TO\,\dot{E}_{ecs-tms}} + \Delta W_{TOWecs} \tag{4.15}$$

w.r.t. $\left\{\vec{X}_{ECS}, \vec{Y}_{ECS}\right\}$

subject to the inequality constraints given in Table 4.2, as well as

$$[P_{bleed}]_{PS} = [P_{bleed}]_{ECS} \;,\; [T_{bleed}]_{PS} = [T_{bleed}]_{ECS} \text{ and } [\dot{E}_{TMS}]_{ECS} = [\dot{E}_{ECS}]_{TMS} \tag{4.16}$$

i.e. the bleed pressures and temperatures must match as well as the energy transferred to the TMS.

ECS the system-level, unit-based Fuel Consumption Problem

Minimize

$$\Delta W_{FUEL\,ECS} = \sum_{i=1}^{n} \left(\lambda_{\dot{m}\,Bleed_{ECS\,i}} \dot{m}_{Bleed_{ECS\,i}} + \lambda_{Decs_i} D_{ECS_i} + \lambda_{\dot{E}ecs-tms_i} \dot{E}_{ECS-TMS_i} + \lambda_{Wecs_i} W_{ECS} \right) \tag{4.17}$$

w.r.t. $\left\{\vec{X}_{ECS}, \vec{Y}_{ECS}\right\}$

Subject to the same constraints as problem (4.15)

ECS system-level, unit-based Total Cost Problem

$$\text{Minimize} \quad \Delta C_{T\,ECS} = C^{P}_{ECS} + \left(\Delta C_{FUEL} + \Delta C_{SS} + \Delta C_{TMS} + \Delta C_{PS}\right)_{ECS} \tag{4.18}$$

subject to the same constraints as problem (4.15).

where the $\Delta C_{T\,ECS}$ is increase in the system's total cost due to the ECS. In the above equation, C^{P}_{ECS} is the capital cost; $\Delta C_{FUEL\,ECS}$ is the cost of the extra fuel due to the ECS penalties (bleed air, ram drag, and ECS weight); and $\Delta C_{SS\,ECS}$, $\Delta C_{TMS\,ECS}$ and $\Delta C_{PS\,ECS}$ are the extra cost of the SS, the TMS, and PS, respectively.

4.2 TMS System-level, Unit-based Synthesis / Design Optimization Problem Definition

The synthesis / design and operational decision variables for the TMS are given in Table 4.3. The ranges of the decision variables are based on existing designs and on the work of Muñoz and von Spakovsky (1999, 2000a).

Table 4.3a. VC/PAOS decision variables and inequality constraints.

Component	Decision Variable		Constraints
	Design Variables		
Bleed air / PAO heat exchanger	L_c	Cold-side length (m)	$0.1<L_r<0.9$
	L_h	Hot-side length (m)	$0.05<L_b<0.9$
	L_n	Non-flow length (m)	$0.1<L_n<0.9$
	No.fin	Number of fins per inch	$11<No.fin<20$
Condenser	L_c	Cold-side length (m)	$0.1<L_r<0.9$
	L_h	Hot-side length (m)	$0.05<L_b<0.9$
	L_n	Non-flow length (m)	$0.1<L_n<0.9$
	No.fin	Number of fins per inch	$11<No.fin<20$
Evaporator	L_c	Cold-side length (m)	$0.1<L_r<0.9$
	L_h	Hot-side length (m)	$0.05<L_b<0.9$
	L_n	Non-flow length (m)	$0.1<L_n<0.9$
	No.fin	Number of fins per inch	$11<No.fin<20$
Ram air / hot PAO heat exchanger	L_c	Cold-side length (m)	$0.1<L_r<0.9$
	L_h	Hot-side length (m)	$0.05<L_b<0.9$
	L_n	Non-flow length (m)	$0.1<L_n<0.9$
	No.fin	Number of fins per inch	$11<No.fin<20$
	Operational Variables		
Vapor Compressor	*Pr*	Pressure Ratio	$1<Pr<9$
Vapor cycle	$\dot{m}_v$	Vapor mass flow(kg/s)	$0.2<m_v<2.2$
Hot PAO cycle	$\dot{m}_{HPAO}$	Hot PAO loop mass flow (kg/s)	$0.2<m_{HPAO}<3.5$
	V_5	Fuel / hot PAO heat exchanger bypass valve position	$0<V_5<0.3$
	V_4	Bleed Air / hot PAO heat exchanger bypass valve position	$0<V_4<0.3$
	V_2	Vapor / hot PAO heat exchanger bypass valve position	$0<V_2<0.3$
	Synthesis Variables		
Ram air / hot PAO heat exchanger	*onoff*	Place or not the Ram air / hot PAO heat exchanger	0 or 1

Table 4.3b. FLS decision variables and inequality constraints.

Component	Decision variable case		Constraints
	Design Variables		
Fuel / Oil heat Exchanger	L_c	Cold-side length (m)	$0.1<L_r<0.9$
	L_h	Hot-side length (m)	$0.05<L_b<0.9$
	L_n	Non-flow length (m)	$0.1<L_n<0.9$
	No.fin	Number of fins per inch	$11<No.fin<20$
Fuel / PAO Heat Exchanger	L_c	Cold-side length (m)	$0.1<L_r<0.9$
	L_h	Hot-side length (m)	$0.05<L_b<0.9$
	L_n	Non-flow length (m)	$0.1<L_n<0.9$
	No.fin	Number of fins per inch	$11<No.fin<20$
Fuel / Ram air heat exchanger	L_c	Cold-side length (m)	$0.1<L_r<0.9$
	L_h	Hot-side length (m)	$0.05<L_b<0.9$
	L_n	Non-flow length (m)	$0.1<L_n<0.9$
	No.fin	Number of fins per inch	$11<No.fin<20$
Fuel / hydraulic heat exchanger	L_c	Cold-side length (m)	$0.1<L_r<0.9$
	L_h	Hot-side length (m)	$0.05<L_b<0.9$
	L_n	Non-flow length (m)	$0.1<L_n<0.9$
	No.fin	Number of fins per inch	$11<No.fin<20$
Ram Air Inlet	A_i	Area of inlet, outlet (cm^2)	$50<A_i<290$
	Operational Variables		
Fuel loop	$\dot{m}_f$	Fuel-mass flow(kg/s)	$0.3<m_F<4$
	$\dot{m}_o$	Oil mass flow(kg/s)	$0.3<m_F<4$
	$\dot{m}_h$	Hydraulic mass flow(kg/s)	$0.3<m_F<4$

Now, as to the coupling functions between the TMS and the PS (the power extraction for the TMS vapor compressor and pumps, the TMS weight and drag), each of these coupling functions demands additional thrust from the PS, which in turn results in an increment in fuel consumption. Again this tight dependence shows the effects the coupling functions have on total fuel consumption and, thus, or the system-level objective function. Furthermore, the coupling function between the TMS and the ECS (the rate of energy transferred between the two sub-systems) affects as well the amount of fuel due to the TMS. As well the case with the ECS in the previous section, the shadow prices of all these coupling functions for the TMS for a given selection of the bleed port, mission leg_i, and optimum fuel weight for leg_i are given by

$$\lambda_{\dot{E}tms-ps_i} = \frac{\partial W^*_{FUEL_i}}{\partial \dot{E}_{TMS-PS}} \tag{4.19}$$

$$\lambda_{Dtms_i} = \frac{\partial W^*_{FUEL_i}}{\partial D_{TMS}} \tag{4.20}$$

$$\lambda_{\dot{E}tms-ecs_i} = \frac{\partial W^*_{FUEL_i}}{\partial \dot{E}_{TMS-ECS}} \tag{4.21}$$

$$\lambda_{Wtms_i} = \frac{\partial W^*_{FUEL_i}}{\partial W_{TMS}} \tag{4.22}$$

where again the weight of the fuel at the i_{th} leg is given by equation (4.5) and the fuel consumed due to the TMS can then be written as

$$W_{FUEL_{TMS}} = \sum_{i=1}^{n}\left(\lambda_{\dot{E}tms-ps_i}\dot{E}_{TMS-PS_i} + \lambda_{Dtms_i}D_{TMS_i} + \lambda_{\dot{E}tms-ecs_i}\dot{E}_{TMS-ECS_i} + \lambda_{Wtms_i}W_{TMS}\right) \tag{4.23}$$

It has been assumed in equation (4.23) that the shadow prices are constant over the range of power, drag, weight, and energy of the TMS. Each term on the right of equation (4.23) can be written with respect to the reference fuel weight W^o_{FUEL} such that

$$W_{FUEL\,\dot{E}tms-ps} = W^o_{FUEL} + \sum_{i=1}^{n}\left(\lambda_{\dot{E}tms-ps_i}\dot{E}_{TMS-PS_i}\right) \tag{4.24}$$

$$W_{FUEL\,Dtms} = W^o_{FUEL} + \sum_{i=1}^{n}\left(\lambda_{Dtms_i}D_{TMS_i}\right) \tag{4.25}$$

$$W_{FUEL\,\dot{E}tms-ecs} = W^o_{FUEL} + \sum_{i=1}^{n}\left(\lambda_{\dot{E}tms-ecs_i}\dot{E}_{TMS-ECS_i}\right) \tag{4.26}$$

$$W_{FUEL\,Wtms} = W^o_{FUEL} + \sum_{i=1}^{n}\left(\lambda_{Wtms_i}W_{TMS}\right) \tag{4.27}$$

where the reference fuel weight W^o_{FUEL} has been set to correspond to the case with no power extraction, TMS drag or weight, and TMS energy exchange with the ECS.

To obtain the impact of these factors on the system-level objective function, for example, the gross takeoff weight, equation (3.1) in *Chapter 3* is solved (i.e. iterated on W_{TO} until convergence is achieved) with the fuel weight values given by equations (4.24) to (4.27). Thus, the increase in the gross take-off weight due to the ECS coupling functions are given by

$$\Delta W_{TO\,\dot{E}tms-ps} = W_{TO}(W_{FUEL\,\dot{E}tms-ps}) - W_{TO}(W^o_{FUEL}) \tag{4.28}$$

$$\Delta W_{TO\,Dtms} = W_{TO}(W_{FUEL\,Dtms}) - W_{TO}(W^o_{FUEL}) \tag{4.29}$$

$$\Delta W_{TO\,\dot{E}tms-ecs} = W_{TO}(W_{FUEL\,\dot{E}tms-ecs}) - W_{TO}(W^o_{FUEL}) \tag{4.30}$$

$$\Delta W_{TOWtms} = W_{TO}(W_{FUELWtms}) - W_{TO}(W^{o}_{FUEL}) \tag{4.31}$$

Note that the choice in the above equations of the rate energy as opposed to, for example, exergy for power and force as opposed to, for example, energy for drag is justified on the basis that the shadow prices for these coupling functions increase monotonically and linearly with this choice of variables.

TMS System-Level, Unit-Based Synthesis / Design Optimization Problem

$$\text{Minimize} \quad \Delta W_{TOTMS} = \Delta W_{TO\dot{E}tms-ps} + \Delta W_{TODtms} + \Delta W_{TO\dot{E}tms-ecs} + \Delta W_{TOWtms} \tag{4.32}$$

w.r.t. $\left\{\vec{X}_{TMS}, \vec{Y}_{TMS}\right\}$

subject to the inequality constraints given in Table 4.4. as well as the equality constraints of the TMS model.

TMS System-Level, Unit-Bases Fuel Consumption Optimization Problem

Minimize

$$\Delta W_{FUELTMS} = \sum_{i=1}^{n}\left(\lambda_{\dot{E}tms-ps_i}\dot{E}_{TMS-PSi} + \lambda_{Dtms\,i}D_{TMSi} + \lambda_{\dot{E}tms-ecs\,i}\dot{E}_{TMS-ECSi} + \lambda_{Wwtms\,i}W_{TMS}\right) \tag{4.33}$$

w.r.t. $\left\{\vec{X}_{TMS}, \vec{Y}_{TMS}\right\}$

subject to the same constraints as in problem (4.32).

TMS System-Level, Unit-Based Total Cost Optimization Problem

$$\text{Minimize } \Delta C_{TTMS} = C^{P}_{TMS} + \left(\Delta C_{FUEL} + \Delta C_{SS} + \Delta C_{ECS} + \Delta C_{PS}\right)_{TMS} \tag{4.34}$$

subject to the same constraints as in problem (4.32).

where the ΔC_{TTMS} is increase in the system's total cost due to the ECS. In the above equation, C^{P}_{TMS} is the capital cost; $\Delta C_{FUELTMS}$ is the cost of the extra fuel due to the TMS penalties (power extraction, ram drag, and TMS weight); and ΔC_{SSTMS}, ΔC_{ECSTMS} and ΔC_{PSTMS} are the extra cost of the SS, ECS and the PS, respectively.

4.3 PS Unit-Level Design Optimization Problem Definition

The following types were selected for various of the PS components:

- Inlet: 2D external compression
- Nozzle: 2-D convergent-divergent
- Combustor: single-dome
- Mixer: Forced mechanical mixer.

The fan and high-pressure compressor are designed with constant tip radius. Both of these components have inlet guide vanes (variable in the case of the high pressure compressor (HPC)). The high-pressure turbine (HPT) and low-pressure turbine (LPT) have constant mean and tip radii, respectively. They use metallic blades. In addition, some important geometric, thermodynamic and aerodynamic decision variables held fixed during the optimization for the rotating turbo-machinery are given in Table 4.4. The decision variables and inequality constraints are given in Table 4.5.

The number of stages for the fan and HPC are calculated by the engine sizing code (WATE) based on the design pressure ratio. The HPT and LPT have one stage each.

Table 4.4. Some important thermodynamic, geometric and aerodynamic parameter values for the PS optimization.

Parameter	fan	HPC	Parameter	HPT	LPT
$Mach_{in}$	0.50	0.45	$Mach_{in}$	0.20	0.17
$Mach_{exit}$	0.50	0.45	$Mach_{exit}$	0.30	0.32
Max. 1st stage PR	1.80	1.40	Ratio of exit to entrance radius	1.20	1.00
Hub to tip ratio	0.40	0.46	Blade solidity	0.71	1.22
Blade solidity	1.10	0.84	Blade thickness ratio	0.20	0.20
Blade thickness ratio	0.10	0.08	1st stage aspect ratio	1.20	1.20
1st stage aspect ratio	2.00	1.00	Last stage aspect ratio	1.80	1.80
Last stage aspect ratio	1.50	1.00	Blade taper ratio	1.00	1.00
Blade taper ratio	0.556	0.83	Stator solidity	0.92	1.11
Stator solidity	0.80	0.75	Isentropic efficiency	0.90	0.90
Polytropic efficiency Hub Tip	 0.89 0.88	0.88	Turbine loading parameter	0.35	0.30

Table 4.5. PS decision variables and inequality constraints.

Component	Design Decision Variables		Constraints
Fan	α	Fan bypass ratio	$0.3 \le \alpha \le 0.6$
	PR_{fan}	Fan design pressure ratio (tip and hub)	$3.0 \le PR_{fan} \le 5.0$
Compressor	PR_{hpc}	High pressure compressor design pressure ratio	$4.0 \le PR_{hpc} \le 8.0$
Turbine	PR_{hpt}	High pressure turbine design pressure ratio	$1.8 \le PR_{hpt} \le 3.0$
	PR_{lpt}	Low pressure turbine design pressure ratio	$1.8 \le PR_{lpt} \le 3.0$
Mixer	M_{mixer}	Mixer Mach number	$M_{mixer}=0.4$
	Operational Decision Variables		
Compressor	BP_{low}	Low pressure bleed port[9]	$BP_{low}=0,1$
	BP_{high}	High pressure bleed port	$BP_{high}=0,1$
Turbine	T_{it}	Turbine inlet temperature	$T_{it} \le 1778$ K
	Dependent Variables		
Afterburner	T_{aft}	Afterburner temperature[10]	$T_{aft} \le 2000$ K
Fan	φ_{hub}	Fan (hub) % stall margin[8]	$\varphi_{hub} > 10$
	φ_{tip}	Fan (tip) % stall margin[8]	$\varphi_{tip} > 10$
Fan and compressor	PR_{cp}	Overall pressure ratio	$17.0 \le PR_{cp} \le 32.0$
Compressor	φ_{hpc}	Compressor % stall margin[8]	$\varphi_{hpc} > 10$
	N/A	Bleed port selection[8]	$BP_{low}+BP_{high}=1$

As to the coupling functions between the PS and ECS and the PS and TMS, they are as already described in the previous section. Thus, we proceed with the definition of the PS, unit-level design optimization problem[11] which is as follow:

[9] Binary variable: 0 means no bleed air is taken from the bleed port.

[10] This variable takes different values at different mission segments.

[11] Note that we define a unit-level as opposed to a system-level, unit-based optimization problem here since we apply ILGO-A instead of ILGO-B to the PS.

PS Unit-Level Gross Takeoff Weight Problem

$$\text{Minimize} \quad W_{TO} = w_{SS}(W_{TO}) + W_{PS} + W_{ECS} + W_{TMS} + W_{FUEL} + W_{PPAY} + W_{EPAY} \quad (4.35)$$

w.r.t. $\left\{\bar{X}_{PS}, \bar{Y}_{PS}\right\}$

subject to the inequality constraints of Table 4.5. and the equality constraints of the PS and SS models the latter of which include the flight dynamics equation for the entire aircraft system i.e.

$$T_i = \alpha T_{SL} = q_i S\left[K_1\left(\frac{n_i}{q_i}\frac{\beta_i W_{TO}}{S}\right)^2 + C_{D_0} + \frac{D_{ECS_i} + D_{TMS_i}}{q_i S}\right] + \frac{\beta_i W_{TO}}{V_i}\frac{d}{dt}\left(h_i + \frac{V_i^2}{2g}\right) \quad (3.21)$$

Furthermore, note that for this unit-level optimization problem (as opposed to the system-level optimization, equations (3.1)), W_{ECS} and W_{TMS} are held constant, i.e.

$$W_{ECS} - W^o_{ECS} = 0 \quad (4.36)$$

$$W_{TMS} - W^o_{TMS} = 0 \quad (4.37)$$

In addition, the following constraints are also imposed:

$$\dot{m}_{bleed\,i} - \dot{m}^o_{bleed\,i} = 0 \quad (4.38)$$

$$Port_{Bleed\,low_i} - Port^{\,o}_{Bleed\,low_i} = 0 \quad (4.39)$$

$$Port_{Bleed\,high_i} - Port^{\,o}_{Bleed\,high_i} = 0 \quad (4.40)$$

$$\dot{E}_{TMS-PS\,i} - \dot{E}^0{}_{TMS-PS\,i} = 0 \quad (4.41)$$

$$D_{SS} - D^o_{SS} = 0 \quad (4.42)$$

$$D_{TMS} - D^o_{TMS} = 0 \quad (4.43)$$

$$D_{ECS} - D^o_{ECS} = 0 \quad (4.44)$$

Constraints (4.36) through (4.44) indicate that the weight and drag of the ECS and TMS, the bleed air flow rate, the bleed port from which it is taken, the pressure and temperature of the bleed, the power extracted by the TMS and the drag of the SS are set equal to the values indicated with the superscript *0*. These values are set externally. In addition the necessary initial estimates of the weight fractions β_i in equation (3.21) are given by Nicolai (1975) or Mattingly et al. (1987).

PS Unit-Level Fuel Problem

$$\text{Minimize} \quad W_{FUEL} = w_{fuel}(W_{TO}, \vec{X}_{PS}, \vec{Y}_{PS}, mission) \tag{4.45}$$

w.r.t. $\left\{\vec{X}_{PS}, \vec{Y}_{PS}\right\}$

subject to the same constraints as in problem (4.36)

PS Unit-Level Total Cost Problem

$$\text{Minimize} \quad C_T = C_{SS}^P + C_{PS} + C_{ECS} + C_{TMS} + C_{FUEL} \tag{4.46}$$

w.r.t. $\left\{\vec{X}_{PS}, \vec{Y}_{PS}\right\}$,

subject to the same constraints as in problem (4.36)

4.4 Solution Approach using ILGO

The implementation of ILGO-A for the PS and ILGO-B for the ECS and TMS B requires the following steps:

1. The first step is to optimally design the PS (i.e. perform problem (4.35)) for an initial estimate of the necessary amount of bleed air, ECS drag and weight, power extraction, and TMS drag and weight. Since no information about the ECS and TMS exists at this stage of the synthesis design process, estimates are used based on Muñoz and von Spakovsky (2000a) and Figliola (1997). Initial values of the amount of bleed air, power extraction, TMS and ECS drag and weight are estimated from theses references

2. After completing the PS optimal design, the bleed port thermodynamic conditions are calculated at all operating conditions (mission segments). The fuel-based shadow prices for each of the mission legs are calculated as well in this step. The entire modeling/optimization process for the PS design optimization is depicted in Figure 4.2.

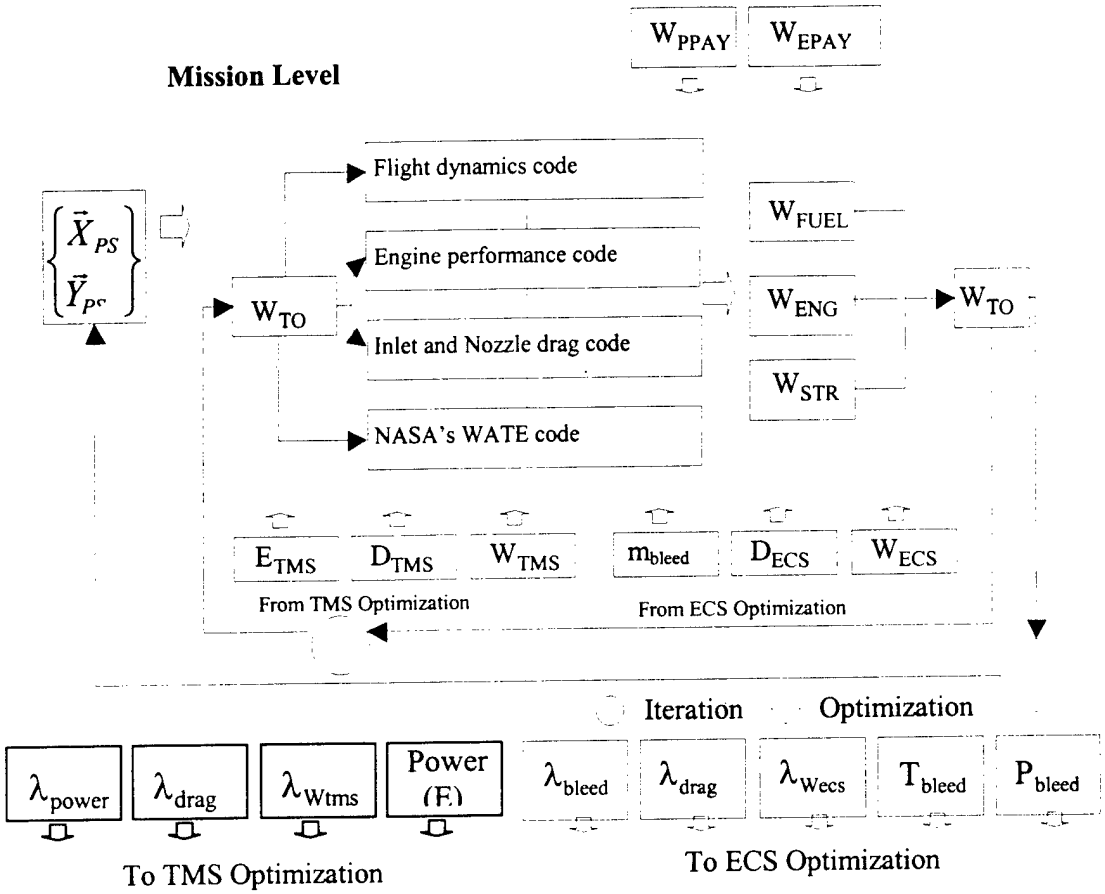

Figure 4.2. The PS unit-level modeling and optimization procedure.

3. The bleed air temperature and pressure values for each of the mission legs along with the shadow prices are used to carry out the synthesis / design optimization of the ECS (problem (4.15)). Based on the previous work of Muñoz and von Spakovsky (2000a) and what was presented in *Chapter 3*, the shadow prices are assumed constant over the synthesis / design space, which allows the coupling function take arbitrarily large or small values[12]. To begin the solution of problem (4.15), the bleed pressure and temperature maps presented by Muñoz and von Spakovsky (1999) are used. The initial coupling functions from the TMS required for the ECS to be optimmaly synthesized / designed are estimated based on Hudson (1975) and Figliola (1997). The total number of variables is 109. Given the large number of variables and the fact that 4 of them are integer for the ECS problem, time decomposition is used in the manner described in Muñoz and von Spakovsky (2000b) and in *Chapter 2*. The work of Muñoz and von Spakovsky (1999) shows that the most demanding operating condition for the ECS and TMS corresponds to the mission segment

[12] Note that this assumption is based on a priori knowledge of the system-level ORS being a hyper plane. For cases where it is not, i.e. it is convex, the assumption must be tightened to include only a part of the synthesis / design space. This, however, simple means that the method will take somewhat longer to converge

with high altitude and subsonic speed. This point is critical because of a combination of relatively low bleed pressures, high cooling temperatures, and low ram air availability. Thus, the selected synthesis / design or reference condition corresponds to the second subsonic cruise climb leg (scc_2) of Table 4.1.

4. The second subsonic cruise climb leg is used to obtain a set of the most promising solutions. Each of these (typically 5) provides values for the ECS synthesis / design decision variables, which are then used in the off-design optimization. At the operational-level, fourteen problems are resolved each with respect to the operational decision variables for each leg. The optimization procedure for the ECS is shown in Figure 4.3.

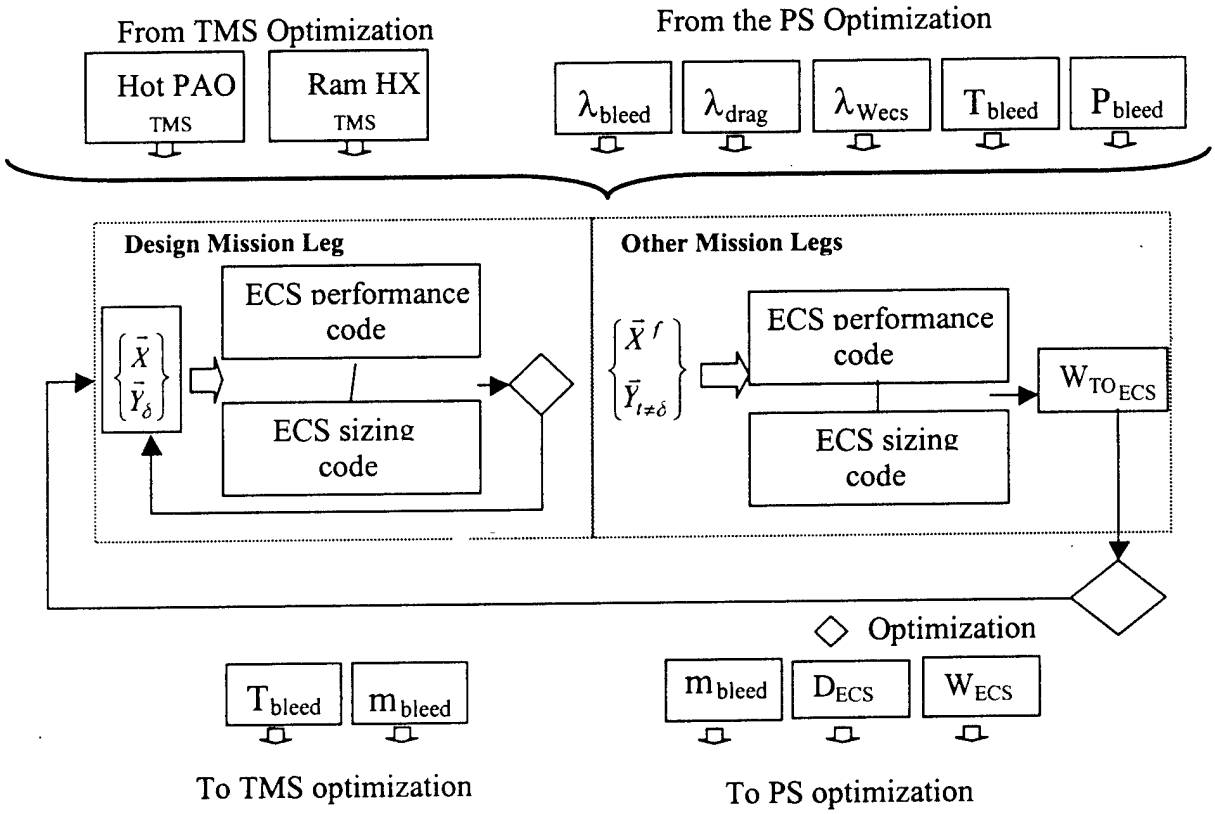

Figure 4.3. ECS system-level, unit-based modeling and optimization procedure.

5. Once completed, the ECS synthesis / design provides updated values for the coupling functions of the ECS. These values a long with the corresponding shadow prices are used to carry out the synthesis / design optimization of the TMS. As in step 3 the shadow prices are held constant. The second subsonic cruise climb leg is used to find a set of the most promising solutions for the

TMS. Afterwards, the operational-level problem is solved. The procedure is shown in Figure 4.4.

6. Once completed, the ECS and TMS syntheses / designs provides updated values for the coupling functions of the ECS and TMS. These values are used in step 1 to optimally redesign the PS. The iterative process continues until no improvement in the system-level objective function is observed.

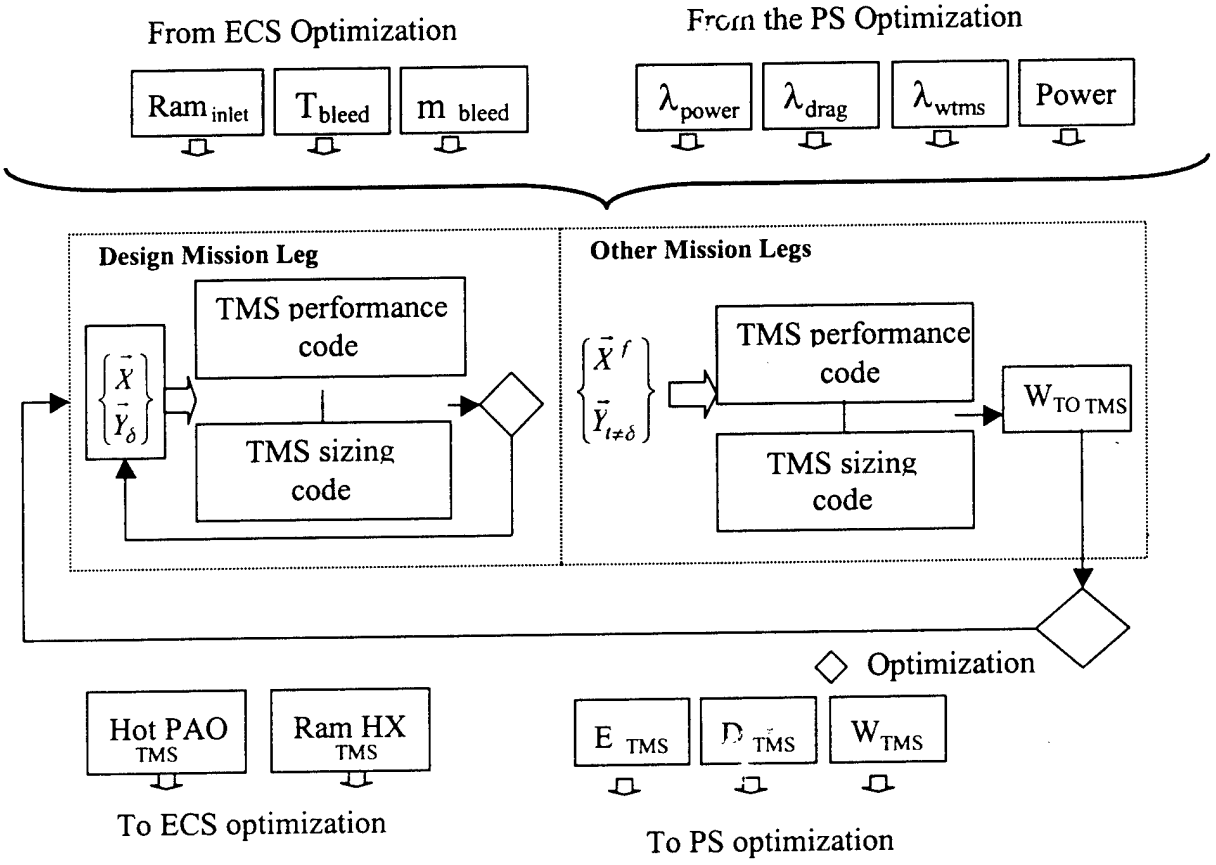

Figure 4.4. TMS system-level, unit-based modeling and optimization procedure.

The procedure described above is the same regardless of whether the objective function is the total take-off gross weight or the fuel consumed to carry out the mission or the total cost. Figure 4.5. shows the coupling function flows between sub-systems and the system optimization scheme.

All of the optimization problems are solved using the commercial optimization package iSIGHT (1999). Each optimization iteration typically consists of two steps. The first uses a Genetic Algorithm (GA) in order to effectively deal with the mixed integer variables and possible local minima problems in each of the sub-system (unit-

level for the PS and system-level, unit-based for the ECS and TMS) optimizations. Each GA optimization run has a minimum population size equal to three times the number of variables with a minimum of 50. The minimum number of iterations for the GA is set to 100 times the population size for the PS and 1000 times the population size for the TMS and the ECS optimization problems. In the first step, the convergence criterion for the calculation of the take-off gross weight is set at 0.2 %. This means that the value of W_{TO} sent to the optimization algorithms has an error of approx. ±200 N. The second step uses the top two or three solutions obtained with the GA to narrow down the best solutions using a gradient-based algorithm (Method of Feasible Directions). For the second step, the convergence criterion on the take-off gross weight calculation is set at 0.1 %.

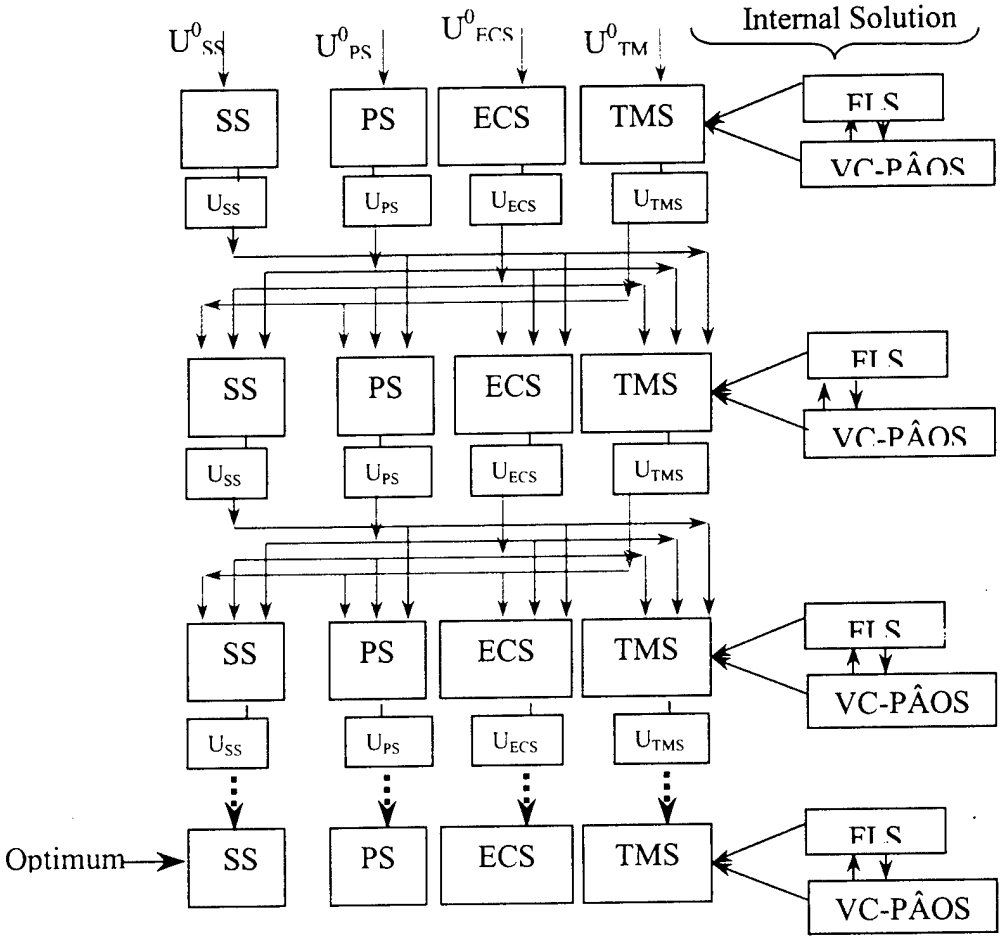

Figure 4.5. System ILGO Optimization Scheme.

CHAPTER 5

5. THERMAL MANAGEMENT SUB-SYSTEM SYNTHESIS / DESIGN MODELING AND OPTIMIZATION

It is common to choose a single operating point (the one with the most stringent requirements) as the synthesis / design point. A system's sub-systems are then optimized with respect to this point using a suitable criterion (gross takeoff weight, fuel consumption, total cost, etc.) for the specified conditions and tested for performance. throughout the whole mission profile. The mission profile of the vehicle corresponding to the TMS being optimized can be seen in Figure 4.1 and Table 4.1. As indicated in *Chapter 4*, The synthesis/design of the TMS (its heat exchangers, compressor, pumps, and the ram air inlet, exit and ducts) is carried out for the second subsonic cruise climbing mission segment in the context of the overall aircraft system (i.e. PS, ECS, TMS and SS) using ILGO. What following a more in-depth look into the modeling and optimization of the TMS itself.

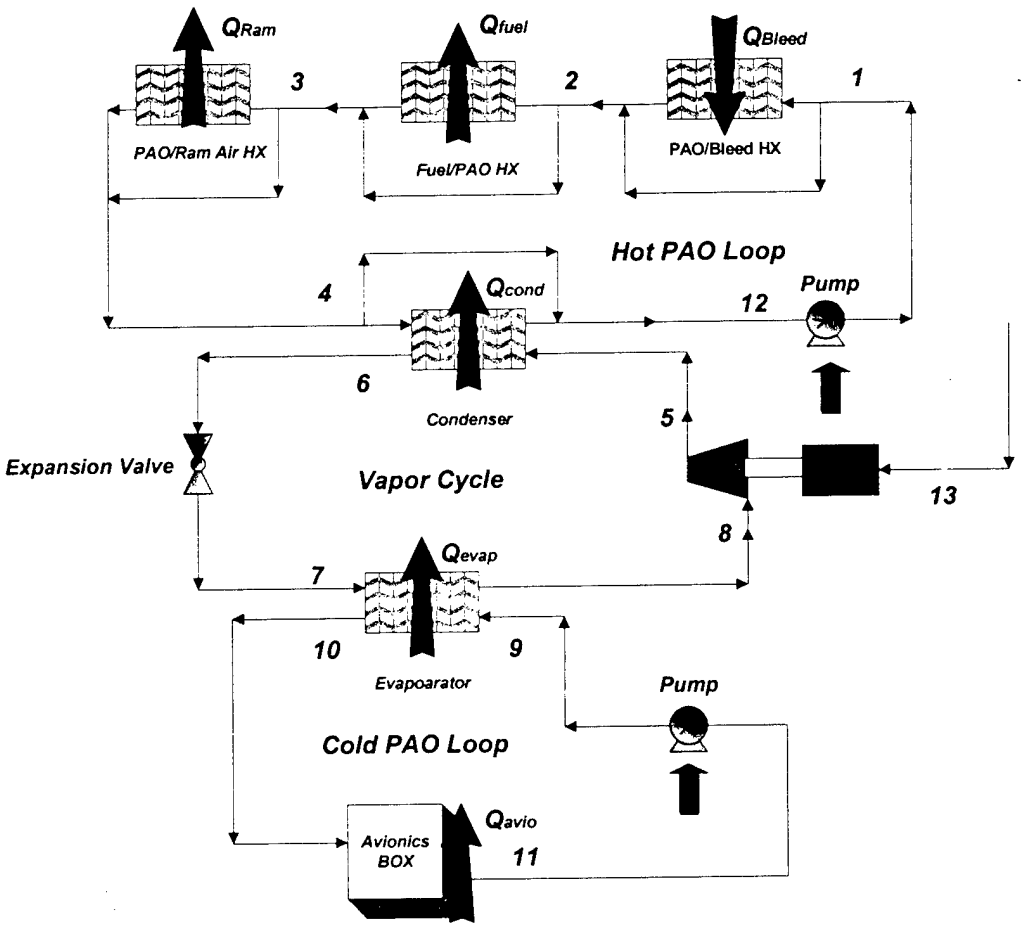

Figure 5.1. Schematic of the VC/PAOS of the TMS.

5.1 Vapor Compression Refrigeration / PAO Loops Sub-system (VC / PAOS)

In order to approach the highly transient behavior exhibited by the TMS, it was decomposed into two new sub-systems, the Vapor Compression Refrigeration / PAO Loops Sub-system (VC / PAOS) and the Fuel Loop Sub-system (FLS). Figure 5.1. shows the VC / PAOS in detail and the connecting streams to the other sub-systems. The energy (exergy) of Q_{fuel}, which connects this sub-system with the FLS, provides the necessary thermodynamic and cost link between the two subsystems. Q_{Bleed} provides the thermodynamic and cost link between the TMS and the ECS, while stream (13) provides the energy (exergy) and cost link between the TMS and the PS. Figure 3.2 in *Chapter 3* shows the physical boundaries between systems and their coupling functions.

The VC / PAOS includes three loops and the ducts that connect them as follow: the cold PAO loop, the vapor cycle, and the hot PAO loop. The cold PAO loop includes an avionics box, a pump, and a heat exchanger (evaporator) which is shared with the vapor compression cycle. The vapor cycle includes, in addition to the evaporator, a centrifugal compressor, an expansion valve, and a heat exchanger (condenser) which is shared with the hot PAO loop. The hot PAO loop includes, in addition to the condenser, a pump, a ram heat exchanger, a bleed air / PAO heat exchanger, which interconnects the ECS and the TMS, and a fuel / PAO heat exchanger which links the VC / PAOS with the FLS.

The only PS product being used directly by the VC / PAOS is the power required to drive the vapor compressor and PAO loops pumps. This power and the VC /PAOS drag penalty also represent feedbacks to the PS as do the VC/PAOS weight. Each translates into excess thrust. The FLS cooling capacity is used as resource by the VC / PAOS. Finally, An additional feedback is the energy transferred from the ECS to the VC / PAOS through the bleed / PAO heat exchanger. All of these products and feedbacks for the basis for the coupling functions connecting the VC/PAOS with the other sub-system.

Let us now define the shadow prices of these feedbacks (power taken from the PS, energy transferred to the FLS) and products (VC/PAOS weight and drag, and energy transferred from the ECS) for different mission legs. The shadow prices based on the optimum fuel weight for a fixed leg *i* are given by

$$\lambda_{\dot{E}vc/paos-ps_i} = \frac{\partial W^*_{FUEL_i}}{\partial \dot{E}_{VC/PAOS-PS}} \tag{5.1}$$

$$\lambda_{Dvc/paos_i} = \frac{\partial W^*_{FUEL_i}}{\partial D_{VC/PAOS}} \tag{5.2}$$

$$\lambda_{Wvc/paos_i} = \frac{\partial W^*_{FUEL_i}}{\partial W_{VC/PAOS}} \tag{5.3}$$

$$\lambda_{\dot{E}ecs-vc/paos_i} = \frac{\partial W^*_{FUEL_i}}{\partial \dot{E}_{ECS-VC/PAOS}} \tag{5.4}$$

$$\lambda_{\dot{E}fls-vc/paos_i} = \frac{\partial W^*_{FUEL_i}}{\partial \dot{E}_{FLS-VC/PAOS}} \tag{5.5}$$

where the weight of the fuel at the i_{th} leg is given by equation (4.5) and the fuel consumed due to the VC/PAOS can then be written as

$$W_{FUEL_{vc/paos}} = \sum_{i=1}^{n} \left(\begin{array}{l} \lambda_{\dot{E}vc/paos-ps_i} \dot{E}_{VC/PAOS-PS_i} + \lambda_{Dvc/paos_i} D_{VC/PAOS_i} + \lambda_{Wvc/paos_i} W_{VC/PAOS} + \\ \lambda_{\dot{E}ecs-vc/paos_i} \dot{E}_{ECS-VC/PAOS_i} + \lambda_{\dot{E}fls-vc/paos_i} \dot{E}_{FLS-VC/PAOS_i} \end{array} \right) \tag{5.6}$$

It has been assumed in equation (5.6) that the shadow prices are constant over the ranges of power, drag, weight and rate of energy exchange of the VC / PAOS. Equation (5.6) can be written as in Chapter 4 with respect to the reference fuel weight W^o_{FUEL}, i.e.

$$W_{FUEL\,\dot{E}vc/paos-ps} = W^o_{FUEL} + \sum_{i=1}^{n} \left(\lambda_{\dot{E}vc/paos-ps_i} \dot{E}_{VC/PAOS-PS_i} \right) \tag{5.7}$$

$$W_{FUEL\,Dvc/paos} = W^o_{FUEL} + \sum_{i=1}^{n} \left(\lambda_{Dvc/paos_i} D_{VC/PAOS_i} \right) \tag{5.8}$$

$$W_{FUEL\,Wvc/paos} = W^o_{FUEL} + \sum_{i=1}^{n} \left(\lambda_{Wvc/paos_i} W_{VCR/PAOS} \right) \tag{5.9}$$

$$W_{FUEL\,\dot{E}ecs-vc/paos} = W^o_{FUEL} + \sum_{i=1}^{n} \left(\lambda_{\dot{E}ecs-vc/paos_i} \dot{E}_{ECS-VC/PAOS_i} \right) \tag{5.10}$$

$$W_{FUEL\,\dot{E}fls-vc/paos} = W^o_{FUEL} + \sum_{i=1}^{n} \left(\lambda_{\dot{E}fls-vc/paos_i} \dot{E}_{FLS-VC/PAOS_i} \right) \tag{5.11}$$

where the reference fuel weight W^o_{FUEL} has been set to correspond to the case with no power extraction, no VC / PAOS drag or weight, and no energy transfer from or toward any other sub-system.

To obtain the impact of these factors on the system-level objective function, for example the gross take-off weight, problem (3.1) is solved (i.e. iterated on W_{TO} until convergence is achieved) with the fuel weight values given by equations (5.7) to (5.8). Thus, the increase in the gross takeoff weight due to the VCR/PAOS products and feedback are given by

$$\Delta W_{TO\,\dot{E}vc/\,paos-ps} = W_{TO}(W_{FUEL\,\dot{E}vc/\,paos-ps}) - W_{TO}(W^{o}_{FUEL}) \tag{5.12}$$

$$\Delta W_{TO\,Dvc/\,paos} = W_{TO}(W_{FUEL\,Dvc/\,paos}) - W_{TO}(W^{o}_{FUEL}) \tag{5.13}$$

$$\Delta W_{TO\,Wvc/\,paos} = W_{TO}(W_{FUEL\,Wvc/\,paos}) - W_{TO}(W^{o}_{FUEL}) \tag{5.14}$$

$$\Delta W_{TO\,\dot{E}fls-vc/\,paos} = W_{TO}(W_{FUEL\,\dot{E}fls-vc/\,paos}) - W_{TO}(W^{o}_{FUEL}) \tag{5.15}$$

$$\Delta W_{TO\,\dot{E}ecs-vc/\,paos} = W_{TO}(W_{FUEL\,\dot{E}ecs-vc/\,paos}) - W_{TO}(W^{o}_{FUEL}) \tag{5.16}$$

With the above comments and taking into account that there are additional feedbacks and products being used by the VC/PAOS, the system-level, unit-based synthesis / design optimization problem is set up as follows:

VC/PAOS System-Level, Unit-Based Gross Takeoff Weight Optimization Problem

$$\text{Minimize} \quad \Delta W_{TO\,vc/\,paos} = \begin{pmatrix} \Delta W_{TO\,\dot{E}vc/\,paos-ps} + \Delta W_{TO\,Dvc/\,paos} + \Delta W_{TO\,Wvc/\,paos} \\ + \Delta W_{TO\,\dot{E}ecs-vc/\,paos} + \Delta W_{TO\,\dot{E}fls-vc/\,paos} \end{pmatrix} \tag{5.17}$$

w.r.t. $\left\{\vec{X}_{VC/\,PAOS}, \vec{Y}_{VC/\,PAOS}\right\}$

subject to the inequality constraints given in Table 5.1. as well as the equality constraints of the VC/PAOS model.

VC/PAOS System-Level, Unit-Based Fuel Consumption Optimization Problem

Minimize

$$\Delta W_{FUEL\,vc/\,paos} = \sum_{i=1}^{n} \begin{pmatrix} \lambda_{\dot{E}vc/\,paos-ps_i} \dot{E}_{VC/\,PAOS-PS\,i} + \lambda_{Dvc/\,paos_i} D_{VC/\,PAOS\,i} + \lambda_{Wvc/\,paos_i} W_{VC/\,PAOS} \\ + \lambda_{\dot{E}ecs-vc/\,paos_i} \dot{E}_{ECS-VC/\,PAOS\,i} + \lambda_{\dot{E}fls-vc/\,paos_i} \dot{E}_{FLS-VC/\,PAOS\,i} \end{pmatrix} \tag{5.18}$$

w.r.t. $\left\{\vec{X}_{VC/\,PAOS}, \vec{Y}_{VC/\,PAOS}\right\}$

subject to the same constraints as in problem (5.17).

VC/PAOS System-Level, Unit-Based Total Cost Optimization Problem

$$\text{Minimize } \Delta C_{T\,vc/\,paos} = C^{P}{}_{VC/\,PAOS} + \left(\Delta C_{FUEL} + \Delta C_{SS} + \Delta C_{PS} + \Delta C_{ECS} + \Delta C_{FLS}\right)_{VC/\,PAOS} \tag{5.19}$$

subject to the same constraints as in problem (5.17).

$\Delta C_{T\,vc/paos}$ is the increase in the system's total cost due to the VC/PAOS. In the above equation, $C^{P}_{VC/PAOS}$ is the capital cost; $\Delta C_{FUEL\,vc/paos}$ is the cost of the extra fuel due to the VC/PAOS penalties (power, ram drag, and VC/PAOS weight, and rate of FLS energy exchange); $\Delta C_{SS\,vc/paos}$, $\Delta C_{PS\,vc/paos}$, $\Delta C_{ECS\,vc/paos}$ and $\Delta C_{FLS\,vc/paos}$ are the extra cost of the SS, PS, ECS and FLS respectively.

From Muñoz and von Spakovsky (1999) the shadow prices in equation. (5.2.) and equation. (5.3) are correctly considered as constant, since they are of the same nature as their counterparts in the ECS. However, the assumption that the shadow prices for the power exchange and energy exchange with other subsystems must be proved. To this end, the effect of power extraction and energy exchange variations on total fuel consumption for a turbofan engine was studied. An engine deck from one of our industrial partners, which dynamically simulates the real performance characteristics of an aircraft engine, was used[1]. The model of an F-109 turbofan engine to perform the calculations was used.

The functions that describe the shadow prices of extracted power and energy exchange are dependent on flight conditions and on the aerodynamic and thermodynamic behavior of the main engine of a particular aircraft. When the shadow prices are calculated on a unit cost basis, i.e. in terms of mass flow rates of fuel, they can be seen as the penalties that a given sub-system imposes on the overall aircraft system.

Figure 5.2 shows the change in the non-dimensional total fuel consumption as a function of the additional power required for the VC/PAOS, while keeping the energy exchange and the additional thrust constant. Figure 5.3. shows the changes in the non-dimensional total fuel consumption as a function of the energy exchange, while keeping constant the required power and additional thrust. The non-dimensional total fuel consumption is defined as

$$W_f^{*} = \frac{W_f - W_{f_o}}{W_{f_o}} \tag{5.20}$$

where W_{f_o} is the total fuel consumption without power extraction or energy transfer and W_f is the fuel consumption including the power and energies penalties. The slope of the curves (shadow prices) in Figures 5.2 and 5.3 clearly indicates that the assumption of constant shadow prices for power extraction and energy is fully justified. Prior knowledge of the functions describing the shadow prices as a function of altitude and Mach number allows one to effectively decompose the system and optimize the VC/PAOS and other sub-systems without simultaneously simulating during the optimization process the PS.

[1] Note that industrial engine decks such as the one we have employed use values from average engines and employ a number of simplifying assumptions and, therefore, fail to capture all the important factors involved.

Table 5.1. VC/PAOS decision variables, fixed parameters, and inequality constraints.

Component	Decision variable		Constraints
	Design Variables		
Bleed air / PAO heat exchanger	L_c	Cold-side length (m)	$0.1<L_r<0.9$
	L_h	Hot-side length (m)	$0.05<L_b<0.9$
	L_n	Non-flow length (m)	$0.1<L_n<0.9$
	No.fin	Number of fins per inch	$11<No.fin<20$
Condenser	L_c	Cold-side length (m)	$0.1<L_r<0.9$
	L_h	Hot-side length (m)	$0.05<L_b<0.9$
	L_n	Non-flow length (m)	$0.1<L_n<0.9$
	No.fin	Number of fins per inch	$11<No.fin<20$
Evaporator	L_c	Cold-side length (m)	$0.1<L_r<0.9$
	L_h	Hot-side length (m)	$0.05<L_b<0.9$
	L_n	Non-flow length (m)	$0.1<L_n<0.9$
	No.fin	Number of fins per inch	$11<No.fin<20$
Ram air / hot PAO heat exchanger	L_c	Cold-side length (m)	$0.1<L_r<0.9$
	L_h	Hot-side length (m)	$0.05<L_b<0.9$
	L_n	Non-flow length (m)	$0.1<L_n<0.9$
	No.fin	Number of fins per inch	$11<No.fin<20$
	Operational Variables		
Vapor Compressor	*Pr*	Pressure Ratio Vapor Compressor	$1<Pr<9$
	m_v	Vapor mass flow(kg/s)	$0.2<m_v<2.2$
Hot PAO cycle	m_{HPAO}	Hot PAO loop mass flow	$0.2<m_{HPAO}<3.5$
	V_5	Fuel / hot PAO heat exchanger bypass valve position	$0<V_5<0.3$
	V_4	Bleed Air / hot PAO heat exchanger bypass valve position	$0<V_4<0.3$
	V_2	Vapor / hot PAO heat exchanger bypass valve position	$0<V_2<0.3$
	Synthesis Variables		
Ram air / hot PAO heat exchanger	*onoff*	Place or not Ram air / hot PAO heat exchanger	0 or 1
	Fixed Parameter		
Fuel / PAO Heat Exchanger	L_c	Cold-side length (m)	$0.1<L_r<0.9$
	L_h	Hot-side length (m)	$0.05<L_b<0.9$
	L_n	Non-flow length (m)	$0.1<L_n<0.9$
	m_{fuel}	Fuel side mass flow (kg/s)	$0.3< m_{fuel}<4.0$
	No.fin	Number of fins per inch	$11<No.fin<20$
Ram Air Inlet	A_i	Area of inlet, outlet (cm^2)	$95<A_i<290$
Bleed Air Inlet	T_{bi}	Bleed air inlet temperature (K)	$380<T_{bi}<480$
	Derived variables		
Heat Exchangers	R_{er}	Reynolds number, ram air-side	$R_{er}<5000$
	R_{eb}	Reynolds number, bleed air-side	$R_{eb}<5000$
	R_{eb}	Reynolds number, fuel-side	$R_{eb}<5000$

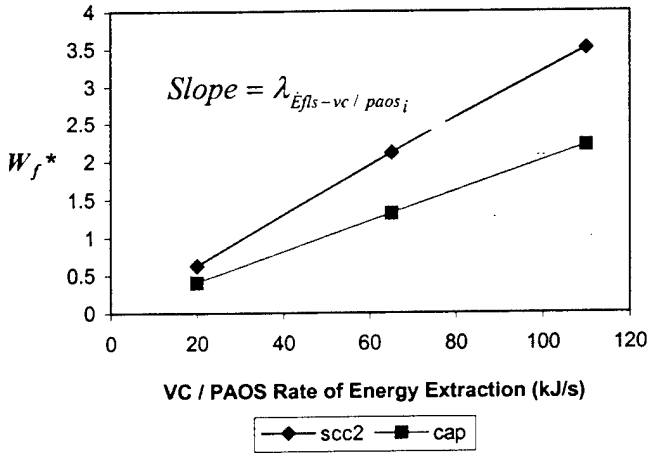

Figure 5.2. Non-dimensional total fuel consumption versus power extraction.

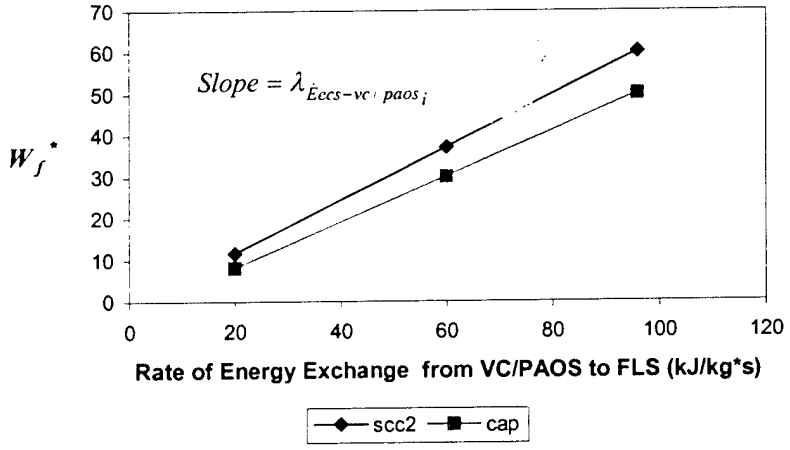

Figure 5.3. Non-dimensional total fuel consumption vs. rate of energy exchange.

The types of heat exchangers considered for the VC/PAOS and FLS sub-systems are compact heat exchangers. Due to their low weight to capacity ratio, these exchangers are commonly used in aircraft energy systems. There is a wide range of available geometries and types of fins that can be used (see for example the classic book on compact heat exchangers by Kays and London, 1998). Here we arbitrarily select offset-strip fins for the design of the heat exchangers in the TMS since this is one of the most commonly used plate-fin geometries.

In general, once the particular type and geometry of the fin are selected, the only remaining degrees of freedom are the height, width and length of the heat exchanger core and the number of fins per inch. It is assumed here that the design of the manifolds and other accessories has no effect on heat transfer performance. A model for estimating the core weight is given in Muñoz and von Spakovsky (1999). This model correlates extremely well with observed mass values. A linear least squares equation that relates core mass to total mass (i.e. core plus manifolds and insulation) was used to estimate the total heat exchanger weight. The heat transfer and pressure drop models used are based on the work of Shah (1981) and Kays and London (1998) as shown in the same work. Both sides of the heat exchangers have one pass unless stated otherwise.

As can be seen from Table 5.1., decision variables and inequality constraints other than those for the heat exchangers are also considered in the synthesis / design optimization, i.e. those for the ram air intake. For this component, it was assumed that the VC / PAOS and the FLS use scoop-type of ram air inlets. The mass flow rate of air entering the inlet is given by

$$\dot{m} = k\,\rho_{\infty} V_{\infty} A_i \tag{5.21}$$

where the subscript ∞ refers to ambient conditions and k is a factor which depends on whether the flight speed is subsonic or supersonic. The performance of the supersonic inlet is based on a typical scoop-type of inlet. The ducts and exit were modeled using a compressible model with a typical friction factor of 0.01. Details of the thermodynamic and physical model are given in Muñoz and von Spakovsky (1999). The area of the ducts and exit were assumed to be equal to the area of the inlet. The ducts connecting the ram air inlet and the heat exchangers were assumed to have a length of 2 m and be made of an aluminum alloy with a wall thickness of 0.1 cm.

As indicated in Table 5.1 there are 23 decision variables for the VC/PAOS, of which six are operational variables. Whether or not to place a PAO / ram heat exchanger into the hot POA loop is a synthesis decision variable, which is used as a binary variable in the optimization problem. Figure 5.4. shows the VC / PAOS optimization procedure.

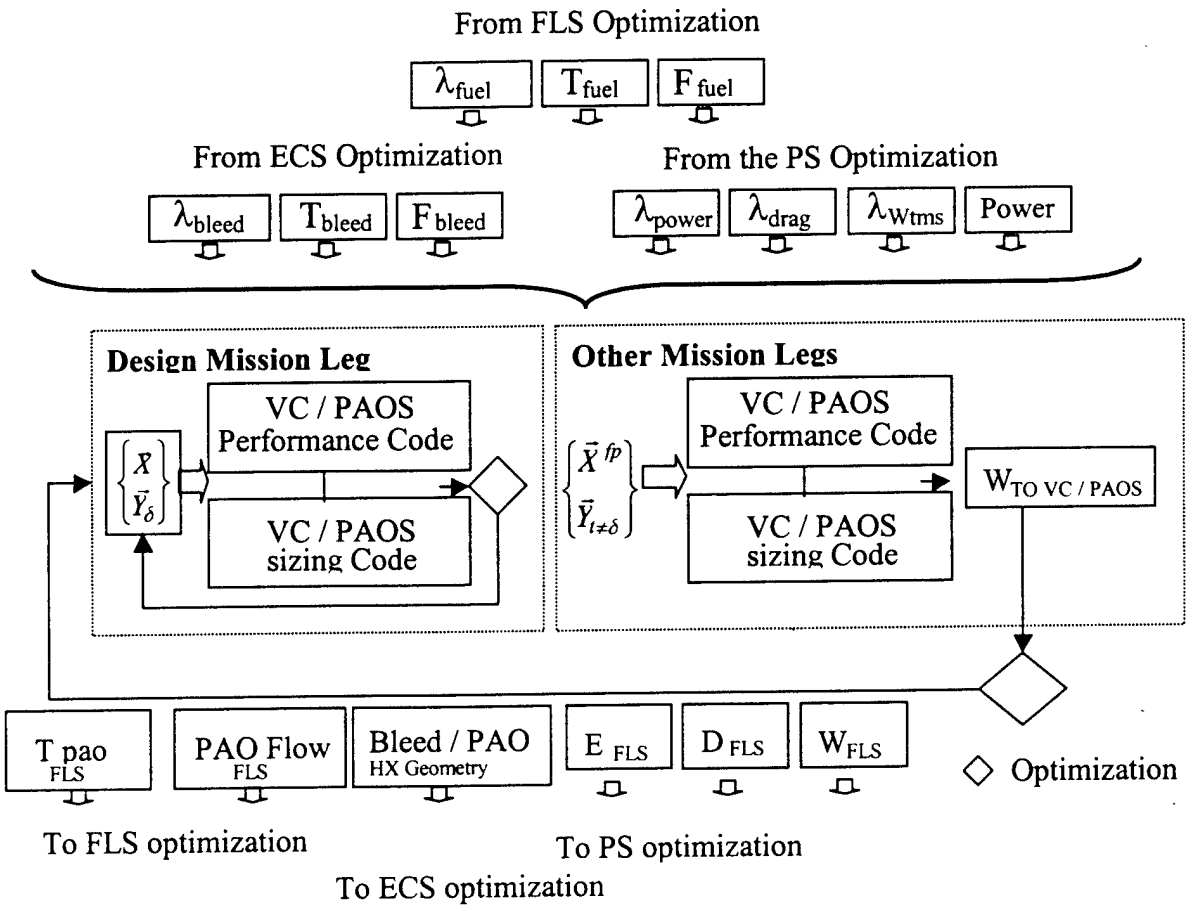

Figure 5.4. The VC / PAOS system-level, unit-based modeling and optimization procedure.

5.2 Fuel Loop Sub-system (FLS)

The FLS is composed of a fuel tank, which serves as a sink for the heat taken from the VC / PAOS, a fuel / hot PAO heat exchanger, a fuel / oil heat exchanger, a fuel / hydraulic heat exchanger, a fuel / ram heat exchanger, a pump, and ducts to connect the different components. This sub-system is used to extract heat from different sub-systems (i.e. the VC / PAOS, the PS, and the hydraulic sub-systems). In order to do this, the FLS consumes resources from the PS. The different subsystems linked to the FLS use its cooling capacity as a resource, which must be taken into account in their respective synthesis / design optimization problems. Here we consider the FLS taking resources only from the PS. The feedbacks from the VC / PAOS, the PS, and the hydraulic sub-systems are the loads imposed on the FLS, which change according with the different mission segments.

As with the VC/PAOS, the second subsonic climb was selected as the base for the synthesis / design optimization. The best five cases are employed to solve for the operational optimization problem through the entire mission, which is not only subject to heat load constraints but also to the fuel tank maximum temperature. The operational variables to be determined by the optimization are the fuel mass flow, which is time dependent, as well as the hydraulic mass flow and the oil mass flow. The initial fuel tank temperature range is based on data from Hudson et al. (1975).

The thermodynamic and physical model for the heat exchangers, the pump, and ram air inlet are the same as the ones for the VC / PAOS. Table 5.2 shows the operational and synthesis / design decision variables, the fixed parameter, which are input from the VC / PAOS, the derived variables and the inequality constraints.

The only PS product being used directly by the FLS is the power extracted to drive the fuel pump. This power, and the FLS drag penalty also represent feedbacks to the PS as do the FLS weight. Each translates into excess thrust. The VC / PAOS heat load represents an additional feedback. The two subsystems being optimized, the FLS and VC / PAOS, make use of the same source for extracted power (i.e. PS), the shadow price for extracted power ($\lambda_{\dot{E}vc/paos-ps}$) appearing in the optimization problem definitions is the same for both sub-systems. Moreover, the penalties produced by the drag and weight due to the FLS and VC / PAOS are of the same nature as those produce by the ECS. Therefore, the ECS shadow prices (λ_D *and* λ_W) due to drag and weight can be used for the FLS synthesis / design optimization.

Table 5.2. FLS decision variables, fixed parameters, and inequality constraints.

Component	Decision variable		Constraints
	Design Variables		
Fuel / Oil heat Exchanger	L_c	Cold-side length (m)	$0.1<L_r<0.9$
	L_h	Hot-side length (m)	$0.05<L_b<0.9$
	L_n	Non-flow length (m)	$0.1<L_n<0.9$
	No.fin	Number of fins per inch	$11<No.fin<20$
Fuel / PAO Heat Exchanger	L_c	Cold-side length (m)	$0.1<L_r<0.9$
	L_h	Hot-side length (m)	$0.05<L_b<0.9$
	L_n	Non-flow length (m)	$0.1<L_n<0.9$
	No.fin	Number of fins per inch	$11<No.fin<20$
Fuel / Ram air heat exchanger	L_c	Cold-side length (m)	$0.1<L_r<0.9$
	L_h	Hot-side length (m)	$0.05<L_b<0.9$
	L_n	Non-flow length (m)	$0.1<L_n<0.9$
	No.fin	Number of fins per inch	$11<No.fin<20$
Fuel / hydraulic heat exchanger	L_c	Cold-side length (m)	$0.1<L_r<0.9$
	L_h	Hot-side length (m)	$0.05<L_b<0.9$
	L_n	Non-flow length (m)	$0.1<L_n<0.9$
	No.fin	Number of fins per inch	$11<No.fin<20$
Ram Air Inlet	A_i	Area of inlet, outlet (cm^2)	$50<A_i<290$
	Operational Variables		
Fuel loop	M_F	Initial Fuel mass flow(kg/s)	$0.3<m_F<4$
	mo	Oil mass flow(kg/s)	$0.3<m_F<4$
	mh	Hydraulic mass flow(kg/s)	$0.3<m_F<4$
	T tank	Initial fuel tank temperature (K)	300<T tank<320
	Fixed Parameter		
Hot PAO loop	m_{HPAO}	Hot PAO loop mass flow	
	Tin	PAO inlet temperature to Fuel / hot PAO heat exchanger	
	Tout	PAO outlet temperature to Fuel / hot PAO heat exchanger	
Bleed Air Inlet	T_{bi}	Bleed air inlet temperature (K)	
	Derived variables		
Fuel Tank	T_{Ti}	Fuel tank initial temperature (K)	$300<T_{Ti}<320$
Heat Exchangers	R_{er}	Reynolds number, ram air-side	$R_{er}<5000$
	R_{eb}	Reynolds number, oil air-side	$R_{eb}<5000$
	R_{eh}	Reynolds number, hydraulic-side	$R_{eh}<5000$

Let us now define the shadow prices of the coupling functions (products and feedbacks) for different mission legs. The shadow prices based on the optimum fuel weight for a fixed leg i are given by

$$\lambda_{\dot{E}fls-ps_i} = \frac{\partial W^*_{FUEL_i}}{\partial \dot{E}_{FLS-PS}} \tag{5.22}$$

$$\lambda_{Dfls_i} = \frac{\partial W^*_{FUEL_i}}{\partial D_{FLS}} \tag{5.23}$$

$$\lambda_{Wfls_i} = \frac{\partial W^*_{FUEL_i}}{\partial W_{FLS}} \tag{5.24}$$

$$\lambda_{\dot{E}vc/paos-fls_i} = \frac{\partial W^*_{FUEL_i}}{\partial \dot{E}_{VC/PAOS-FLS}} \tag{5.25}$$

where as before the weight of the fuel at the i_{th} leg is given by equation (4.5) and the fuel consumed due to the FLS can then be written as

$$W_{FUEL_{FLS}} = \sum_{i=1}^{n}\left(\lambda_{\dot{E}fls-ps_i}\dot{E}_{FLS-PS_i} + \lambda_{Dfls_i}D_{FLS_i} + \lambda_{Wfls_i}W_{FLS} + \lambda_{\dot{E}vc/paos-fls_i}\dot{E}_{VC/PAOS-FLS_i}\right) \tag{5.26}$$

As before it is assumed in equation (5.26) that the shadow prices are constant over the ranges of power, drag, weight, and rate of energy exchange of the FLS. Equation (5.26) can be written as in *Chapter 4* with respect to the reference fuel weight W^o_{FUEL}, i.e.

$$W_{FUEL\,\dot{E}fls-ps} = W^o_{FUEL} + \sum_{i=1}^{n}\left(\lambda_{\dot{E}fls-ps_i}\dot{E}_{FLS-PS_i}\right) \tag{5.27}$$

$$W_{FUEL\,Dfls} = W^o_{FUEL} + \sum_{i=1}^{n}\left(\lambda_{Dfls_i}D_{FLS_i}\right) \tag{5.28}$$

$$W_{FUEL\,Wfls} = W^o_{FUEL} + \sum_{i=1}^{n}\left(\lambda_{Wfls_i}W_{FLS}\right) \tag{5.29}$$

$$W_{FUEL\,\dot{E}vc/paos-fls} = W^o_{FUEL} + \sum_{i=1}^{n}\left(\lambda_{\dot{E}vc/paos-fls_i}\dot{E}_{VC/PAOS-FLS_i}\right) \tag{5.30}$$

where the reference fuel weight W^o_{FUEL} has been set to correspond to the case with no power extraction, FLS drag or weight, and no energy transfer from or toward any other subsystem.

To obtain the impact of these factors on the system-level objective function, for example, the gross take-off weight, problem (3.1) is solved (i.e. iterated on W_{TO} until convergence is achieved) with the fuel weight values given by equations (5.27) to (5.30). Thus, the increase in the gross take-off weight due to the FLS products and feedback are given by

$$\Delta W_{TO\,\dot{E}fls-ps} = W_{TO}(W_{FUEL\,\dot{E}fls-ps}) - W_{TO}(W^{o}_{FUEL}) \tag{5.31}$$

$$\Delta W_{TO\,Dfls} = W_{TO}(W_{FUEL\,Dfls}) - W_{TO}(W^{o}_{FUEL}) \tag{5.32}$$

$$\Delta W_{TO\,Wfls} = W_{TO}(W_{FUEL\,Wfls}) - W_{TO}(W^{o}_{FUEL}) \tag{5.33}$$

$$\Delta W_{TO\ \dot{E}vc\ /\ paos\ -\ fls} = W_{TO}(W_{FUEL\ \dot{E}vc\ /\ paos\ -\ fls}) - W_{TO}(W^{o}_{FUEL}) \tag{5.34}$$

The constant behavior of the power extraction, drag and weight shadow prices has been already demonstrated. The assumption the VC/PAOS rate of energy transfer shadow price is constant was demonstrated in the previous section (Figure 5.3) and will be demonstrated further in this section. With the above comments the system-level, unit-based synthesis / design optimization problem is set up as follows:

FLS System-Level, Unit-Based Fuel Consumption Optimization Problem

$$\text{Minimize} \quad \Delta W_{TO\,fls} = \Delta W_{TO\,\dot{E}fls-ps} + \Delta W_{TO\,Dfls} + \Delta W_{TO\,Wfls} + \Delta W_{TO\,\dot{E}vc/paos-fls} \tag{5.35}$$

$$\text{w.r.t.} \quad \left\{\vec{X}_{FLS}, \vec{Y}_{FLS}\right\}$$

subject to the inequality constraints given in Table 5.2, the equality constraints of the FLS model as well as

$$\left[\dot{E}_{FLS}\right]_{VC/PAOS} = \left[\dot{E}_{VC/PAOS}\right]_{FLS} \tag{5.36}$$

FLS System-Level, Unit-Based Fuel Consumption Optimization Problem

Minimize

$$\Delta W_{FUEL\,FLS} = \sum_{i=1}^{n}\left(\lambda_{\dot{E}fls-ps_i}\dot{E}_{FLS-PS\,i} + \lambda_{Dfls_i}D_{FLS\,i} + \lambda_{Wfls_i}W_{FLS\,i} + \lambda_{\dot{E}vc/paos-fls_i}\dot{E}_{VC/PAOS-FLS\,i}\right) \tag{5.37}$$

$$\text{w.r.t.} \quad \left\{\vec{X}_{FLS}, \vec{Y}_{FLS}\right\}$$

subject to the same constraints as in problem (5.35).

FLS System-Level, Unit-Based Total Cost Optimization Problem

$$\text{Minimize} \quad \Delta C_{T\,fls} = C^{P}_{FLS} + \left(\Delta C_{FUEL} + \Delta C_{SS} + \Delta C_{PS} + \Delta C_{ECS} + \Delta C_{CV/PAOS}\right)_{FLS} \tag{5.38}$$

$$\text{w.r.t.} \quad \left\{\vec{X}_{FLS}, \vec{Y}_{FLS}\right\}$$

subject to the same constraints as problem (5.35).

$\Delta C_{T\,fls}$ is increase in the system's total cost due to the FLS. In the above equation, C_{FLS}^{P} is the capital cost; $\Delta C_{FUEL\,FLS}$ is the cost of the extra fuel due to the FLS penalties (power, ram drag, FLS weight, and rate of energy exchange); $\Delta C_{SS\,FLS}$, $\Delta C_{PS\,FLS}$, $\Delta C_{ECS\,FLS}$ and $\Delta C_{CV\,/\,PAOS\,FLS}$ are the extra cost of the SS, PS, ECS and VC/PAOS, respectively.

Now returning once more to the shadow price for the rate of rate of energy transfer, Figure 5.5 shows the change in the non-dimensional total fuel consumption as a function of the energy exchange between the FLS and the CV/PAOS, while keeping the required power and the additional thrust constant. The non-dimensional total fuel is defined as in equation (5.20).

The slope of the curve in Figure 5.5 clearly shows that the assumption of a constant shadow price is fully justified in this case.

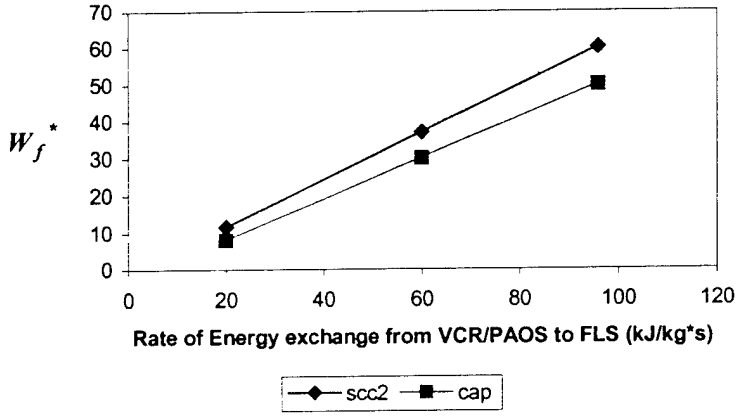

Figure 5.5. Non-dimensional total fuel consumption versus rate of energy exchange with the VC/PAOS.

The FLS is shown in detail in Figure 5.6. The operation of the FLS is dependent on the temperature of the thermal storage tank (i.e. fuel tank) and the heat loads from the PS, hydraulics, and VC / PAOS. The temperature of the fuel tank should be kept within a certain range in such a way that the difference between the fuel inlet temperature and the hot PAO inlet temperature to the fuel/PAO heat exchanger allows the effectiveness to reach reasonable values and the fuel-side to operate within a certain acceptable flow range. The main constraints for the FLS, which are indeed extremely stringent, are to keep constant the flow conditions on the hot PAO side and the amount of heat going from the hot PAO loop to the FLS. In order to do this, it must be taken into account that the temperature of the tank, which in turn is the inlet fuel temperature to the fuel/PAO heat exchanger, is increasing with time. Therefore, the fuel mass flow has to be increased. One can define the FLS problem in terms of the mass fuel required at any time, subject to the fuel tank temperature increment and the VC/PAOS heat load.

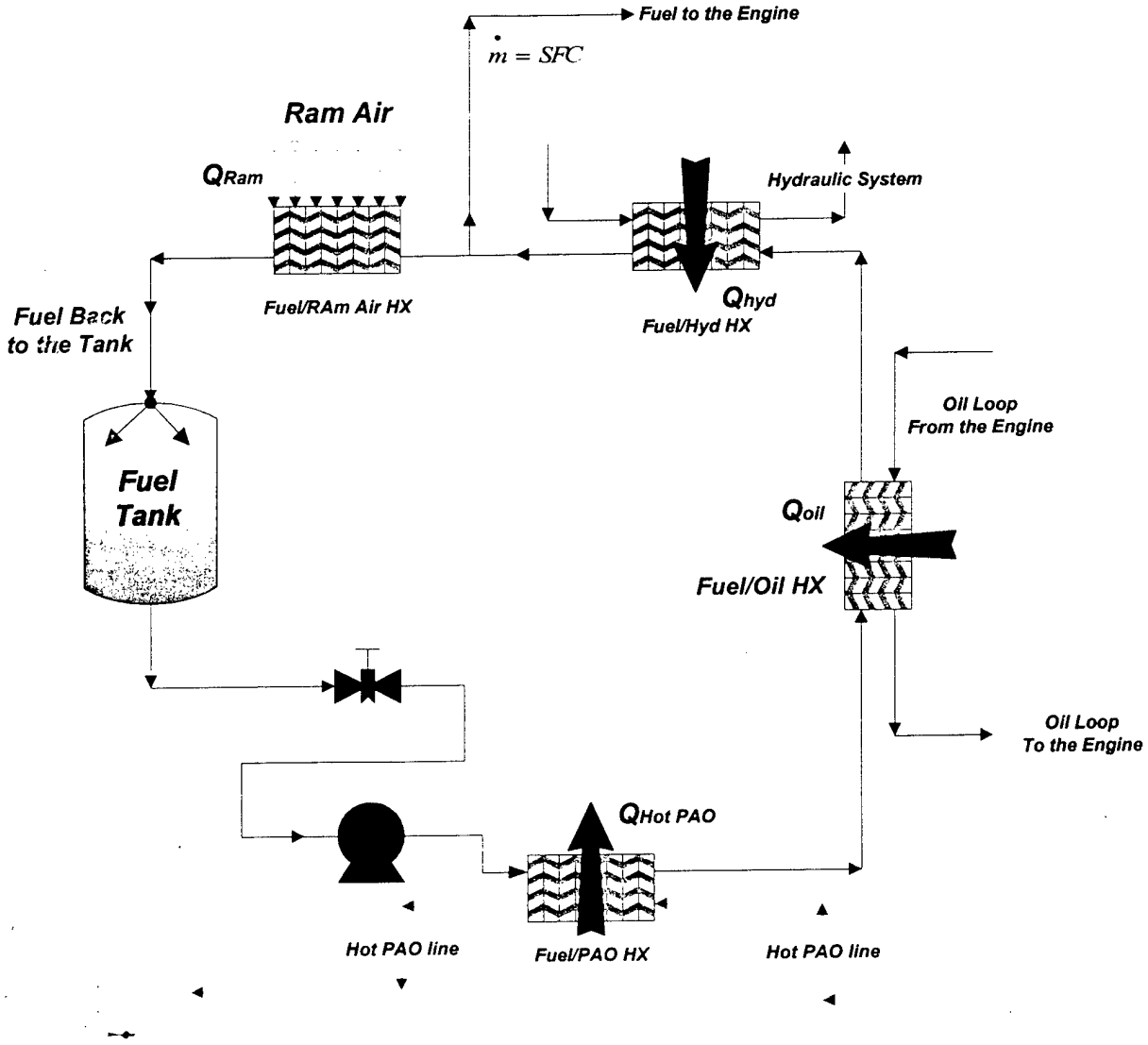

Figure 5.6. Fuel loop sub-system.

Now, the inlet and outlet conditions of the hot PAO loop in the fuel/PAO heat exchanger are kept constant for each mission segment during the FLS synthesis / optimization problem.. This fact allows us to have an amount of energy transfer through the fuel/PAO heat exchanger which in turn is constant during each mission segment.

As to the fuel tank temperature (T_{tank}), it is a function of time and is determined by the flight conditions, the amount of ram air, the heat loads from the PS and hydraulics (which are constant for each mission segment), and the heat loads from the VC / PAOS. Data from Hudson et al. (1975) are used to defined the initial condition required to solve this highly dynamic problem.

The effectiveness of the fuel / hot POA heat exchanger is given by

$$\varepsilon_{fuel/PAO} = \frac{Q_{actual}}{Q_{max}} = \frac{(\dot{m}C_p)_{pao}(T_{pao\_in} - T_{pao\_out})}{(\dot{m}C_p)_{min}(T_{pao\_in} - T_{fuel\_in})} \tag{5.39}$$

or

$$\varepsilon_{fuel/PAO} = \frac{Q_{actual}}{Q_{max}} = \frac{(\dot{m}C_p)_{fuel}(T_{fuel\_out} - T_{fuel\_in})}{(\dot{m}C_p)_{min}(T_{pao\_in} - T_{fuel\_in})} \tag{5.40}$$

where T_{pao_in} and T_{pao_out} are the inlet and outlet PAO side temperatures and T_{fuel_in} is equal to the fuel tank temperature. As can be seen, since (T_{tank}) is changing with time the fuel / PAO heat exchanger effectiveness is also changing with time. In general $(\dot{m}C_p)_{min}$ is equal to $(\dot{m}C_p)_{pao}$. If it is not, the effectiveness has to be expressed in terms of the fuel flow, which is also changing with time. This in fact must be verified in the optimization model.

The effectivenesses of the fuel /oil and fuel / hydraulics heat exchangers are given by equations (5.41) and (5.42), respectively. In the presence of a variable fuel mass flow and temperature, the constant heat rate through these heat exchanger is controlled by varying the oil and hydraulics mass flows. This sub-problem is part of the optimization. In order to set the constraint required to solve the FLS model, the temperature of the fuel leaving the fuel / PAO heat exchanger has to be set to a fixed value for each leg. This temperature is in fact an operational decision variable in the sub-system level optimization problem.

$$\varepsilon_{fuel/oil} = \frac{(\dot{m}C_p)_{oil}(T_{oil\_in} - T_{oil\_out})}{(\dot{m}C_p)_{min}(T_{oil\_in} - T_{fuel\_in})} \tag{5.41}$$

$$\varepsilon_{fuel/hyd} = \frac{(\dot{m}C_p)_{hyd}(T_{hyd\_in} - T_{hyd\_out})}{(\dot{m}C_p)_{min}(T_{hyd\_in} - T_{fuel\_in})} \tag{5.42}$$

The effectiveness of the fuel / ram air heat exchanger is given by

$$\varepsilon_{fuel/ram} = \frac{Q_{actual}}{Q_{max}} = \frac{(\dot{m}C_p)_{ram}(T_{ram\_out} - T_{ram\_in})}{(\dot{m}C_p)_{min}(T_{fuel\_in} - T_{ram\_in})} \tag{5.43}$$

or

$$\varepsilon_{fuel/ram} = \frac{Q_{actual}}{Q_{max}} = \frac{(\dot{m}C_p)_{fuel}(T_{fuel\_in} - T_{fuel\_out})}{(\dot{m}C_p)_{min}(T_{fuel\_in} - T_{ram\_in})} \tag{5.44}$$

From equations (5.43) and (5.44) and considering that the ram air mass flow is constant for each leg and the fuel mass flow and temperature are changing with time, it can be deduced that both the effectiveness and the energy transferred through the fuel / ram air heat exchanger are also changing with time.

Now, taking into account all the heat sources and the change in mass of the fuel in the tank, an energy balance on the tank yields (assuming constant specific heats)

$$\frac{\partial E}{\partial t} = MC_p \frac{\partial T_{tank}}{\partial t} + \frac{\partial M}{\partial t} C_p * T_{tank} = \dot{m}C_p(T_{fuel\_out} - T_{fuel\_in}) \tag{5.45}$$

where heat loss through the tank walls is negligible. The variable T_{fuel_out} in equation (5.45) is equal to T_{tank}, since no losses are considered between the output of the tank and the inlet of the fuel / PAO heat exchanger. M is the fuel mass in the tank at any time, which is expressed as

$$M(t) = M_o - SFC \quad t \tag{5.46}$$

M_o is the initial fuel mass in the tank at the beginning of the leg. SFC is the specific fuel consumption, which is given by the PS and is fixed for each leg. The derivative of equation (5.46) with respect to time is

$$\frac{\partial M}{\partial t} = -SFC \tag{5.47}$$

The expression for the fuel mass flow exiting the tank is determined from the heat rate in the fuel / PAO heat exchanger, where the hot PAO side conditions are constant, i.e.

$$\dot{Q}_{fuel/PAO\_HX} = \dot{m}_{fuel} C_p (T_{fuel\_out} - T_{fuel\_in}) \tag{5.48}$$

where $\dot{m}_{fuel}$ is the required amount of fuel through the fuel / PAO heat exchanger in order to maintain constant the heat exchange. Combining equations (5.43) and (5.48) gives the following output fuel mass flow expression:

$$\dot{m}_{fuel\_out} = \frac{(\dot{m}_{PAO} C_p)_{PAO} (T_{PAO\_in} - T_{PAO\_out})}{C_{p\,fuel}\left[T_{fuel\_out} + \left(\frac{(T_{PAO\_in} - T_{PAO\_out})}{\varepsilon_{fuel/PAO\_HX}} - T_{PAO\_in}\right)\right]} \tag{5.49}$$

where all the terms except the effectiveness of the fuel/PAO heat exchanger do not change with time. Now, a mass balance on the tank yields the following expression for the inlet fuel mass flow:

$$\dot{m}_{fuel\_in} = \dot{m}_{fuel\_out} - SFC \tag{5.50}$$

Thus, the only term left in equation (5.45) which requires and expression is the inlet fuel temperature (T_{fuel_in}). From equation (5.39) and (5.40) this temperature is expressed as

$$T_{Fuel\_in} = T_{Fuel\_to\_engine} - \frac{\varepsilon_{RAM\_HX} (\dot{m} C_p)_{\min} T_{Fuel\_to\_engine} - T_{RAM\_in})}{C_{p\,fuel} \dot{m}_{fuel\_in}} \tag{5.51}$$

where the inlet fuel temperature to the fuel / ram air heat exchanger is equal to the temperature of the fuel going to the PS ($T_{Fuel\_to\_engine}$), which is known since the heat load from the PS and hydraulics are constant. Combining equation (5.39) to (5.51) and after some algebraic manipulation yields a new expression for the energy balance, Equation (5.48), i.e.

$$\frac{\partial T_{tank}}{\partial t} = \frac{(\alpha + \beta) T(t)_{tank} + \lambda}{\mu - t\alpha} \tag{5.52}$$

where

$$\alpha = Cp_{fuel} SFC \tag{5.52.1}$$

$$\beta = \frac{\varepsilon_{fuel/PAO\_HX}(C_p \dot{m})_{PAO}(T_{PAO\_in} - T_{PAO\_out})}{C_{p\,fuel}(T_{PAO\_out} - T_{PAO\_in} + \varepsilon_{fuel/PAO\_HX}(T_{fuel\_out\_fuel/POA\_HX} - T_{pao\_in})} \quad (5.52.2)$$

$$\lambda = \varepsilon_{fuel/RAM\_HX}(C_p \dot{m})_{RAM}(T_{fuel\_to\_engine} - T_{RAM\_in}) - T_{fuel\_to\_engine} \quad (5.52.3)$$

$$\mu = C_{p\,fuel} M_o \quad (5.52.4)$$

Equation (5.52) shows that the fuel tank temperature is a function of, among others, the effectiveness of the fuel / PAO and fuel / ram air heat exchangers. These effectivenesses are not constant with time, since the fuel mass flow and fuel temperature are changing with time. To introduce them into equation (5.52) in terms of time, fuel mass flow, and fuel temperature yields a differential equation with no analytical solution. Therefore, a quasi-static approach is used in which each mission segment is divided in n sub-intervals, in each of which the effectiveness can be treated as constant. This approach yields the following analytical expression for the fuel tank temperature at any given instance of time

$$T_{tank} = \frac{\frac{-\lambda}{\lambda+\beta} + (t\ \alpha - \mu)^{\frac{-\alpha-\beta}{\alpha}}\left[T_{0\_tank} + \frac{\lambda}{\lambda+\beta}\right]}{\left[\mu^{\frac{-\alpha-\beta}{\alpha}}\right]} \quad (5.53)$$

where T_{0_tank} is the fuel tank initial temperature. Knowing the temperature of the tank at any time allows one to compute the fuel mass flow through the fuel / PAO heat exchanger in order to keep the energy transfer rate constant, while the fuel tank temperature is kept below certain limits. Finally , the quasi-static optimization problem was solved using gPROMS® , which is a state-of-the art dynamic modeling, simulation and optimization software by PS Enterprise Ltd. Figure 5.7 shows the FLS optimization procedure.

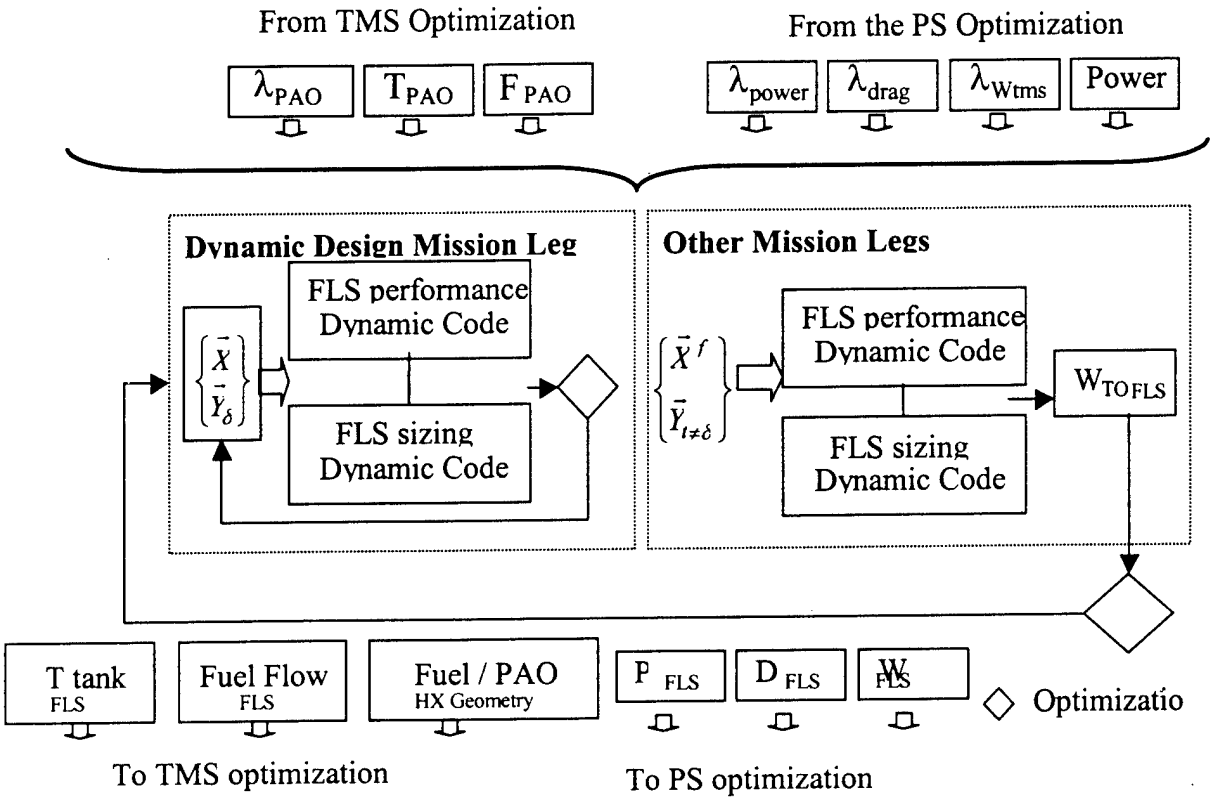

Figure 5.7. The FLS system-level, unit-based modeling and optimization procedure.

CHAPTER 6

6. STRUCTURAL SUB-SYSTEM DESIGN MODELING AND OPTIMIZATION

In Chapter 3 the SS was analyzed. However the SS has up to this point in all the presentations of the previous chapters only played a passive role in the optimization process, i.e. no decision variables have been active such as, for example, aspect ratio and sweep angle. Values for these parameters were selected based on statistical data and well-known design practice. The fact that the SS optimization problem stated in problem (3.27) must be solved in terms of the drag polar relation (equation (3.19)) and the ratio of thrust at sea level to the gross take off weight (equation 3.21) opens up the possibility of using ILGO to solve the SS unit-level optimization problem along with the PS, TMS, and ECS optimization problems. Moreover, the drag and the drag due to the lift depend not only on the flight conditions and requirements (e.g., Mach number) but also on the SS geometry and weight. In this Chapter we will show the influence that the SS geometry (i.e. the aerodynamics) has on the system-level optimization problem.

6.1 Aerodynamics

The SS in this work is defined as the actual empty aircraft, which includes all sub-systems (e.g., fuselage, wings, tail, gear, etc.) excluding the fuel weight, the payload, the PS, the TMS and the ECS. Designers can take advantage of the fact that the SS can be separated into sub-components (e.g., fuselage, wings, tail, gear, etc.) in order to introduce new sub-systems into the system-level optimization problem.

The SS has two characteristics especially interesting from a optimization point of view, which are weight and geometry. These characteristics influence each other (e.g., variations in weight produce changes in the optimum geometry and changes in geometry affect the final gross takeoff weight). This interdependence leads to the fact that improvements (reductions) in weight generated by the use of new technologies such as composite materials, lead to improvements in geometry (e.g., reductions in the wing surface area), which in turn means reductions in wing weight. This synergistic behavior can be effectively exploited using the optimization strategy propose in this work

Structural weight and geometry are not only the base for solving the unit-level optimization problem but are also the link between the SS and the other sub-systems. For instance, equations (6.1) to (6.24) show the effect of weight and geometry (i.e. aerodynamics, drag and lift) on thrust for each mission leg, which determines the performance requirements and constraints for the PS, which in turn will yield the engine weight to be used in the SS optimization problem. Similar interactions between the SS and the ECS and TMS as witnessed by the coupling functions of Figure 3.2. in Chapter 3 affect the optimizations of these sub-systems as well.

In Section 3.2.1 an energy balance on the aircraft was performed. A similar analysis is followed here. However, in contrast to *Chapter 3* we will focus on the aerodynamics. Furthermore, the constraint analysis will be completed for the most stringent mission segments in order to illustrate the selection of decision variables. In order to do this, some of the equations presented in *Chapter 3* are repeated here. However they are disaggregated even further, which is necessary in order to understand the complex relationship between the SS and the different sub-systems that make up an aircraft.

The energy balance for the aircraft yields

$$\{T-(D+R)\}V = W\frac{dh}{dt} + W\frac{d}{dt}\left\{\frac{V^2}{2g}\right\} \tag{6.1}$$

Note that the total resistance (D + R) is the sum of the drag of the "clean" aircraft (D) and any additional drag (R) associate with protuberances. Here, R represents the drag due to the TMS and ECS. The term on the left-hand-side of equation (6.1) is the rate of mechanical energy input. The first and second terms on the right-hand-side represent the storage of potential and kinetic energy, respectively. If the installed thrust is defined as

$$T_i \equiv \alpha T_{SL} \tag{6.1a}$$

where α is the installed full throttle thrust lapse, i.e. the fraction of the sea level take-off thrust, which depends on altitude and speed. The instantaneous weight is given by

$$W \equiv \beta_i W_{TO} \tag{6.1b}$$

where β_i is the fraction of the take-off weight at leg *i*, which depends on how much fuel has been consumed. Substituting this definition into equation (6.1) results in

$$\frac{T_{SL}}{W_{TO}} = \frac{\beta}{\alpha}\left[\frac{D+R}{W_{TO}\beta}\right] + \frac{1}{V_i}\frac{d}{dt}\left(h_i + \frac{V_i^2}{2g}\right) \tag{6.2}$$

The lift and drag analysis for this equation begins with the well-known aircraft relationships

$$L = nW = qC_L S \tag{6.3}$$

$$\text{and } D = qC_D S \tag{6.4}$$

where n is the load factor, which is equal to the number of g's perpendicular to the direction of the velocity. A lift-drag polar relationship of the form (Mattingly et al., 1987; Raymer, 1999) is assumed. Such that

$$C_D = K_1 C_L^{\,2} + K_2 C_L + C_{D_0} \tag{6.5}$$

where $K_2 = -2K''C_{L_{min}}^2$ (6.6)

$$K_1 = K' + K'' \tag{6.7}$$

$$C_{D_0} = C_{D\min} + K''C_{L_{min}}^2 \tag{6.8}$$

In equation (6.8) C_{D_0} is the drag coefficient at zero lift. Also, for modern high performance aircraft $C_{L_{min}} \approx 0$, and therefore, $K_2 \approx 0$. This leads to a following expression for the drag coefficient:

$$C_D = K_1 C_L^2 + C_{D_0} \tag{6.9}$$

where $C_{D_0} = C_{D\min} = C_{fe}\frac{S_{wet}}{S_{ref}}$ (Subsonic) (6.10)

$$C_{D_0} = C_{fe}\frac{S_{wet}}{S_{ref}} + C_{Dwave} \quad \text{(Supersonic)} \tag{6.11}$$

$$K' = \frac{1}{A_R e\pi} \quad \text{(Subsonic)} \tag{6.12}$$

$$K' = \frac{A_R(M^2-1)}{4A_R\sqrt{M^2-1}} - 2\cos A_{LE} \quad \text{(Supersonic)} \tag{6.13}$$

$$0.001 \le K'' \le 0.03 \tag{6.14}$$

Here C_{fe} is the skin friction factor, C_{Dwave} is the drag coefficient due to wave shocks, A_R is the aspect ratio, M is the mach number, A_{LE} is the quarter chord sweep angle, and e is the span efficiency factor. Different expressions for C_{fe}, C_{Dwave}, and e can be found in the literature. These expression can be general formulations to be used during the preliminary design phase or fairly elaborate statistical regressions to be used for the detailed design phase or analysis. However, they all are function of aerodynamic parameters such as aspect ratio, sweep angle, wing area, etc.

From the lift and drag analysis just performed, it can be concluded that there is a strong dependence of the drag coefficient on the SS geometry (i.e. aerodynamics). This dependence will be exploited to find the optimum value for the drag coefficient. The dependence of the subsonic lift coefficient on the same parameters can be concluded from

$$C_L = C_{L\alpha}\alpha \tag{6.15}$$

where C_L is the wing lift coefficient, $C_{L\alpha}$ is the wing lift curve slope, and α is the angle of attack. A further analysis yields

$$C_{L\alpha_{Subsonic}} = \frac{2A_R\pi}{2+\sqrt{4+\frac{A_R{}^2\beta^2}{\eta^2}\left(1+\frac{\tan^2 A_{maxt}}{\beta^2}\right)}}\left(\frac{S_{exposed}}{S_{ref}}\right)(F) \tag{6.16}$$

where $\beta^2 = 1 - M^2$ (6.17)

$$\eta = \frac{C_{\ell\alpha}}{2\pi/\beta} \tag{6.18}$$

$$F = 1.07(1 + d/b)^2 \tag{6.19}$$

and where A_{maxt} is the sweep of the wing at the chord location where the airfoil is thickest. $C_{\ell\alpha}$ is the airfoil lift curve slope, $S_{exposed}$ is the exposed wing platform, F is the fuselage lift factor, d is the fuselage maximum equivalent diameter, b is the wing span. As before A_R is the wing geometric aspect ratio of the complete reference platform. However, A_R can be replaced by the effective aspect ratio when wing endplates or winglets are used, i.e..

$$A_{R_{effective}} = A_R(1 + 1.9h/b) \tag{6.20}$$

where h is the endplate height.

Now for purely supersonic wing the lift curve slope is given by

$$C_{L\alpha_{Supersonic}} = \frac{4}{\beta} \tag{6.21}$$

$$\text{when } M > \frac{1}{Cos A_{LE}} \tag{6.22}$$

For a mix flow wing (i.e. supersonic and subsonic), which is generally the case for high Mach number sweep wings, it is difficult to predict the lift curve slope. However, it can be done using sophisticated and accurate databases. To use these databases, geometric parameters are required, i.e. aspect ratio, taper ratio, and leading edge sweep angle. If required, these databases can be added to the optimization code or specialized software to compute the lift curve slope can be used along with state of the art parsing programs, which allow data exchange in real time between two or more codes built for different platforms (e.g. Perl, 2001).

With the lift and drag analysis shown above in mind, equations (6.2) through (6.14) can be manipulated to produce the thrust equation for the i_{th} mission leg, namely,

$$\frac{T_i}{W_i} = \frac{q_i S}{W_i}\left[K_1\left(\frac{n_i}{q_i}\frac{W_i}{S}\right)^2 + C_{D_0} + \frac{D_{ECS_i} + D_{TMS_i}}{q_i S}\right] + \frac{1}{V_i}\frac{d}{dt}\left(h_i + \frac{V_i^2}{2g}\right) \tag{6.23}$$

where the only additional drag, R, being considered is the momentum drag created by the ECS and the TMS (i.e. $R = D_{ECS} + D_{TMS}$). In equation (6.23), the velocity (V) and the rates of climb (dh/dt) and acceleration (dV/dt) are directly or indirectly given by the mission specifications. The drag created by the ECS and TMS are also leg-dependent as will be discussed below.

An alternative version of equation (6.23) can be given as a function of the thrust at sea level take-off (T_{SL}) and the gross take-off weight (W_{TO}), namely,

$$T_i = \alpha T_{SL} = q_i S\left[K_1\left(\frac{n_i}{q_i}\frac{\beta_i W_{TO}}{S}\right)^2 + C_{D_0} + \frac{D_{ECS_i}}{q_i S}\right] + \frac{\beta_i W_{TO}}{V_i}\frac{d}{dt}\left(h_i + \frac{V_i^2}{2g}\right) \tag{6.24}$$

Equation (6.24) represents the required thrust for each mission leg as a function of the gross takeoff weight, the mission weight fraction, additional drag, performance requirements, and aerodynamic parameters. Equation (6.24) comprises the most important set of constraints to be used to the PS optimization problem, as was explained in chapter 3, which will produce the propulsion system optimum weight of the PS. The fact that the engine weight is part of the gross take-off weight allows the designer to use this term as a coupling function to the SS optimization problem.

Equations (6.2) through (6.22) hint at the tight integration issues associated with the synthesis / design of an aircraft. The synthesis / design and operation of any given sub-system is highly influenced by and in turn influences the synthesis / design and operation of all the others. Take the case of the TMS, for example. The TMS's weight and energy and extra thrust requirements affect the required total thrust which leads to higher fuel consumption and higher take-off gross weight. Equation (6.24) clearly shows that an increase in W_{TO} is associated with higher thrust, which in turns affects the size of the PS. The weight of the SS is also affected as indicated by equation (6.28) below.

The characteristics just mentioned above along with the aerodynamic analysis define a highly dynamic system where "everything affects everything else". Therefore, it is very worthwhile to include the SS into the system-level optimization problem. Moreover, the ILGO-B approach can be use, in spite of the "non-energy" nature[1] of the SS. In order to establish the SS unit-level optimization problem a suitable set of which can be decision variables must be defined. Table 6.1. shows a group of twelve viable decision variables which can be used. The designer can decide whether or not any given variable should be introduced into the optimization problem or whether or not a fixed value is assigned based on the available information. This decision should be made taking into account several factors such as information accuracy and availability during the design phase, deadlines, etc.

[1] Even though energy, of course, plays a major role in the SS, we use the term "energy" and "non-energy" here to distinguish between what are traditionally known as energy conversion sub-systems (e.g., PS, ECS, and TMS) and those that are not (e.g., SS).

Table 6.1. Set of possible decision variables for the SS unit-level optimization problem.

STRUCTURE			REQUIREMENTS	SENSITIVITY STUDIES
Aerodynamics (design)	**Configuration (synthesis)**	**Advance technologies**		
AR, Λ, t/c, λ	Variable sweep	Composite Materials	Range/payload/crew	Dead weight
Fuselage fineness ratio	High-lift devices		Loiter time	C_{Do} and KC_{Dwave}
T/W and W/S	Tail type		Speed, Time to climb	C_{lmax}
Airfoil camber	Airfoil shape		Runway length	SFC, Fuel price

Sensitivity studies on the importance of each of these variables can be done to determine how much the aircraft weight is impacted if various parameters such as drag or specific fuel consumption should increase. Also, changes in external factors such as the fuel price are analyzed as is the expected impact of carrying more dead weight (e.g., two more external missiles or avionics). In such a case, the internal density (i.e. takeoff weight divided by the internal volume) should be kept constant.

6.2 Constraint Analysis

Equation (6.24) can be manipulated to yield equation (6.25), which is a "master equation" for the flight performance of aircraft in terms of take-off thrust loading (T_{SL}/W_{TO}) and wing loading (W_{TO}/S), i.e.

$$\frac{T_{SL}}{W_{TO}} = \frac{\beta}{\alpha}\left\{\frac{q_i S}{W_{TO}}\left[K_1\left(\frac{n\rho}{q}\frac{W_{TO}}{S}\right)^2 + C_{D_0} + \frac{D_{ECS_i} + D_{TMS_i}}{qS}\right] + \frac{1}{V_i}\frac{d}{dt}\left(h_i + \frac{V_i^2}{2g}\right)\right\} \tag{6.25}$$

This equation is based on energy considerations and for each mission leg will provide relationships between (T_{SL}/W_{TO}) and (W_{TO}/S), which represent, in fact, the boundaries of the optimization problem. The derivation and study of these boundaries is known as constraint analysis. In equation (6.25), β is unknown. Consequently, and initial numerical value of this weight fraction for each mission leg is required. This initial value is based on experience (i.e. regression of data from recent aircraft and new technology considerations). The actual values are found in the weight fraction analysis, which in turn requires TSFC information from the PS unit-level optimization problem. Actual values are used to update the constraint analysis. This shows the iterative nature of the aircraft design and optimization process.

The fraction of the sea-level takeoff thrust, α, is also based on experience. It depends on the Mach number and whether or not there is an afterburner, which is determined once the actual values are produced by the PS unit-level optimization problem.

The constraint analysis is performed on the most stringent mission legs, generally 4 or 5. To show how it works, only the supersonic penetration and escape dash leg curve is developed here. A complete constraint analysis for the aircraft optimized in this work is shown in Figure 6.1. This constraint analysis yields feasible values for the take-off thrust loading (T_{SL}/W_{TO}) and wing loading (W_{TO}/S)

For supersonic penetration and escape dash (mission leg 6-7), there are no changes in velocity or altitude. During the first stage of the synthesis / design optimization, the initial drag is neglected. However, once the conceptual stage is performed, the computed W_{TO} and S are used to bring into consideration the additional drag D_{ECS_i} and D_{TMS_i}, which work as coupling functions coming from two of the energy sub-systems (the TMS and the ECS) to the non-energy sub-system (the SS). Equation (6.25), thus, yields

$$\frac{T_{SL}}{W_{TO}} = \frac{\beta}{\alpha}\left\{K_1 \frac{\beta}{q_i}\left(\frac{W_{TO}}{S}\right) + \frac{C_{D_0}}{\frac{\beta}{q_i}\left(\frac{W_{TO}}{S}\right)}\right\} \tag{6.26}$$

For a given set of aerodynamic variables (i.e. aspect ratio, sweep angle, angle of attack, taper ratio, etc.) and with the inputs from other sub-systems (e.g. coupling functions), all the terms, but $\frac{T_{SL}}{W_{TO}}$ and $\frac{W_{TO}}{S}$, in equation (6.26) are known. Therefore, tabulated data of $\frac{T_{SL}}{W_{TO}}$ versus $\frac{W_{TO}}{S}$ must be developed to understand the range of values these terms can take. A numerical example for the mission leg being analyzed is given in Table 6.2.

Table 6.2. Supersonic penetration and escape dash constraint analysis data.

$\frac{T_{SL}}{W_{TO}}$	2.35	1.77	1.2	0.913	0.746
$\frac{W_{TO}}{S}(N/m^2)$	1915	2105	2900	3880	5050

This data is plotted on a graph of $\frac{T_{SL}}{W_{TO}}$ vs. $\frac{W_{TO}}{S}$ along with that generated by the execution of the constraint analysis over the other most stringent legs. Figure 6.2 is a real representation of the constraint analysis realized in this project for given values of the aerodynamic variables. Figure 6.2 also represents the constraints given by the request for proposal (RFP) for an air-to-air fighter (AAF) and shows the functional relationship between the take-off thrust loading (T_{SL}/W_{TO}) and wing loading (W_{TO}/S). This diagram shows all the possible thrust and wing loading values that lead to syntheses / designs that comply with the requirements of the RFP.

The shaded area indicated in Figure 6.2. represents the synthesis / design optimization space for a given set of values of the aerodynamic variables. Notice that any point in this area meets the RFP constraints. However, this area will change for different values of the aerodynamic variables. This allows the take-off thrust loading (T_{SL}/W_{TO}) and wing loading (W_{TO}/S) to be treated as decision variables in the SS unit-level optimization problem. Table 6.3 shows some suitable ratios for the AAF, which will be used in the weight fraction analysis in order to determine the total gross take-off weight.

Table 6.3. Suitable values for T_{SL}/W_{TO} and W_{TO}/S to be used into the SS unit-level optimization problem.

$\frac{T_{SL}}{W_{TO}}$	1.2	1.3	1.4	1.5
$\frac{W_{TO}}{S}(N/m^2)$	3065	2800	3100	1950

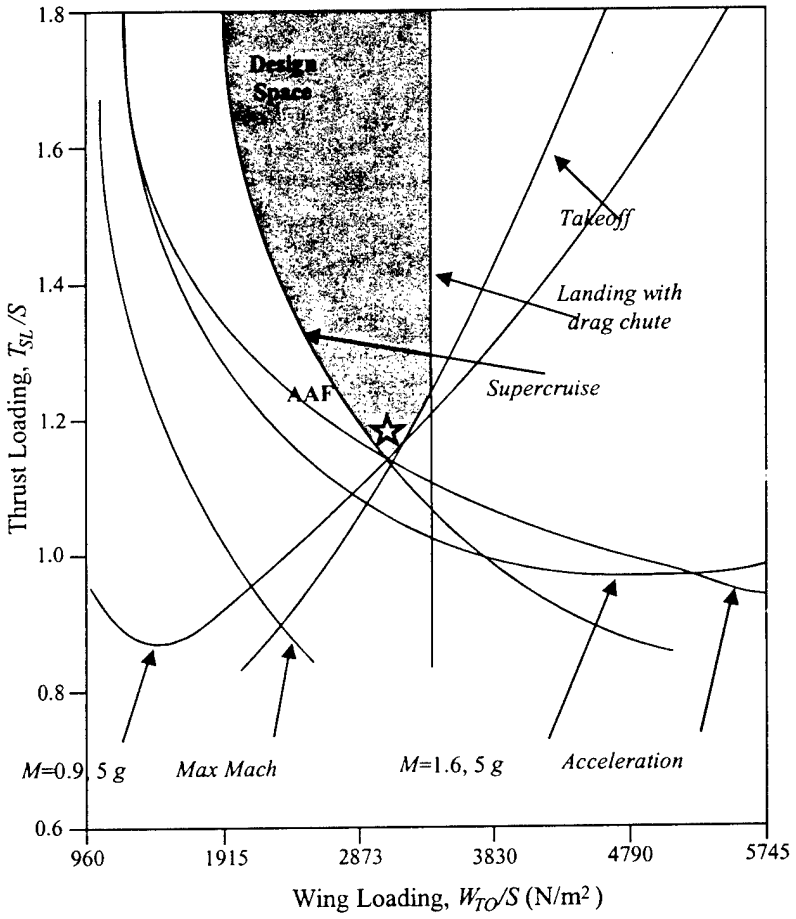

Figure 6.1. Complete AAF constraint analysis diagram.

6.3 Mission Analysis, Weight Fractions and Sizing

6.3.1 Mission Analysis

With suitable values of the take-off thrust loading (T_{SL}/W_{TO}) and wing loading (W_{TO}/S), the next step is to establish the scale of the aircraft (i.e. wing area, fuselage length, empty weight, fuel weight) via the computation of the gross take-off weight (W_{TO}). This is accomplished by flying the aircraft through the entire mission on paper. The fuel weight is calculated based on engine performance and mission requirements and depends on the system synthesis / design and mission requirements. The weight of the ECS, the TMS, and the PS result from the sub-system optimization problems. The weight of the SS depends on a number of synthesis / design considerations: materials, aerodynamic performance, durability, strength and stability among many others. The gross take-off weight (W_{TO}) is given by

$$W_{TO} = W_{SS} + W_{PS} + W_{ECS} + W_{TMS} + W_{FUEL} + W_{PPAY} + W_{EPAY} \tag{6.27}$$

where W_{SS} is the weight of the SS, which refers to all sub-systems present in the aircraft (wing, fuselage, hydraulics, power distribution, etc.) with the exception of the ECS, TMS, weapons, and the PS[2]. W_{PS} is the weight of the engine (PS), W_{ECS} is the weight of the ECS, W_{TMS} the weight of the TMS, W_{FUEL} the weight of fuel necessary to carry out the mission, W_{PPAY} the weight of the permanent payload (crew, equipment) and W_{EPAY} the expendable payload (ammo and missiles).

In the optimization problem posed in Chapter 4 and 5, no decision variables were include for the SS and the weight of the SS corresponded to values in agreement with existing design practices. To this end, the data given Muñoz and von Spakovsky, 1999 was used. This data shows the empty weight (SS plus PS plus ECS plus TMS) as a function of the gross take-off weight for a number of high performance jet aircraft. However, analytical expressions of the empty weight and the engine weight as a function of the gross take-off weight are also available (see equation (6.28)) below. Those expressions are based on sophisticated state of the art statistical regressions.

$$\frac{W_E}{W_{TO}} = 2.34 W_{TO}^{-0.13} \tag{6.28}$$

$$\text{where } W_E = W_{SS} + W_{PS} + W_{ECS} + W_{TMS} \tag{6.29}$$

From equations (6.28), it is possible to obtain the weight of the SS for a given value of the take-off weight. Thus, the weight of the SS is the empty weight (equation (6.28)) minus the engine weight multiplied by the factors k_{ecs} and k_{tms} to reflect the fact that the empty weight also includes the weight of the ECS and TMS. It will be shown that once a first

[2] Obviously our decomposition could be extended by breaking out as separate sub-systems the hydraulics, power distribution, etc. from the SS.

estimation of W_{TO} is made, the empty weight can be more accurately computed as function not only of the gross take-off weight but also of the aerodynamic and SS synthesis / design decision variables. The new empty weight is used to find the final gross take-off weight.

6.3.2 Weight Fraction

What follows is dedicated to the development of the weight fraction (π) equations needed for the different mission legs. The fuel consumption analysis is based on calculations which require relatively little information. In addition, it shows the best way to fly certain legs for minimum fuel usage. The fuel expended in each mission leg is expressed as a fraction of the weight starting the leg.

As to the fuel weight in equation (6.27), it is a complex function of the thermodynamic performance of the engine, the mission requirements, the technology used, and some stability considerations. In general, it is given by

$$W_{FUEL} = g \sum_{mission} \dot{m}_i \Delta t_i = g \sum_{mission} TSFC \cdot T \cdot \Delta t_i \tag{6.30.1}$$

or Minimize $$W_{FUEL} = w_{fuel}(W_{TO}, \vec{X}_{PS}, \vec{Y}_{PS}, mission) \tag{6.30.2}$$

where the rate of fuel consumption has been written in terms of the thrust specific fuel consumption (*TSFC*). Equation (6.30), however, is fairly inconvenient due to the fact that the specifications of each of the mission legs are given in terms of different parameters. As seen in Table 3.1 of *Chapter 3*, some of the legs have specified range, others specified duration, while still others have specific maneuvers to be carried out. In addition, the duration of some of the legs changes as the decision variables are varied. Therefore, it is useful to employ a transformation, which puts all mission segments under a unified measure. Fuel consumed in each leg written in terms of the weight ratio is such a measure. The ratio of the final to the initial weight for leg *i* is defined as

$$\pi_i = W_{final} / W_{initial} \tag{6.31}$$

In order to proceed with the calculation of the weight ratios, consider the rate at which aircraft weight diminishes due to the consumption of fuel, namely

$$\frac{dW}{dt} = -TSFC \cdot T \tag{6.32}$$

$$\text{or} \quad \frac{dW}{W} = -TSFC \frac{T}{W} dt = -TSFC \frac{T}{W} \frac{dt}{ds} ds = -TSFC \frac{T}{W} \frac{ds}{V} \tag{6.33}$$

Equation (6.33) represents the weight-time and weight-velocity transformation that is used to unify the different requirements of the mission. The integration of equation (6.33) is done by breaking each mission segment into several (typically 5) intervals. The flight and operating conditions for each sub-segment are assumed to be constant at some representative value so that the integration can be accomplished explicitly. It was found that in most cases, five intervals are sufficient to ensure excellent accuracy. Proper

integration of equation (6.33) requires knowledge of the behavior of the specific fuel consumption and the instantaneous thrust loading as a function of time along the flight path. The integration can be carried out according to the weight specific excess power (P_s). This approach yields equation (6.34.1) for $P_s > 0$ and equation (6.34.2) for $P_s = 0$. The derivation of these equations is not presented, since it does not provide any additional help in understanding the development of the stated optimization problem.

$$\frac{W_f}{W_i} = \exp\left\{ -\frac{TSFC}{V\left(1-\frac{D+R}{T}\right)} \Delta\left(h + \frac{V^2}{2g_o}\right) \right\} \tag{6.34.1}$$

$$\frac{W_f}{W_i} = \exp\left\{ -TSFC\left(\frac{D+R}{W}\right)\Delta t \right\} \tag{6.34.2}$$

where Δt is the total mission leg flight time.

The engine installed TSFC is a complex function of the combination of altitude, speed, and throttle setting, especially if the engine has the option of afterburning. Since for the first iteration of the ILGO problem there is no information from the PS unit-level optimization, it is required to find an adequate starting point for the TSFC estimation. A satisfactory solution is found by assuming that

$$TSFC = C\sqrt{\theta} \tag{6.35}$$

where C is a constant which is estimated in advance and θ represents the usual thermodynamic cycle improvement due to a lower ambient temperature at higher altitude. Note that once the PS unit-level optimization problem can be solved, the actual specific fuel consumption will be used in the SS optimization problem to perform the weight fraction analysis. Table 6.4. shows the weight ratio for different mission legs. There is a special case, however, which deviates from the above calculations and corresponds to the mission segment when the expendable payload is delivered. If it is assumed that the delivery is done at some point j in the mission, then

$$\frac{W_j - W_{EPAY}}{W_j} = 1 - \frac{W_{EPAY}}{W_j} \tag{6.36}$$

With equation (6.27) and the weight ratios and after some manipulation, the fuel consumption can be written as:

$$W_{FUEL} = W_{TO}\left(1 - \prod_{i=1}^{n} \pi_i\right) - W_{EPAY}\left(1 - \prod_{i=j}^{n} \pi_i\right) \tag{6.37}$$

where n is the number of legs being considered. The weight fractions depend on the design of the PS and other sub-systems, the required thrust, the afterburner setting and power requirements of the other sub-systems, ambient conditions, and a number of other factors. However, it should be noted that the weight fraction depends also on the aerodynamic, e.g., geometric decision variables. These complex set of factors are addressed by means of solving equation (6.34) for each leg.

Table 6.4. Weight ratio calculations for different mission legs.

Case	$\pi = W_{final}/W_{initial}$
Constant speed climb	$\exp\left\{\frac{-TSFC}{V}\left[\frac{\Delta h}{1-\frac{D+D_{ECS}}{T}}\right]\right\}$
Horizontal acceleration	$\exp\left\{\frac{-TSFC}{V}\left[\frac{\Delta\left(V^2/2g\right)}{1-\frac{D+D_{ECS}}{T}}\right]\right\}$
Climb and acceleration	$\exp\left\{\frac{-TSFC}{V}\left[\frac{\Delta\left(h+V^2/2g\right)}{1-\frac{D+D_{ECS}}{T}}\right]\right\}$
Constant altitude/speed cruise	$\exp\left\{\frac{-TSFC}{V}\left(\frac{D+D_{ECS}}{W}\right)\Delta s\right\}$
Constant altitude/speed turn[3]	$\exp\left\{-TSFC\cdot n\cdot\left(\frac{D+D_{ECS}}{W}\right)\frac{2\pi NV}{g\sqrt{n^2-1}}\right\}$
Loiter	$\exp\left\{-TSFC\left(\frac{D+D_{ECS}}{W}\right)\Delta t\right\}$
Warm-up	$1-TSFC\left(\frac{T}{W_{TO}}\right)\Delta t$
Take-off rotation	$1-TSFC\left(\frac{T+D_{ECS}}{W_{TO}}\right)\cdot t_R$

Algebraic manipulation of equations (6.27), (6.36), and (6.37) yields the following expression for the gross take-off weight

[3] N is the number of turns.

$$W_{TO} = \frac{W_{PP} + W_{PE} \prod_{j\_n}}{\prod_{1\_n} - \frac{W_E}{W_{TO}}} \tag{6.38}$$

where $\frac{W_E}{W_{TO}} = 2.34 W_{TO}^{-0.13}$ (6.28)

This equation not only allows the straightforward calculation of the gross take-off weight, but also reveals its dependence on the critical parameters of the mission represented by W_{PP}, W_{PE}, the $\Pi's$, $\frac{W_E}{W_{TO}}$, and of course the aerodynamics. An initial estimation of W_{TO} must be made during this part of the process to solve equation (6.38). Note that the weight fractions have already been computed. If the initial estimation is far from the value given by equation (6.38), then an iterative solution is required. The iteration process should converge rapidly.

Now, with the value the gross take-off weight, the values of the sea-level thrust, wing area, weight of the fuel, and size of the fuselage can be determined from equations (6.28), (6.27) and from the definition of takeoff thrust loading (T_{SL}/W_{TO}) and wing loading (W_{TO}/S) also, equation (6.24) can be solved to generate the value of the thrust for each mission segment, which in turn is a coupling function to be used by the PS optimization problem.

Finally, during the construction of the constraints analysis graph, it was necessary to make some assumptions on the weight ratios for several mission segments. These assumptions should be verified before proceeding any further.

6.3.3 Sizing

The gross take-off weight calculation can be improved by the use of the refined sizing method. This method gathers the different subcomponents of the SS into groups, expressing their weights as a function of the gross take-off weight and SS decision variables and parameters. This is done by applying statistical equations based upon sophisticated regression analysis. When the component weights are estimate using this method, they are tabulated and summed to determine the actual empty weight. If the empty weight is different from the one estimated initially, this must be corrected by resizing the aircraft. The new empty weight is replaced in equation (6.38) and the new gross take-off weight is computed by iteration. This new gross take-off weight in turn is used to finds a new empty weight by using the group weight technique. The process continues until convergence is reached. Table 6.5 shows some group weight equations for fighter aircraft taken from Raymer, 2001.

Table 6.5. Fighter group weights.

Group Name	Group Weight (kg)
Wing	$0.0103\mathrm{K_{dw}K_{vs}}\left(\mathrm{W_{dg}N_z}\right)^{0.5} S_w^{0.622} AR^{0.785}\left(t/c\right)_{root}^{-0.4}\left(1+\lambda\right)^{0.005}\left(\cos \mathrm{A}\right)^{-1} S^{0.04} csw$
Horizontal tail	$3.316\left(1+\frac{F_w}{B_h}\right)\left(\frac{W_{dg}N_z}{1000}\right)^{0.260} S_{ht}^{0.806}$
Landing gear	$K_{cb}K_{tpg}\left(W_t N_t\right)^{0.25} L_m^{0.973}$
Fuselage	$0.499 K_{dwf} W_{dg}^{0.35} N_z^{0.25} L^{0.5} D^{0.849} W^{0.685}$

6.4 SS System-level Unit-based Design Optimization Problem Definition

As was the case for the ECS and TMS in Chapter 4 and 5, we defined a system-level, unit-based synthesis / design optimization problem for the SS since ILGO-B will be applied to this sub-system in the work that we will do over the next several months. This problem is defined in terms of the set of decision variables given in Table 6.1, the set of constraints represented by the constraint analysis, and the coupling functions, which appear in Table 6.6 and represent the information flow between the SS and other sub-systems.

Table 6.6. SS system-level, unit-based optimization problem coupling functions (u_{ij}).

COUPLING FUNCTION	FROM	TO
TMS weight	TMS	SS
TMS drag	TMS	SS
ECS weight	ECS	SS
ECS drag	ECS	SS
PS weight	PS	SS
PS drag	PS	SS
TSFC	PS	SS
SS weight	SS	PS
SS drag	SS	PS
Goss take-off weight	SS	PS
Required thrust	SS	PS

However, we first define the unit-level SS optimization problem in total cost[4] such that[5]

[4] Note that writing the optimization problem on a total cost basis is more general than writing it on a gross take-off weight or fuel weight basis since the latter two are in effect special cases or subsets of the cost problem.

[5] This parallel is the definition given for the other sub-systems in Chapter 3.

$$\text{Minimize } C_{SS} = \int_{time} c_{f_n} (\dot{m}_f^w + \dot{m}_f^D + \dot{m}_f^{DL} + \dot{m}_f^f)\, dt + \sum_n C_n^p \tag{6.39}$$

w.r.t. $\{\bar{X}_{SS}, \bar{Y}_{SS}\}$

subject to the set of inequality and inequality constraints given by the constraint analysis and the coupling functions.

Here C_{SS} is the total cost of the SS, c_f is the unit cost of fuel, $\dot{m}_f^w$ is the rate of fuel needed to carry the total weight of the sub-system, $\dot{m}_f^D$ is the rate of fuel necessary to overcome the drag penalty created by the interaction between the system and the air, $\dot{m}_f^{DL}$ is the rate of fuel necessary to overcome the drag penalty due to lift, and $\dot{m}_f^f$ is the rate of fuel needed to carry the fuel itself. C_n^p is the component capital and capital related costs such as those for equipment purchase, research and development, maintenance, etc.

The cost model used was developed by Resetar et al. (1991). The model provides separate costs for the following major cost elements: non-recurring engineering, non-recurring tooling, development support, flight test, recurring engineering, recurring tooling, recurring manufacturing labor, recurring manufacturing material, and recurring quality assurance. The cost model is derived from a database consisting of 13 military aircraft with first flight dates ranging from 1960 to 1978: A-6, A-7, A-10, C-5, C-141, F-4, F-14, F-15, F-16, F-18, F-111, S-3A, and T-39. Empty weights for the sample aircraft range from under 10,000 lbm to over 300,000 lbm, while speeds range from 400 kn to over 1,300 kn.

The airframe cost refers to the cost of the assembled structural and aerodynamic components of the air vehicle that support sub-systems essential to a particular mission. It includes not only the basic structure (wing, fuselage, empennage, and nacelles) but also the air induction sub-system, starters, exhausts, fuel control sub-system, inlet control sub-system, alighting gear (tires, tubes, wheels, brakes, hydraulics, etc.), secondary power, furnishings (cargo, passenger, troop, etc.), engine controls, instruments (flight navigation, engine, etc.), environmental control, racks, mounts, intersystem cables and distribution boxes, etc. inherent to and inseparable from the assembled structure, dynamic sub-systems, and other equipment homogeneous to the airframe.

The airframe costs also encompass the integration and installation of the propulsion, avionics, and armament sub-systems into the airframe but not those efforts directly related to their development and manufacture. The cost estimate does not include training, support equipment, data, and spares. Since the structures cost already includes the ECS and TMS cost, the former was multiplied by a factor of 0.945. This factor is obtained from assuming a linear relationship between cost and weight. This assumption proved to be valid as shown in the following sections. For cost calculation purposes, it was assumed that 4 test and 350 production aircraft are built, respectively. These numbers agree with current military aircraft programs (Tirkap, 2000).

Now, turning to the system-level, unit-based SS optimization problem, it is written on a cost basis as

Minimize

$$C_{Total} = C_{ss\,total} + \lambda_{ps}\Delta\bar{u}_{ps} + \lambda_{tms}\Delta\bar{u}_{tms} + \lambda_{ecs}\Delta\bar{u}_{ecs} + C^{o}{}_{ps} + C^{o}{}_{tms} + C^{o}{}_{ecs} \tag{6.40}$$

w.r.t. $\left\{\bar{X}_{SS}, \bar{Y}_{SS}\right\}$

subject to a set of equality and inequality constraints which include

$$T_i = \alpha T_{SL} = q_i S\left[K_1\left(\frac{n_i}{q_i}\frac{\beta_i W_{TO}}{S}\right)^2 + C_{D_0} + \frac{D_{ECS_i}}{q_i S}\right] + \frac{\beta_i W_{TO}}{V_i}\frac{d}{dt}\left(h_i + \frac{V_i^2}{2g}\right) \tag{6.24}$$

where it should be pointed out that for the system-level, unit-based optimization (as opposed to the system-level optimization), $C^{o}{}_{ecs}$, $C^{o}{}_{tms}$, $C^{o}{}_{ps}$ are held constant, i.e.

$$C_{ecs} - C^{o}_{ecs} = 0 \tag{6.41}$$

$$C_{tms} - C^{o}_{tms} = 0 \tag{6.42}$$

$$C_{ps} - C^{o}_{ps} = 0 \tag{6.43}$$

In addition, the following constraints are also imposed:

$$D_{ps} - D^{o}_{ps} = 0 \tag{6.44}$$

$$D_{tms} - D^{o}_{tms} = 0 \tag{6.45}$$

$$D_{ecs} - D^{o}_{ecs} = 0 \tag{6.46}$$

where D is the drag produced by each sub-system. Let us now define the shadow prices for the coupling functions of the SS. The shadow prices based on the optimum cost for a given leg i are given by

$$\bar{\lambda}_{PS_i} = \frac{\partial C^{\bullet}_{PS}}{\partial \bar{u}_{PS}} \tag{6.47}$$

$$\bar{\lambda}_{TMS_i} = \frac{\partial C^{\bullet}_{TMS}}{\partial \bar{u}_{TMS}} \tag{6.48}$$

$$\bar{\lambda}_{ECS_i} = \frac{\partial C^{\bullet}_{ECS}}{\partial \bar{u}_{ECS}} \tag{6.49}$$

where $\bar{u}$ represents the coupling function vectors between the SS and the PS, TMS, and ECS. Constraints (6.41) through (6.46) indicate that the weight and drag of the ECS, PS and TMS are set equal to the values indicated with the superscript *0*. These values are set externally. The necessary initial estimates of the weight fractions β_i were discussed earlier.

Now, on a fuel basis, the system-level, unit-based SS optimization problem is written as

$$\text{Minimize} \quad W_{FUEL} = w_{fuel}(W_{SS}, \vec{X}_{SS}, \vec{Y}_{SS}, mission, \lambda^f_{ps}, \Delta\bar{u}_{ps}, \lambda^f_{tms}, \Delta\bar{u}_{tms}, \lambda^f_{ecs}, \Delta\bar{u}_{ecs}) \tag{6.50}$$

w.r.t. $\{\vec{X}_{SS}, \vec{Y}_{SS}\}$

subject to

$$\vec{H}_{SS} = \vec{0}, \quad \vec{G}_{SS} \le \vec{0} \tag{6.51}$$

It is implicit in the formulation of the above problem that the fuel consumption over the entire mission is calculated using proper values for the coupling functions and shadow prices of the ECS, TMS and PS. Note that the subscript "*f*" indicates that the shadow prices are calculated on the basis of optimal fuel as opposed to optimal cost (i.e. as in equations (6.47) to (6.49)).

Finally, on a weight basis, the system-level, unit-based SS optimization problem is expressed as

$$\text{Minimize} \quad W_{TO} = w_{SS}(W_{TO}, W_{FUEL}, \lambda^w_{ps}, \Delta\bar{u}_{ps}, \lambda^w_{tms}, \Delta\bar{u}_{tms}, \lambda^w_{ecs}, \Delta\bar{u}_{ecs}) \tag{6.52}$$

w.r.t. $\{\vec{X}_{SS}, \vec{Y}_{SS}\}$,

subject to

$$\vec{H}_{SS} = \vec{0}, \quad \vec{G}_{sSS} \le \vec{0} \tag{6.53}$$

As with the previous problems, it is implicit that the SS weight over the entire mission is calculated using proper values for the coupling functions and shadow prices of the ECS, TMS and PS. Note that the subscript "*w*" indicates that the shadow prices are calculated on the basis of optimal weight as opposed to optimal cost (i.e. as in equations (6.47) to (6.49)). Furthermore, it is important to note that although the minimization of weight is not a thermoeconomic problem, it shares many of its characteristics. For example, the synthesis / design and operation of any given sub-system forces the sub-systems with which it interacts to change their size. In problem (6.52), that change is reflected in different weights and in problem (6.40) in different costs.

CHAPTER 7

7. PRELIMINARY RESULTS AND DISCUSSION

As indicated in Chapter 1 and 4, it is our intention at the completion of this project to have solve in its entirety the air craft synthesis / design problem posed in this report. In the mean time, however, for the purpose of this report, we will present some preliminary results showing the influence of the various coupling functions on the unit-level and system-level, unit-based synthesis / design optimization of the PS, ECS, and TMS (i.e. FLS and VC/PAOS). Furthermore, for the time being no decision variables are used for the SS, which is solved as and integral part of the PS. With all of this in mind, we proceed now with a presentation of our preliminary results.

The shadow prices are indicative of the relative importance of the intermediate products (i.e. coupling functions) going from one sub-system to the others and the corresponding feedback coming from the different subsystems. The shadow prices (the slopes of the curves) of the coupling functions going from the ECS to the PS for the first iteration of ILGO and for select mission legs are given in Figure 7.1. The constant behavior of the shadow prices for both design and off-design conditions is clearly manifest. This behavior is observed even though no energy or exergy quantities were used. The fact that the shadow prices represented by the slopes of the curves in Figure 7.1 are constant will help the relatively fast overall convergence of the ILGO scheme used. In Muñoz and von Spakovsky (2000b), it was theorized that constant shadow prices would lead to the final solution in only one iteration. This was not the case in this application, primarily due to the initial mismatch between bleed conditions used in the ECS optimization and those obtained from running the PS optimization.

A graphical representation of the impact of the coupling functions such as that given in Figure 7.1 becomes very important for identifying promising solutions. Figure 7.1 shows the change in the overall objective function that can be achieved by varying the intermediate products at the most stringent mission segments. Once a potential synthesis / design has been identified (by solving the optimization problem at the synthesis / design point, for example), one could take the intermediate products / feedbacks (ECS weight and drag and bleed air flow rate in this case) and easily evaluate their individual contributions to, say, W_{fuel}, in Figure 7.1.

A first order approximation using the allowable ranges for the ECS decision variables of Table 4.2a,b reveal that the variability of bleed air flow rate, ECS drag and weight are approximately 0.75 ± 0.2 kg/s, 350 ± 300 N and 400 ± 200 kg, respectively. With these values and the shadow prices of Figure 7.1, one can readily conclude that the effect of the ECS weight is significantly higher than that of the bleed air flow rate and momentum drag. Thus, the optimum ECS solution is expected to have the smallest possible weight value. The fact that all of the shadow prices have positive values indicates that a solution with lower bleed air flow rate and drag will be preferred for a given value of ECS weight.

The shadow prices of the coupling functions going from the TMS to the PS for the first iteration of the ILGO and for select mission legs are given in Figure 7.2. As for the ECS, constant behavior of the shadow prices for both design and off-design conditions is observed, again this constant behavior will be helpful in solving the optimization problem. For the TMS, the rate of energy was used to define one of the coupling

functions (i.e. the rate of energy extraction from the PS). The variability of the rate of energy extraction, TMS drag, and weight we found to be approximately 80 ± 60 kJ/s, 250 ± 150 N and 600 ± 300 kg, respectively. Based on this shadow prices values, one can conclude that the effect of TMS weight on the unit-level objective will by far be the most determinant of the TMS coupling functions.

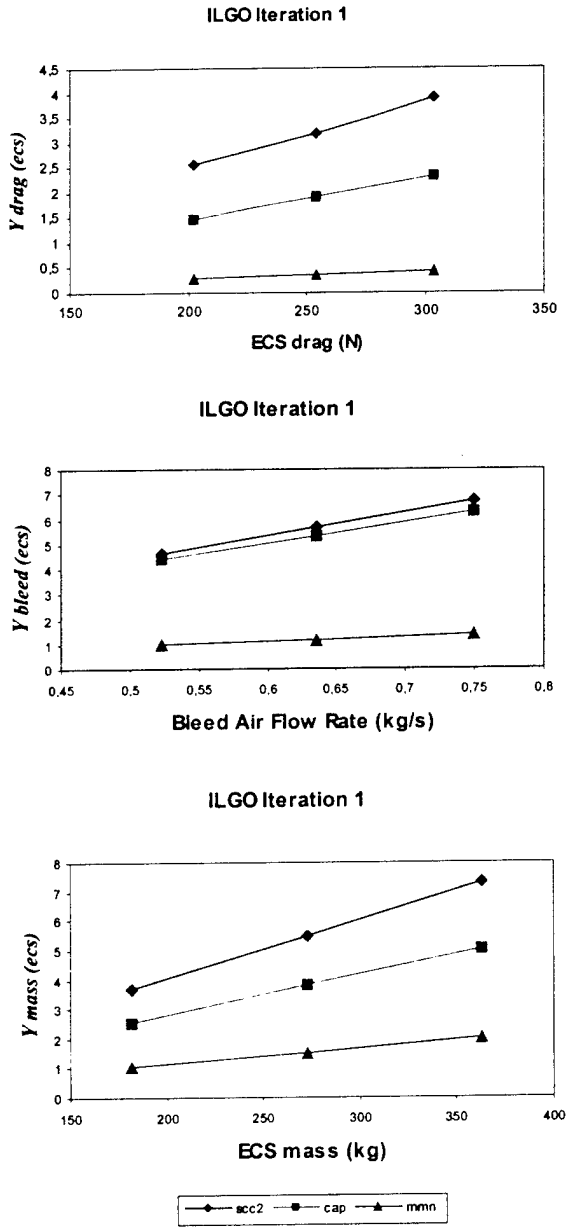

Figure 7.1. ECS drag, mass and bleed air flow rate shadow prices at the scc2 (the design point) and at the cap and mmn mission legs for the first ILGO iteration.

The shadow prices are the slopes of the curves.

$$Y_{drag} \equiv \frac{W_{FUEL}(\dot{m}_{Bleed}, D_{ECS}, W_{ECS}) - W_{FUEL}(\dot{m}_{Bleed}, 0, W_{ECS})}{W_{FUEL}(\dot{m}_{Bleed}, 0, W_{ECS})} x100 \; ; \; Y_{bleed} \equiv \frac{W_{FUEL}(\dot{m}_{Bleed}, D_{ECS}, W_{ECS}) - W_{FUEL}(0, D_{ECS}, W_{ECS})}{W_{FUEL}(0, D_{ECS}, W_{ECS})} x100$$

$$Y_{mass} \equiv \frac{W_{FUEL}(\dot{m}_{Bleed}, D_{ECS}, W_{ECS}) - W_{FUEL}(\dot{m}_{Bleed}, D_{ECS}, 0)}{W_{FUEL}(\dot{m}_{Bleed}, D_{ECS}, 0)} x100$$

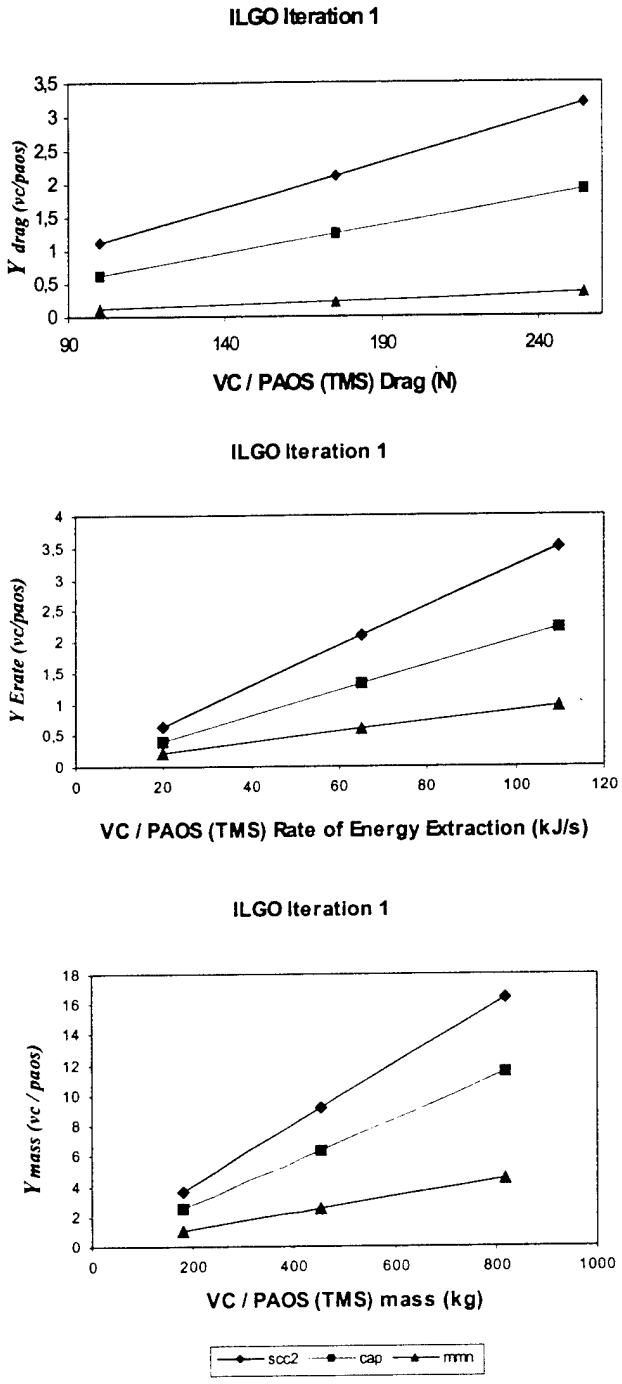

Figure 7.2. TMS (VC/PAOS) drag, mass and rate of energy extraction shadow prices at the scc2 (the design point) and at the cap and mmn mission legs for the first ILGO iteration. The shadow prices are the slopes of the curves

$$Y_{drag} \equiv \frac{W_{FUEL}(\dot{E}, D_{TMS}, W_{TMS}) - W_{FUEL}(\dot{E}, 0, W_{TMS})}{W_{FUEL}(\dot{E}, 0, W_{TMS})} x100 \; ; \; Y_{\dot{E}} \equiv \frac{W_{FUEL}(\dot{E}, D_{TMS}, W_{TMS}) - W_{FUEL}(0, D_{TMS}, W_{TMS})}{W_{FUEL}(0, D_{TMS}, W_{TMS})} x100$$

$$Y_{wtmi} \equiv \frac{W_{FUEL}(\dot{E}, D_{TMS}, W_{TMS}) - W_{FUEL}(\dot{E}, D_{TMS}, 0)}{W_{FUEL}(\dot{E}, D_{TMS}, 0)} x100$$

For the first ILGO iteration the shadow prices (the slope of the curves) of the coupling functions going from the ECS to the VC/PAOS (i.e. the bleed air mass flow through the bleed air / cold PAO heat exchanger) for the most stringent mission segments are shown in Figure 7.3. In graph 7.3 can be seen the considerable effect that the ECS intermediated product has on the VC/PAOS unit-level objective function. The bleed air mass flow through the bleed air / cold PAO heat exchanger represents a significant amount of heat load for the VC/PAOS. Notice that the shadow prices are positive, which again indicates that a lower bleed air mass flow through the bleed air / cold PAO heat exchanger will be preferred with respect to the VC/PAOS unit-level objective. However, this is not necessarily true for the system-level optimization problem.

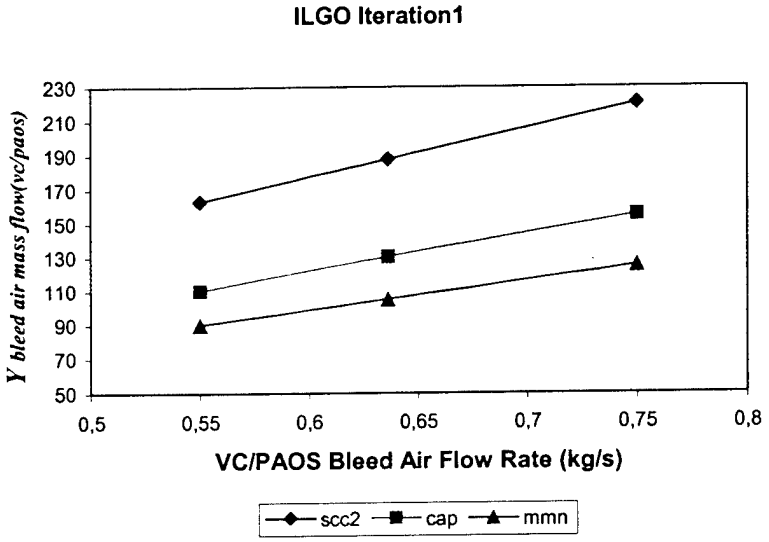

Figure 7.3. VC/PAOS bleed air mass flow through the bleed air / cold PAO heat exchanger shadow prices at the scc2 (the design point) and at the cap and mmn mission segments for the first ILGO iteration. The shadow prices are the slopes of the curves.

$$Y_{vcr\,/\,paos-ecs} \equiv \frac{W_{FUEL_{VCR\_PAOS}}(\dot{m}_{bleed}) - W_{FUEL_{VCR\_PAOS}}(0)}{W_{FUEL_{VCR\,/\,PAOS}}(0)} x100$$

Now, as to the shadow prices (the slope of the curves) of the intermediate product going from the FLS to the VC/PAOS (i.e. the initial fuel tank temperature), they are shown for the most stringent mission segments in Figure 7.4. In Figure 7.4, the considerable effect that the FLS intermediated product has on the VC/PAOS unit-level objective can be seen. Notice that the shadow prices are again positive, which indicates that a lower fuel tank temperature will be preferred in terms of the VC/PAOS unit-level objective. Nonetheless this is not necessarily true for the system-level optimization problem.

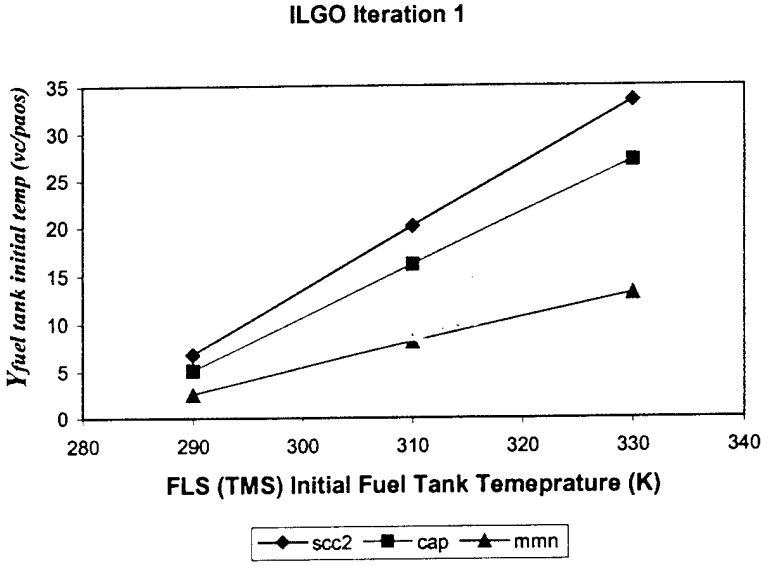

Figure 7.4. FLS (TMS) initial tank temperature shadow prices at the scc2 (the design point) and at the cap and mnn mission segments for the first ILGO iteration. The shadow prices are the slopes of the curves.

$$Y_{vcr\,/\,paos-fls} \equiv \frac{W_{FUEL_{VCR\_PAOS}}(T_{fuel}) - W_{FUEL_{VCR\_PAOS}}(T_0)}{W_{FUEL_{VCR\_PAOS}}(T_0)} x100$$

$$T_0 = 280^{\circ} K$$

For the first ILGO iteration the shadow prices (the slope of the curves) of the coupling function going from the VC/PAOS to the FLS (i.e. heat transfer rate from the VC/PAOS to the FLS through the fuel / cold PAO heat exchanger) for the most stringent mission segments are shown in Figure 7.5. Notice that the shadow prices are positive, which again indicates that a lower rate of energy exchange indicates a lower unit-level objective for the FLS. However, this is not necessarily true for the system-level optimization problem. The shadow prices of the coupling function going from the ECS to the VC/PAOS (i.e. heat transfer rate from the ECS to the VC/PAOS) are shown in Figure 7.6. What is interesting to note in Figure 7.6 is that the shadow prices are negative, which means that a bigger rate of energy exchange between the ECS and the VC/PAOS indicates a lower unit-level objective for the ECS.

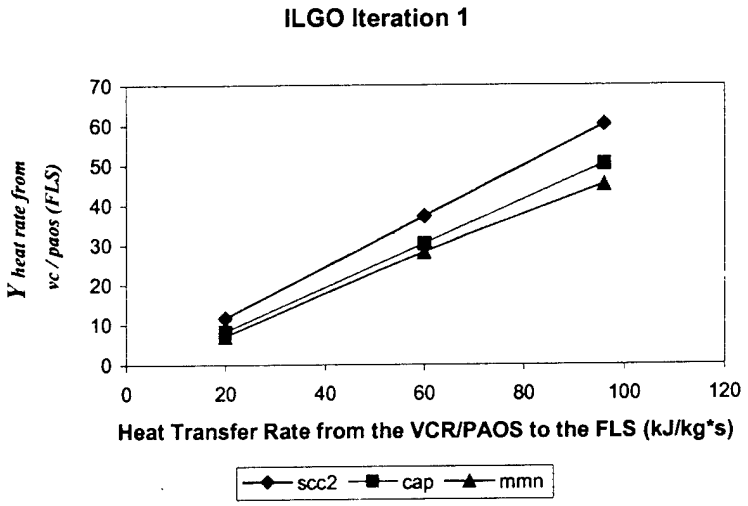

Figure 7.5. Heat transfer rate from the VCR/PAOS to the FLS shadow prices at the scc2 (the design point) and at the cap and mmn mission segments for the first ILGO iteration. The shadow prices are the slopes of the curves.

$$Y_{fls-vcr/paos} \equiv \frac{W_{FUEL_{FLS}}(\dot{E}_{vcr/paos}) - W_{FUEL_{FLS}}(0)}{W_{FUEL_{FLS}}(0)} x100$$

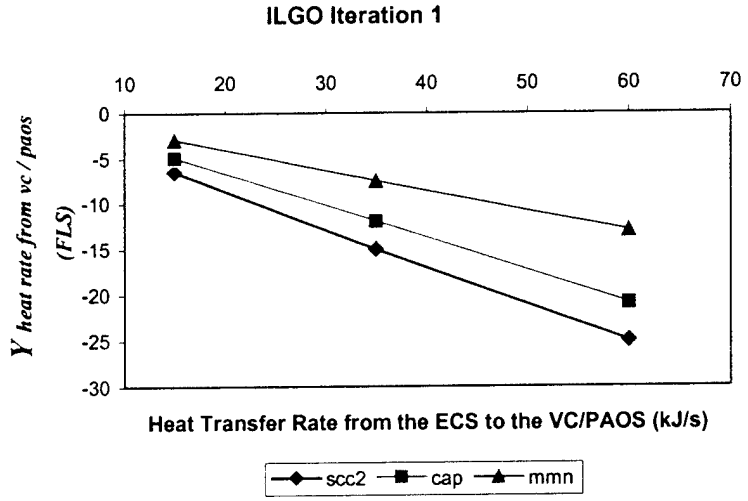

Figure 7.6. Heat transfer rate from the ECS to the VC/PAOS shadow prices at the scc2 (the design point) and at the cap and mmn mission legs for the first ILGO iteration. The shadow prices are the slopes of the curves

$$Y_{ecs-vcr/paos} \equiv \frac{W_{FUEL_{ECS}}(\dot{E}_{VCR/PAOS}) - W_{FUEL_{ECS}}(0)}{W_{FUEL_{ECS}}(0)} x100$$

Table 7.1, 7.2, and 7.3. show the top four solutions in the first ILGO iteration for the synthesis / design segment (scc2) of the ECS, VC/PAOS, and FLS respectively . Notice that for each of these sub-systems the best solution at the synthesis / design point has the lowest possible weight. For the optimum solution the heat exchanger design decision variables tend to be at the lowest values of the constraint range. These top four solutions must be evaluated through the whole mission in order to determine the operational decision variable values for the off-design mission legs. This process yields the mission optimum for each sub-system, as well as the intermediate products and feedbacks required for the next ILGO iteration. At the moment only results for the first ILGO iteration are available. However, the results generated are enough to prove that the shadow prices have constant behavior, which should guarantee (i.e. few iterations) convergence after a few iterations for the system-level optimization problem.

Table 7.1. Top four solutions for the ECS based on the synthesis / design segment (scc_2).

			Solution Ranking			
			1	2	3	4
Primary heat exchangers	L_r	Cold-side length (m)	0.505	0.511	0.504	0.503
	L_b	Hot-side length (m)	0.060	0.063	0.064	0.060
	L_n	Non-flow length (m)	0.504	0.508	0.500	0.502
Secondary heat exchangers	L_r	Cold-side length (m)	0.505	0.500	0.525	0.501
	L_b	Hot-side length (m)	0.061	0.066	0.062	0.060
	L_n	Non-flow length (m)	0.508	0.500	0.523	0.503
Air cycle machine	PR_{cp}	Compressor design pressure ratio	2.7	2.6	2.7	2.8
	PR_{tb}	Turbine design pressure ratio	10.1	8.9	7.5	7.1
Regenerative heat exchangers	L_r	Cold-side length (m)	0.300	0.300	0.300	0.300
	L_b	Hot-side length (m)	0.150	0.150	0.155	0.171
	L_n	Non-flow length (m)	0.300	0.300	0.300	0.300
	Reg_1	Existence-nonexistence	0	0	0	0
	Reg_2		1	1	1	1
Ram air inlet, outlet 1	A_1,	Areas of inlet, outlet (cm^2)	103	113	119	125
Ram air inlet, outlet 2	A_2	Areas of inlet, outlet (cm^2)	103	133	141	149
Heat exchanger fin type: hot sides	Fin_{hot}	Number of fins	14	14	16	19
Heat exchanger fin type: cold sides	Fin_{cold}	Number of fins	14	14	16	19
W_{ECS}/g		Kg	235	253	271	282

Table 7.2. Top four solutions for the VC/PAOS based on the synthesis / design segment.

			Solution Ranking			
			1	2	3	4
Bleed air / PAO heat exchanger	L_r	Length ram side (m)	0.621	0.621	0.514	0.771
	L_b	Length bleed side (m)	0.050	0.186	0.128	0.133
	L_n	Non-flow length (m)	0.866	0.866	0.867	0.326
Condenser	L_r	Length ram side (m)	0.400	0.445	0.404	0.767
	L_b	Length bleed side (m)	0.050	0.156	0.056	0.171
	L_n	Non-flow length (m)	0.593	0.593	0.752	0.361
Evaporator	L_r	Length ram side (m)	0.300	0.390	0.400	0.878
	L_b	Length bleed side (m)	0.050	0.070	0.157	0.243
	L_n	Non-flow length (m)	0.468	0.468	0.732	0.566
Ram air / hot PAO heat exchanger	L_r	Length ram side (m)	0.300	0.351	0.883	0.811
	L_b	Length bleed side (m)	0.050	0.080	0.097	0.177
	L_n	Non-flow length (m)	0.887	0.887	0.692	0.631
Vapor Compressor	Pr	Pressure Ratio Vapor Compressor	4.82	4.82	5.36	5.32
	m_v	Vapor mass flow(kg/s)	2.16	2.16	1.125	0.23
Hot PAO cycle	m_{HPAO}	Hot PAO loop mass flow	1.24	1.24	1.416	0.528
	V_5	Fuel / hot PAO heat exchanger bypass valve position	0.024	0.024	0.016	0.017
	V_4	Bleed Air / hot PAO heat exchanger bypass valve position	0.058	0.058	0.039	0.037
	V_2	Vapor / hot PAO heat exchanger bypass valve position	0.070	0.070	0.023	0.027
Ram air / hot PAO heat exchanger	*On/off*	Place or not ram air / hot PAO heat exchanger	1	1	1	1
W_{ECS}/g		kg	466	483	502	520

Table 7.3. Top four solutions for the FLS based on the synthesis / design segment (scc_2).

			Solution Ranking			
			1	2	3	4
Fuel / Oil heat Exchanger	L_r	Length ram side (m)	0.621	0.621	0.621	0.504
	L_b	Length bleed side (m)	0.050	0.050	0.050	0.064
	L_n	Non-flow length (m)	0.866	0.866	0.866	0.500
Fuel / PAO Heat Exchanger	L_r	Length ram side (m)	0.400	0.400	0.400	0.400
	L_b	Length bleed side (m)	0.050	0.050	0.050	0.050
	L_n	Non-flow length (m)	0.593	0.593	0.593	0.593
Fuel / Ram air heat exchanger	L_r	Length ram side (m)	0.300	0.300	0.300	0.300
	L_b	Length bleed side (m)	0.050	0.050	0.050	0.050
	L_n	Non-flow length (m)	0.468	0.468	0.468	0.468
Fuel / hydraulic heat exchanger	L_r	Length ram side (m)	0.300	0.300	0.300	0.300
	L_b	Length bleed side (m)	0.050	0.050	0.050	0.050
	L_n	Non-flow length (m)	0.887	0.887	0.887	0.887
Ram Air Inlet	A_i	Area of inlet, outlet (cm^2)	523	527	541	556

Figures 7.3, 7.4, and 7.6 show the relationship between the VC/PAOS unit-level objective function and the feedbacks coming from the other sub-systems (i.e. PS, ECS, FLS). In these figures all, the relationships are demonstrated to be linear, which according to Muñoz and von Spakovsky (2000b) facilitates the system-level optimization problem convergence. Upon solving the unit-level optimization problem for the VC/PAOS, a unit-level Optimum Response Surface (ORS) can be generate for this sub-system. This unit-level ORS is a five dimensional hyper-surface and represents the weight, fuel, or cost penalty due to the VC/PAOS as a function of the coupling functions (i.e. corresponding feedbacks from the PS, ECS, FLS).

The unit-level optimum response surface of the VC/PAOS as a function of the fuel tank initial temperature and the bleed air mass flow through the bleed air / cold PAO heat exchanger coming from the ECS is showed in Figure 7.7. This ORS corresponds to a hyper-plane and clearly shows the linear relationship between the unit-level objective function and the corresponding coupling functions. Similar surfaces can be generated from the feedbacks coming from the PS. In this way, any combination of coupling functions can be used to generate the family of ORSs for the VC/PAOS or any other sub-system. Figure 7.7 illustrates how by selecting the coupling functions wisely, the desirable planar behavior and smoothness of the unit-level ORSs follow quite naturally. This type of behavior has also been confirmed by Muñoz and Spakovsky (2000a,b,c,d; 2001a,b).

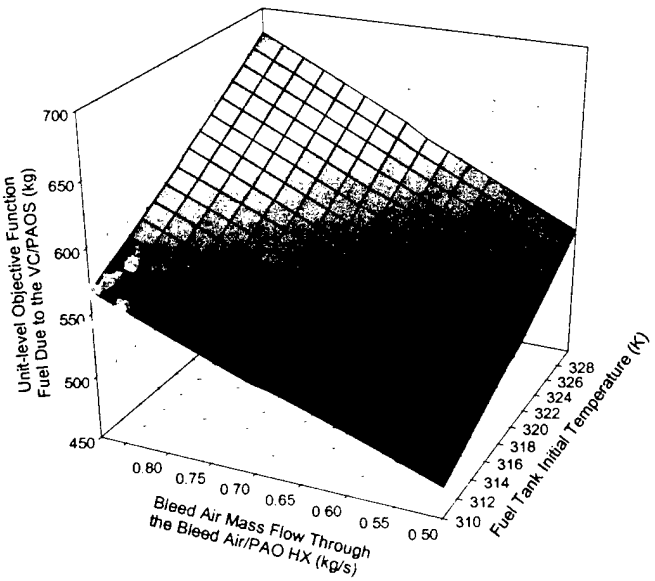

Figure 7.7. Optimum Response Surface (ORS) for the VC/PAOS in the bleed air flow and initial tank temperature directions.

Figure 7.8 shows the dependence of the objective function (on a fuel basis) of the VC/PAOS on the sub-system mass and on the energy required by the compressor. It is clear that the weight is the predominant factor, which determines fuel consumption due to this sub-system. This was expected since from Figure 7.2 it was deduced that the TMS weight effect is by far the most determinant one for this sub-system. On the other hand, the effect that the energy required by the vapor compressor has on the objective function is slight.

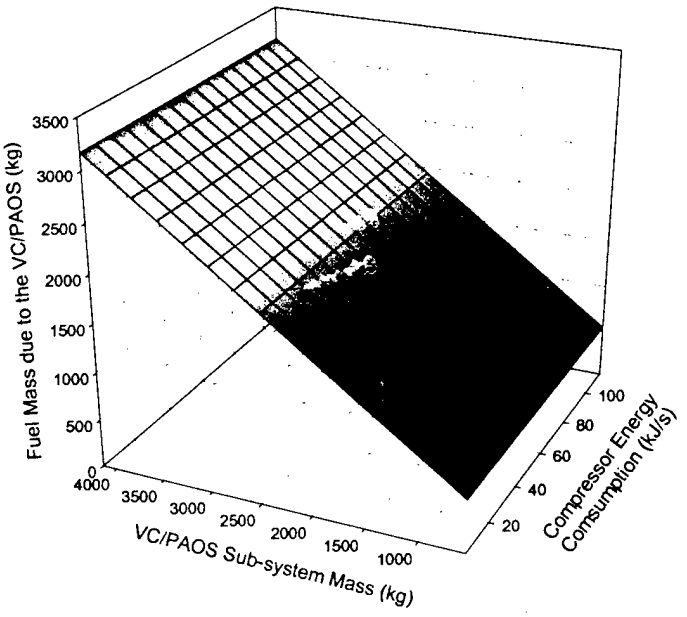

Figure 7.8. VC/PAOS ORS (on a fuel basis) in the sub-system mass and the compressor energy consumption directions.

Finally, Figure 7.9 shows the design space for the fuel mass due to the VC/PAOS as a function of the vapor condenser cold-side and hot-side length, which are geometric decision variables. For the same sub-system, Figure 7.10 shows the design space for unit-level objective function (fuel mass) as a function of two operational decision variables, the vapor compressor pressure ratio and the refrigerant mass flow. Similar sorts of graphs were developed for the PS and the ECS. Figure 7.11 shows the design space for the fuel mass due to the ECS as a function of the primary heat exchanger hot-side and cold-side length, which as for Figure 7.9 are geometric decision variables. Figure 7.12 shows for the PS the mission fuel mass in terms of the low and high pressure turbines pressure ratios. What is interesting to note is that the non-linearities of the problem appear in the surfaces with respect to the unit-level (local) decision variables and that the linearities in contrast appear in the surfaces with respect to the coupling functions. Hence, the basic premise of the ILGO, which is to effectively and intelligently decompose the system-level optimization problem into a set of unit-level problems, is verified.

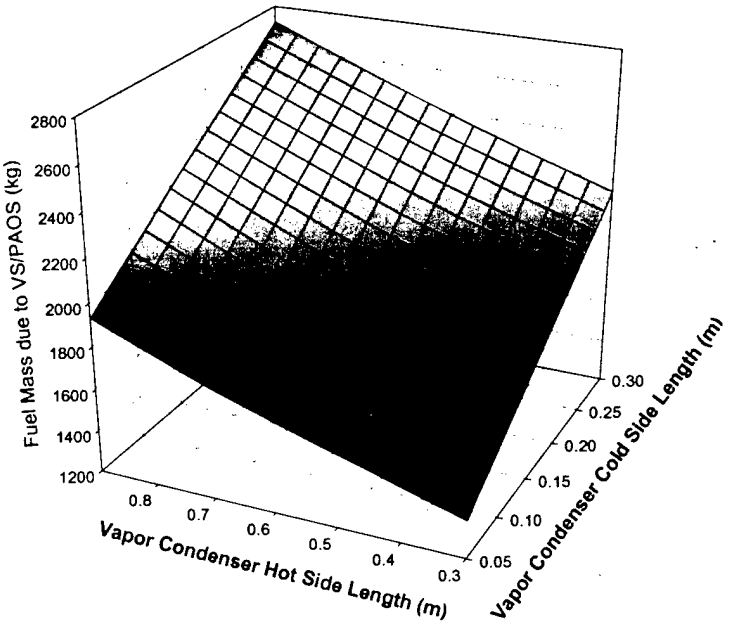

Figure 7.9. Design space for the fuel mass due to the VC/PAOS as a function of the vapor condenser cold-side and hot-side length.

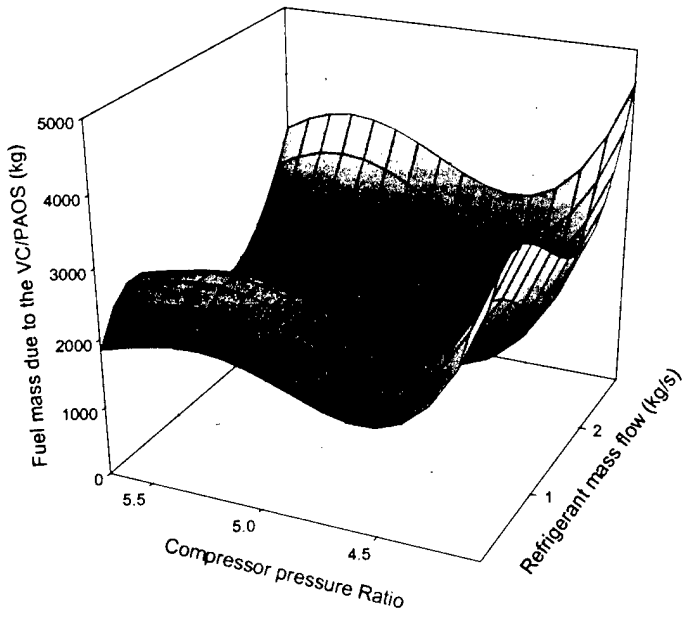

Figure 7.10. Design space for unit-level objective function (fuel mass) as a function of the vapor compressor pressure ratio and the refrigerant mass flow.

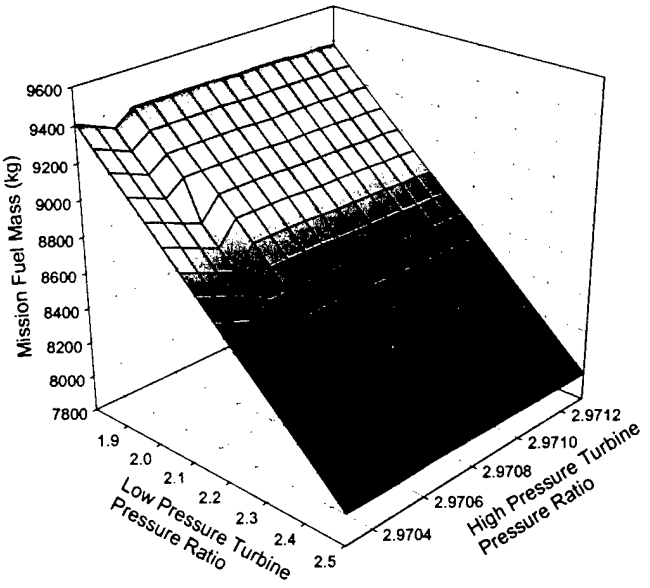

Figure 7.11. Design space for the fuel mass due to the ECS as a function of the primary heat exchanger hot-side and cold-side length.

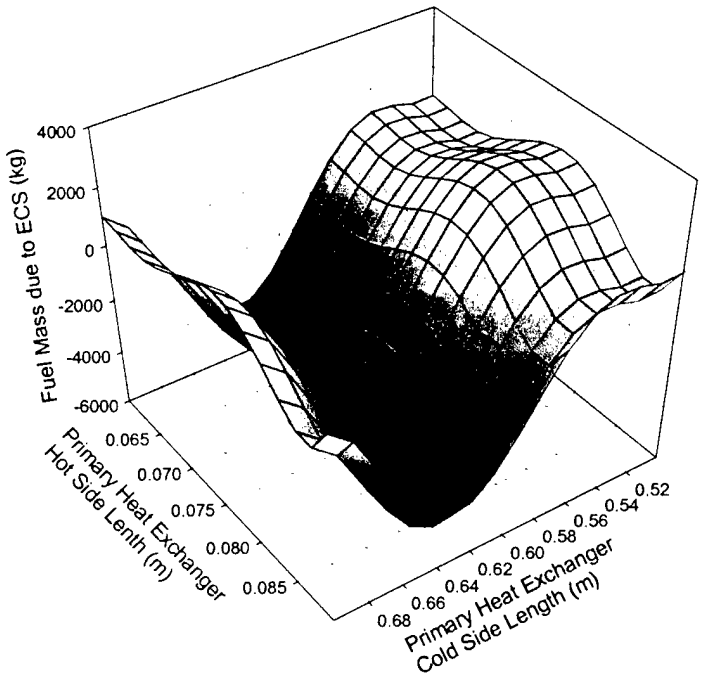

Figure 7.12. The PS the mission fuel mass in terms of the low and high pressure turbines pressure ratios.

CHAPTER 8

8. CONCLUSIONS

The overall problem of *integrated* aircraft synthesis / design *optimization* with variable loads and/or environmental conditions is a very complex and difficult problem to solve. *Decomposition* is seen as a tool for overcoming the mathematical, cultural, and software difficulties that can occur if this synthesis / design problem is formulated as a single problem for the system as a whole. *Decomposition* not only permits the solution of the overall synthesis / design problem but facilitates the difficult task of sub-system integration. The methods presented here are seen to match and enhance existing design practices and are in tune with the current need for concurrent, collaborative environments that make use of multiprocessing as well as parallel and internet capabilities.

As part of this project over the past two years, a general methodology (ILGO) for the decomposed synthesis / design optimization of highly coupled, highly dynamic energy systems has been developed and applied to an aircraft propulsion sub-system (PS) coupled to an environmental control sub-system (ECS) and is currently being applied to a combination of coupled aircraft sub-systems, namely, a PS, an ECS, a TMS (thermal management sub-system) and a SS (structural sub-system). Results for the former application have been presented in previous publications including a Ph.D. dissertation and several conference and journal publications. Some preliminary results for the latter application have been presented in this report. It is our intention at the completion of this project to have solved this problem in its entirety, resulting in the publications and Ph.D. dissertation already mentioned and submitted as our annual report in year one of this project and an M.S. thesis along with some additional conference and journal publications. The M.S. thesis will serve as our final report for the final phase of this project to be completed next year.

Finally, we believe that we have made significant strides in successfully dealing with all of the fundamental issues set forth in our original proposal and enumerated in *Chapter 1* of this report. These include the extension and application of our unique decomposition strategy for the large-scale optimization of highly complex, highly dynamic aircraft systems

- to encompass not only the energy-based sub-systems but the non-energy based sub-systems (e.g., structures / aerodynamics) of an advanced fighter aircraft;
- to optimally account for transient effects such as those related to the fuel loop of the aircraft;
- to enlarge the degrees of freedom possible when optimizing problems of heat and mass transfer in aircraft synthesis/design which require the use of CFD techniques.

Nomenclature

a	Speed of sound
A	Area
AAF	Air-to-Air Fighter
AR	Aspect Ratio
b	Wing span
B_h	Horizontal tail span
BCA	Best cruise altitude
BCM	Best cruise Mach Number
$bleed$	ECS bleed
BP	Bleed port
Cp	Specific heat
C	Objective function, cost
$\dot{C}$	Cost rate
cap	Combat air patrol
cac	Combat acceleration
C_{fe}	Skin friction factor
$C_{l\alpha}$	Airfoil lift curve slope
$C_{L\alpha}$	Wing lift coefficient
C_L	Lift coefficient
C_D	Drag coefficient
C_{D0}	Drag coefficient at zero lift
C_{Dwave}	Drag coefficient due to wave shocks
ct_1	Combat turn 1
LPT	Low pressure turbine
m_{fuek_in}	Rate of fuel going into the fuel tank
m_{fuel_out}	Rate of fuel going out of the fuel tank
$\dot{m}_f$	Rate of fuel
M	Mach number, fuel tank mass
mil	Military
mmn	Maximum Mach number
$MINLP$	Mixed integer non-linear programming problem
$MILP$	Mixed integer linear programming problem
N	Number of turns
N_z	Ultimate load factor
n	Load factor
O	Number of operational variables
P	Product
$p\ \dot{p}$	Product rate
$p, \vec{p}$	Forward feedback function, product vector
PAO	Polyalphaolefin
$PPAY$	Permanent payload
Pr	Vapor compressor pressure ratio
PR	Pressure ratio
PS	Propulsion Sub-system
q	Load factor
R	External input, resource,

ct_2	Combat turn 2
d	Number of design variables, Fuselage maximum equivalent diameter
D	Drag
e	span efficiency factor
E	Exergy, energy, energy transfer rate, energy extraction rate
ECS	Environmental Control Sub-System
$EPAY$	Expendable payload
esc	Escape dash
f	Objective function, feedback vector
F	"Uninstalled" thrust
F	Fuselage lift factor
F_w	Fuselage width at tail intersection
FLS	Fuel Loop Sub-system
g	Acceleration of gravity
G, g	Vector of inequality constraints
h	Altitude, endplate height
H,h	Vector of inequality constraints
HX	Heat exchanger
HPC	High pressure compressor
HPT	High pressure turbine
HX	Heat exchanger
$ILGO$	Iterative Local-Global Optimization
k_i	Conversion Factor
K_1	Aerodynamic Constant
K_2	Aerodynamic Constant
K_{dw}	Constant
K_{vs}	Constant
W_{dg}	Flight design gross weight
L_c	Cold side length
L_h	Hot side length
L_n	Non flow length
LCC	Life cycle cost
loi	Loiter
r	Intermediate resource
R	Additional or "parasitic" drag
Re	Reynolds number
Ri	External Resources
RFP	Request for proposal
Q	Heat transfer
S	Wing planform area
$scc2$	Subsonic cruise climb second
SL	Sea level
Sp	Vehicle speed in kilonots
SS	Structures Sub-system
t	Time
t/c	Thickness Ratio
T	"Installed" thrust, total time for the set of load/environmental conditions, Temperature
T_{SL}	Thrust sea level
$TLCC$	Total Life Cycle Cost
TMS	Thermal Management System
$TSFC$	Thrust specific fuel consumption
V	Velocity, Bypass valve position
VC / PAOS	Vapor Compressor and PAO loops subsystem
V_{TD}	???
u, U	Coupling function
$WATE$	Weight Analysis of Turbine Engines
V	Vector of flow and thermodynamic variables
w	Vector of geometrical variables, weight
W_{TO}	Gross takeoff weight
x	Vector of design variables
y	Vector of operational variables
Z	Capital function (weight, cost)

Greek

α	Step size, thrust fraction, engine bypass ratio, angle of attack
β	Weight fraction
δ	Design point
ε	Small number
$\mathcal{E}$	Heat exchanger Effectiveness
ϕ	Inlet and nozzle drag coefficients
ρ	Air density
γ	Specific heat ratio, input function
Γ	Vector or inequality constraints for dynamic energy systems
H	Vector or equality constraints (analysis system of equations) for dynamic systems
φ	Stall margin (%)
λ, Λ	Marginal cost, shadow price, vector of marginal costs, taper ratio
Λ_{LE}	Quarter chord sweep angle
π	Leg weight ratio
τ	Number of time segments into which the set of load/environmental conditions is divided
ξ	Value of a coupling function
ψ	Value of a coupling function
Y	Vector or operational decision variables for dynamic energy systems
ζ	Cost function

Superscripts

o	Reference, initial value
**	Optimum
p	Capital
*	Restricted optimum
◊	Feasible and "promising" solution

Subscripts

f	Fuel
decs	ECS drag
it	Inlet temperature
o	Reference, initial value
0	Ambient
wecs	ECS weight
*	Optimum

BIBLIOGRAPHY

Anderson, J.D. Jr., 1999, *Aircraft Performance and Design*, WCB/McGraw-Hill

Balling R.J.and Sobieszczanski-Sobieski, J, 1996, "Optimization of Coupled Systems: A Critical Overview of Approaches," *AIAA Journal*, Vol. 34, No. 1, January

Bejan, A., 1995, *Entropy Generation Minimization*, CRC Press, Boca Raton, Florida.

Bejan, A., R., "A Role for Exergy Analysis and Optimization in Aircraft Energy-System Design," AIAA Paper No. 2000-4855, *8th AIAA/USAF/NASA/ISSMO Symposium on Multidisciplinary Analysis and Optimization*, Long Beach, California, September 6-8, 2000.

Bejan, A., Tsatsaronis, G., Moran, M. J., 1996, *Thermal Design and Optimization*, John Wiley and Sons, New York.

Boland, D. and Linnhoff, B., 1979, "The Preliminary Design of Networks for Heat Exchange by Systematic Methods," *Chemical Engineer*, pp 222-228.

Brown, D.A., "Integrated Energy Management System for Uninhabited Combat Air Vehicles (UCAVs)," *IECEC 1999*, Paper No.249. Vancouver, 1999.

Chong, E.K.P., and Zak, S.H., 1996, *An Introduction to Optimization*, Wiley-Interscience, New York, New York.

Curti, V., von Spakovsky, M.R., Favrat, D., 2000, "An Environomic Approach for the Modeling and Optimization of a District Heating Network Based on Centralized and Decentralized Heat Pumps, Cogeneration and/or Gas Furnace (Part I: Methodology)," *International Journal of Thermal Sciences*, vol. 39, no. 6, June, Elsevier, France.

Curti, V., von Spakovsky, M.R., Favrat, D., 2000, "An Environomic Approach for the Modeling and Optimization of a District Heating Network Based on Centralized and Decentralized Heat Pumps, Cogeneration and/or Gas Furnace (Part II: Application)," *International Journal of Thermal Sciences*, vol. 39, no. 6, June, Elsevier, France.

Dieckmann, R.R, Watson, A.C. and Glover, S.F., 1972, *Development of Integrated Environmental Control Systems for Aircraft*, Report No. AFFDL-TR-72-9, Air Force Flight Dynamics Laboratory, WPAFB, OH.

El-Sayed Y., 1989, "A Decomposition Strategy for Thermoeconomic Optimization," *ASME Journal of Energy Resources Technology*, vol. 111, pp 1-15

El-Sayed Y., 1996, "A Second-Law-Based Optimization: Part I Methodology & Part 2," *ASME Journal of Energy Resources Technology*, Vol. 118, pp. 693-703.

El-Sayed, Y.M. and Evans, R.B., 1970, "Thermoeconomics and the Design of Heat Systems," *Journal of Engineering for Gas Turbines and Power*, ASME Transactions, Vol. 92, 27, Jan.

El-Sayed, Y.M., 1996, "A Second-Law-Based Optimization: Parts 1 and 2," *Journal of Engineering for Gas Turbines and Power*, ASME Transactions, vol. 118, October, N.Y.

Evans, R.B. and Tribus, M., 1962, *A Contribution to the Theory of Thermoeconomics*, UCLA Dept. of Engineering: Report No. 62-63, Los Angeles, CA, August.

Evans, R.B. and von Spakovsky, M.R., 1993, "Engineering Functional Analysis (Parts I)," *Journal of Energy Resources Technology*, ASME transactions, Vol. 115, No. 2, N.Y., N.Y., June.

Evans, R.B. and von Spakovsky, M.R., 1993, "Engineering Functional Analysis (Parts II)," *Journal of Energy Resources Technology*, ASME transactions, Vol. 115, No. 2, N.Y., N.Y., June.

Evans, R.B., 1980, "Thermoeconomic Isolation and Essergy Analysis," *Energy: The International Journal*, Vol. 5, Nos. 8-9, 805-821.

Floudas, A., 1995, *Nonlinear and Mixed-Integer Optimization*, Oxford University Press, New York.

Frangopoulos, C. A., 1994, "Application of the Thermoeconomic Functional Approach to the CGAM Problem," *Energy: The International Journal*, Vol. 19, No. 3, pp. 323-342.

Frangopoulos, C.A., 1983, *Thermoeconomic Functional Analysis: A Method for Optimal Design or Improvement of Complex Thermal Systems*, School of Mechanical Engineering, Georgia Institute of Technology, Ph.D. Dissertation.

Frangopoulos, C.A., 1984, "Thermoeconomic Functional Analysis: An Innovative Approach to Optimal Design of Thermal Systems," *Second Law Aspects of Thermal Design*, HTD Vol. 33, ASME, N.Y., N.Y., August.

Frangopoulos, C.A., 1989, "Optimal Synthesis and Operation of Thermal Systems by the Thermoeconomic Functional Approach," *ASME Winter Annual Meeting*, AES 10-3, 49.

Frangopoulos, C.A., and von Spakovsky, M.R., 1993, "The Environomic Analysis and Optimization of Energy Systems (Part I)," *Proceedings of the International Conference on Energy Systems and Ecology: ENSEC'93*, Vol. I, pp. 123-132, ASME, Cracow, Poland, July.

Frangopoulos, C.A., Evans R.B., 1984, "Thermoeconomic Isolation and Optimization of Thermal System Components," *Second Law Aspects of Thermal Design*, HTD Vol. 33, ASME, N.Y., N.Y., August.

Gaggioli R. and El-Sayed Y., 1989, "A Critical Review of Second Law Costing Methods," *Journal of Energy Resources Technology*, ASME Transactions, vol. 111, pp 1-15.

Gaggioli, R., Sama, D.A., Qian, S., and El-Sayed, Y. M., 1991, "Integration of a New Process into an Existing Site: A Case Study in the Application of Exergy Analysis," *Journal for Engineering for Gas Turbines and Power*, ASME Transactions, vol. 113, no. 2.

Goldberg, D. E., 1989, *Genetic Algorithms in Search, Optimization and Machine Learning*, Addison Wesley, Reading, MA.

iSIGHT version 5 User's Guide, 1999, Engineous Software Inc., Morrisville, N.C.

Jane's All the World's Aircraft 1999-2000, 1999, Jane's Information Group, Couldson, UK

Kays, W.M. and London, A.L., 1998, *Compact Heat Exchangers*, Krieger Publishing Company, Malabar, FL.

Kestin, J., 1980, "Availability: The Concept and Associated Terminology," *Energy-The International Journal*, Vol. 5, pp. 679-692.

Lazzaretto, A. and Andreatta, R., 1995, "Algebraic Formulation of a Process-Based Exergo-economic Method," *Thermodynamics and the Design, Analysis and Improvement of Energy Systems*, AES-Vol. 35.

Le Claire, R., 1975, "Evaluation of the Overall Fuel Mass Penalty of an Aircraft System," *Aeronautical Journal*, May, pp 225-228.

Letton, Jr, G., 1976, "Avionics Cooling on USAF Aircraft," *AGARD Conference Proceedings on Avionic Cooling and Power Supplies for Advanced Aircraft*, The Hague, Netherlands, June.

Linnhoff, B., 1993, "Pinch Technology for the Synthesis of Optimal Heat and Power Systems," *Journal of Energy Resources Technology*, ASME Transactions, vol. 111.

Mattingly, J.D., Heiser,W.H. and Daley, D.H., 1987, *Aircraft Engine Design*, AIAA Education Series, New York, New York.

Moran, M. J., 1982, *Availability Analysis. A Guide to Efficient Energy Use*, Prentice Hall, Englewood Cliffs, N.J.

Muñoz J. R., 2000, *Optimization Strategies for the Synthesis / Design of Highly Coupled, Highly Dynamic Energy Systems*, Ph.D. dissertation, Department of Mechanical Engineering, Virginia Polytechnic Institute and State University, Blacksburg, VA, November.

Muñoz J. R., von Spakovsky M.R., 1999, *A Second Law Based Integrated Thermoeconomic Modeling and Optimization Strategy for Aircraft / Aerospace Energy System Synthesis and Design (Phase I - Final Report)*, final report, Air Force Office of Scientific Research, New Vista Program, December.

Muñoz, J.R. and Michaelides, E.E., 1999, "The Effect of the Model of the Environment on Exergy Analyses," *Journal of Energy Resources Technology*, ASME Transactions. Vol. 121. No. 4, pp. 268-276

Muñoz, J.R. and von Spakovsky, M.R., 2000a, "An Integrated Thermoeconomic Modeling and Optimization Strategy for Aircraft / Aerospace Energy System Design," *Efficiency, Costs, Optimization, Simulation and Environmental Aspects of Energy Systems (ECOS'00)*, Twente University, ASME, Netherlands, July 5-7.

Muñoz, J.R. and von Spakovsky, M.R., 2000b, "The Use of Decomposition for the Large-Scale Synthesis/ Design Optimization of Highly Coupled, Highly Dynamic Energy Systems: Part I - Theory," *2000 ASME International Mechanical Engineering Congress and Exposition*, Advanced Energy Systems Division, AES-Vol. 40, Orlando, FL, Nov 5-10.

Muñoz, J.R. and von Spakovsky, M.R., 2000c, "The Use of Decomposition for the Large-Scale Synthesis/ Design Optimization of Highly Coupled, Highly Dynamic Energy Systems: Part II - Applications," *2000 ASME International Mechanical Engineering Congress and Exposition*, Advanced Energy Systems Division, AES-Vol. 40, Orlando, FL, Nov 5-10.

Muñoz, J.R., von Spakovsky, M.R., 2000d, "Decomposition in Energy System Synthesis / Design Optimization for Stationary and Aerospace Applications," *8th AIAA/NASA/USAF/ISSMO Symposium on Multidisciplinary Analysis and Optimization*, AIAA Paper No. 2000-4853, Long Beach, CA, September 6-8.

Muñoz, J.R., von Spakovsky, M.R., 2001a, "The Application of Decomposition to the Large Scale Synthesis/Design Optimization of Aircraft Energy Systems," *International Journal of Applied Thermodynamics*, June, vol. 4, no.2.

Muñoz, J.R., von Spakovsky, M.R., 2001b, "A Decomposition Approach for the Large Scale Synthesis/Design Optimization of Highly Coupled, Highly Dynamic Energy Systems," *International Journal of Applied Thermodynamics*, March, vol. 4, no. 1.

Newberry, C.F., "Exergy - The Aircraft Design Variable of Choice?," AIAA Paper No. 2000-4851, *8th AIAA/USAF/NASA/ISSMO Symposium on Multidisciplinary Analysis and Optimization*, Long Beach, California, September 6-8, 2000.

Nicolai, L., 1975, *Fundamentals of Aircraft Design*, published by the author.

Olsommer, B., von Spakovsky, M.R., Favrat, D., 1999a, "An Approach for the Time-dependent Thermoeconomic Modeling and Optimization of Energy System Synthesis, Design and Operation (Part I: Methodology and Results)," *International Journal of Applied Thermodynamics*, Vol. 2, No. 3.

Olsommer, B., von Spakovsky, M.R., Favrat, D., 1999b, "An Approach for the Time-dependent Thermoeconomic Modeling and Optimization of Energy System Synthesis, Design and Operation (Part II: Reliability and Availability)," *International Journal of Applied Thermodynamics*, Vol. 2, No. 4.

Paulus, D. and Gaggioli, R., "Rational Objective Functions for Vehicles," AIAA Paper No. 2000-4852, *8th AIAA/USAF/NASA/ISSMO Symposium on Multidisciplinary Analysis and Optimization*, Long Beach, California, September 6-8, 2000.

Raymer, D., 2001, *Aircraft Conceptual Design*, AIAA, New York

SAE Aerospace Applied Thermodynamics Manual, 1969, Society of Automotive Engineers, New York.

SAE AIR 1168/8, 1989, *Aircraft Fuel Weight Penalty Due to Air Conditioning SAE Aerospace Applied Thermodynamics Manual*, Warrendale, PA.

Sciubba, E., 1995, "Artificial Intelligence Applications to the Synthesis of Thermal Processes," *Second Law Analysis of Energy Systems: Towards the 21st Century*, ASME, Univ. di Roma.

Sciubba, E., 1998, *Artificial Intelligence in Thermal Systems Design: Concepts and Applications*, Nova Science Publishers, Commack, N.Y.

Shah, R.K. and Webb, R.L., 1982, "Compact and Enhanced Heat Exchangers," in *Heat Exchangers: Theory and Practice*, J. Taborek, G.F. Hewitt, and N. Agfan editors, Hemisphere Publishing Corporation, pp 435-468

Shah, R.S., 1981, "Compact Heat Exchanger Design Procedure," in *Heat Exchangers, Thermal-Hydraulic Fundamentals and Design*, S. Kakac, A.E. Bergles and F. Matinger editors, Hemisphere Publishing Corporation, pp 495-536.

Sobieszczanski-Sobieski, J, 1989, *Optimization by Decomposition: A Step from Hierarchic to Non-hierarchic Systems*, NASA CP-3031, Part 1.

Sobieszczanski-Sobieski, J, 1990, "Sensitivity of Complex, Internally Coupled Systems," *AIAA Journal*, Vol. 28, pp.153-161, January.

Sobieszczanski-Sobieski, J. and Haftka, 1997, "Multidisciplinary Aerospace Design Optimization: Survey of Recent Developments," *Structural Optimization*, Vol. 14, No. 1, pp 1-23.

Tsatsaronis, G. and Pisa, J., 1994, "Exergoeconomic Evaluation and Optimization of Energy Systems-Application to the CGAM Problem," *Energy: The International Journal*, Vol. 19, No. 3, pp. 287-321.

Tsatsaronis, G. and Winhold, M., 1984, *Thermoeconomic Analysis of Power Plants*, EPRI AP-3651 Project 2029-8, Palo Alto, California, Electric Power Research Institute.

Tsatsaronis, G., 1985, *Thermoökonomische Analzse von Energieumwandlungs-prozessen*, Dr. Habilitatus Thesis, Dept. of Mechanical Engineering, Technical University of Aachen, West Germany.

Tsatsaronis, G., and Pisa, J., 1994, "Exergoeconomic Evaluation and Optimization of Energy Sytsems: Application to the CGAM Problem," *Energy: The International Journal*, Vol. 19, No. 3, pp. 287-321, Pergamon, Great Britain.

Tsatsaronis, G., et al., 1989, "Thermodynamic Analysis and Improvement of Energy Systems," *Proceeedings of the International Symposium*, Beijing, China, Pergamon Press, pp. 195-200.

Valero, A., Tsatsaronis, G., Frangopoulos, C.A., von Spakovsky, M.R., Lozano, M., M., Pisa, J., 1994, "CGAM Problem: Definition and Conventional Solution," *Energy: The International Journal*, Vol. 19, No. 3, pp. 279-286.

Valero, A., Serra, L., Lozano, M.A., 1993, "Structural Theory of Thermoeconomics," *Thermodynamics and the Design, Analysis and Improvement of Energy Systems*, ASME, AES-Vol. 30, N.Y., N.Y..

Valero, A., Serra, L., Lozano, M.A., and Torres, C., 1994, "Application of the Exergetic Cost Theory to the CGAM Problem," *Energy: The International Journal*, Vol. 19, No. 3, pp. 365-381, Pergamon, Great Britain.

von Spakovsky M.R., 1986, *A Practical Generalized Analysis Approach for the Optimal Thermoeconomic Design and Improvement of Real-World Thermal Systems*, School of Mechanical Engineering, Georgia Institute of Technology, Ph.D. Dissertation, December.

von Spakovsky M.R., Evans R.B., 1984, "Detailed Second Law Design of Components in Complex Thermal Systems," *Second Law Aspects of Thermal Design*, HTD Vol. 33, ASME, N.Y., N.Y., August.

von Spakovsky M.R., Frangopoulos, C.A., 1994, "The Environomic Analysis and Optimization of a Gas Turbine Cycle with Cogeneration," *Thermodynamics and the Design, Analysis and Improvement of Energy Systems*, ASME, AES-Vol. 33, N.Y., N.Y., November.

von Spakovsky, M.R., 1994, "Application of Engineering Functional Analysis to the Analysis and Optimization of the CGAM Problem," *Energy: The International Journal*, Vol. 19, No. 3, pp. 343-364, Pergamon, Great Britain.

von Spakovsky, M.R., and Evans, R.B., 1993, "Engineering Functional Analysis (Part I)," *Journal of Energy Resources Technology*, ASME Transactions, Vol. 115, No. 2, N.Y., June.

WATE User's Guide, 1999, NASA Lewis Research Center.